FFIE/685/116

Approved
Kjeller 2 July 1996

Paul Narum
Chief Scientist

REALTIME SYSTEM FOR STRUCTURE MONITORING OF SHIPS USING WAVELETS FOR TRANSIENT CHARACTERIZATION AND DETECTION

ERIKSEN Roger

FFI/RAPPORT–96/03149

FORSVARETS FORSKNINGSINSTITUTT
Norwegian Defence Research Establishment
Postboks 25, 2007 Kjeller, Norge

CONTENTS

REALTIME SYSTEM FOR STRUCTURE MONITORING OF SHIPS USING WAVELETS FOR TRANSIENT CHARACTERIZATION AND DETECTION

1 INTRODUCTION

In the resent years an increasing need for structural monitoring of mechanical loads and damages on constructions has emerged. In our case, surveillance of load, pressure and vibrations during use of vessels in rough sea condition. Critical loads must be measured to verify design criteria. Structural monitoring is necessary to avoid overload resulting in delamination and other damaging or degrading processes.

The development of Fibre Bragg Grating (FBG) strain sensors in the resent years have really opened the possibility for good structure monitoring of hulls. These sensors can be embedded in the hull, and be a part of the structure. In future structure monitoring systems there will be a large number of sensor elements, several hundreds, maybe thousands, and sufficient data power for real time signal processing and display of results will be required. When such a sensor system is used, it is useless without intelligent detection and characterization algorithms. These implemented algorithms must be fast if one require that the system shall run in real time.

A realtime system must have several properties. It must have efficient routines for data logging, data compression and detection/characterization of important events in analyzed signals. To be useful in real time, any graphical user interface (GUI) needs fast pre–processing before viewing results.

These systems will be very important during testing of ship designs. We will then give additional requirement to the realtime system. Data must be stored for careful detail analysis later. This analysis is supposed to be a tool for the designer of the ship. Using these analysis, an optimal construction may be achieved with respect to weight and determining limits for structural capacities.
On a long view this structure monitoring system is supposed to be fully automatic during active use of the vessel. A full realtime detection and characterization of transients or interesting events followed by a comparison to typical events must be carried out before any warnings or messages can be given to the crew.

This thesis work is a part of a preliminary study for a technical feasibility project where a fibre optic sensor system is going to be developed, installed and evaluated on a high speed naval vessel. This will be a collaboration, the CHESS (Composite Hull Embedded Sensor System) project, between Forsvarets Forskningsinstitutt (FFI) and Naval Research Laboratory (NRL), Optical Science Division.

The thesis is a study of application of wavelets for detection and characterization of transients phenomena. The background for choosing the wavelet approach is that wavelet theory today is a complete mathematical tool which represents a foundation for a

Of course many of the references explain almost the same, but as a new–beginner on wavelets without proper guidance, the learning process got very much harder. Because of this, the really interesting work has been done in the last few months of the available time. I hope that readers of this thesis will get a much shorter learning process on wavelets than me. Since learning wavelet theory consumed a great deal of time, there were either enough time for a comparison of wavelets with other techniques for solving the same problems, or proper experiments. Practical application of wavelet required insight in a number of computable technical details which are not well documented in the literature. And therefore time consuming for this author.

Wavelet theory is a relatively new concept in the signal processing field, just as it is in many other branches of science.
The first use of wavelets where introduced by J. Morlet in the late 1970's for analyzing seismic data. To convince his colleagues about the importance of his theory, he looked for help, and found it at A. Grossmann. They developed the inverse transform and some of the mathematical background of the wavelet transform. Later (1985), Y. Meyer realized that the analysis and synthesis[1] was a rediscovery of A. Calderón's theory form the 1960's.
First in the late 1980's did wavelet theory start to enter the signal processing field, after some important work of I. Daubechies and S. G. Mallat (3). In the 1990's the number of published papers on the topic has grown at an enormous rate. The large quantities of papers might be a problem when trying to learn the basic theory about wavelets. Therefore I think it is wise to use tutorial papers that are based on one's own science, i.e. the field of signal processing in my case. On the Internet there will also be found much information on this topic. Several wavelet toolboxes for Matlab and other wavelet programs are available as shareware.
During my work, I have run into examples of applications where wavelets today are used. Some of these are: Image compression, earthquake prediction and analysis, earthquake excitation and response of tall buildings, stresses in Dolos armor units, turbulence analysis and surveillance, analysis of seismic data, physics, solving mathematical problems, for removal of noise, and transient detection in signal processing.

1. General term for reconstruction or inverse transform.

2 SENSOR PRINCIPLE

This chapter will explain the principle of a fibre optic Bragg grating (FBG) sensor used for detecting mechanical strains. Several of these sensors are part of a structure monitoring system. A sensor system will be attached onto the hull of a ship to measure mechanical deformations. The hull of such a vessel will mainly consist of composite materials, i.e. glass fibre reinforced polyester.

The sensor is a special optical fibre, with a grating in the core, that utilizes the Bragg effect. This effect is known as Bragg reflection in solid state physics. When we have an optical fibre with a core structure as shown in Figure 2.1, and expose this to broadband illumination, the grating structure will reflect light at a wavelength according to Bragg's law (4)

$$2d \sin\theta = m\lambda_r, \tag{2.1}$$

where θ is the angle between the light vector and the lattice, λ_r is the wavelength of the returned light, m is the order of reflection, and d is the grating period (4). Equation (2.1) is known as the Bragg condition.

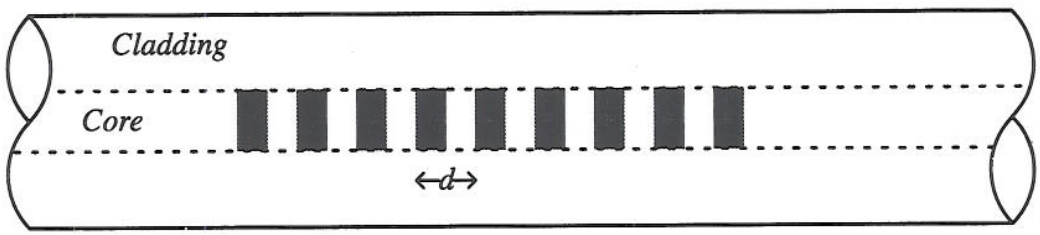

Figure 2.1 Optical fibre section with a Bragg grating. The index of refraction along the grating is modulated like a sine (or cosine) curve with period d. Source: (4)

In an optical fibre the angle of incidence will usually be normal to the grating interface, and hence $\theta = 90^o$. We will achieve highest reflection of the light with the condition $m = 1$. This gives:

$$\lambda_r = 2d, \tag{2.2}$$

and thus we have a linear relationship between the physical layer period d and the wavelength (or frequency) of the reflected light.

With such a relationship, it is clear that a tension which results in a contraction or elongation of the optical fibre along its axis will give a detectable change in wavelength of the reflected light.

Figure 2.2 illustrates the working principle of this strain sensor. The techniques used in detection and demodulation are not a topic for this report, however, there exists a large number of methods that can be used. From a signal processing point of view, one only need to know that the voltage out of the sensor is proportional to the longitudinal strain

in the fibre. For this fiber sensor, this implies a linear relationship between the optical wavelength shift and elongation or contraction.

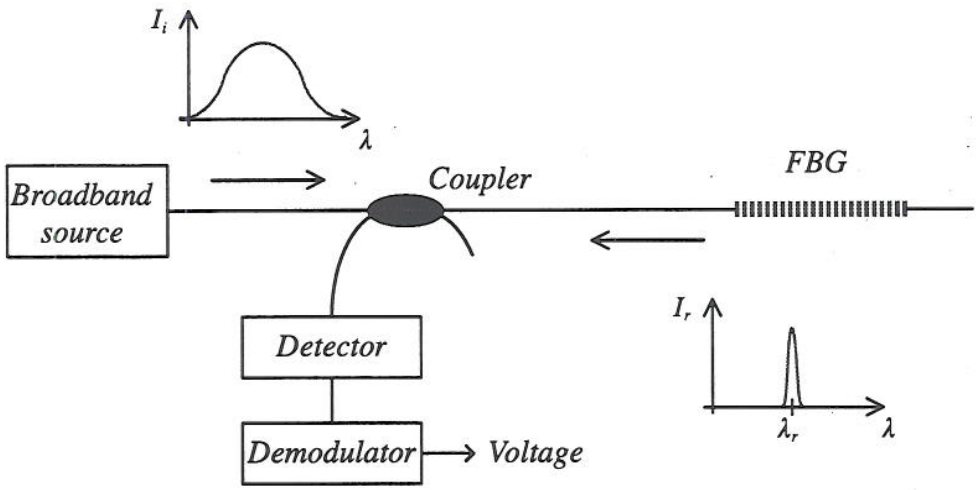

Figure 2.2 A schematic overview of the sensor principle

The sensor, or more specifically the optical fibre, can contain more than one FBG element. An example of an array with such gratings is illustrated in Figure 2.3. This system will clearly require a more complex management/treatment of the optical and electrical signals, and an example of one scheme that does this is shown if Figure 2.3. In this particular scheme, a combination of time and wavelength division multiplexing is used to address the various sensors (the 32 FBG's).

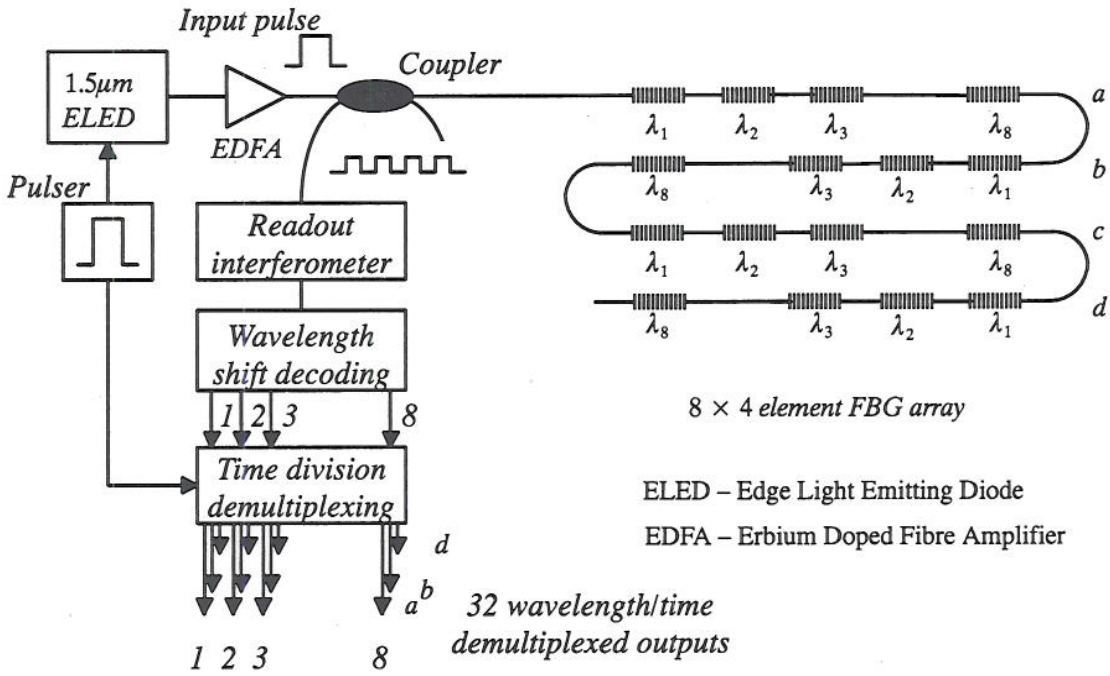

Figure 2.3 A 32 FBG array topology[2]

The FBG sensor can tolerate longitudinal strains up to about 3%.

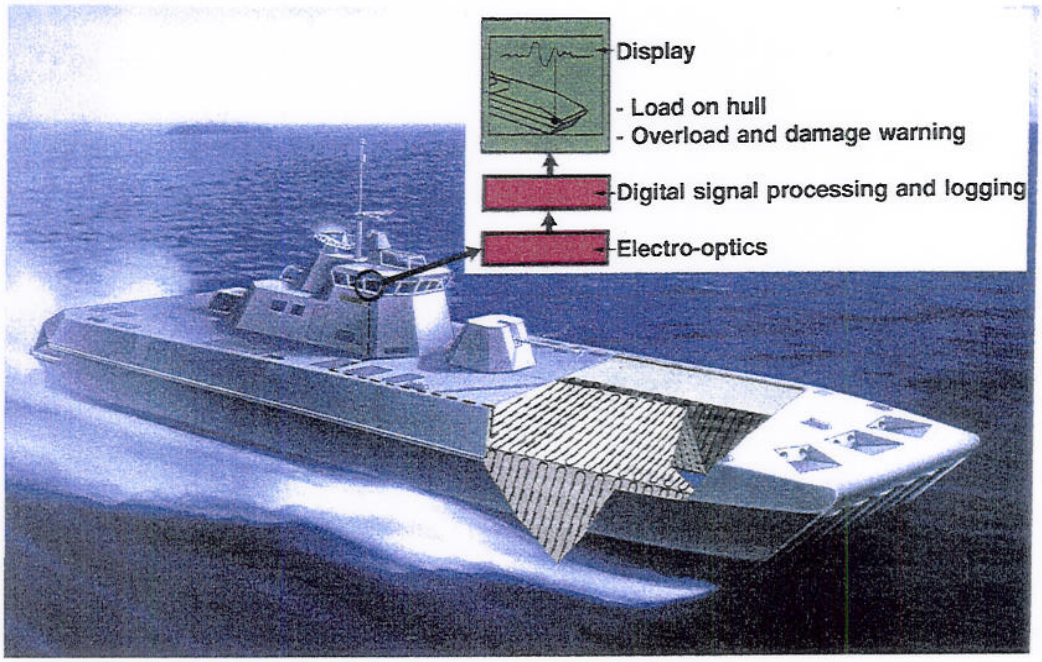

Figure 2.4 Sketch of a vessel with structure monitoring system. Inset schematically shows how signals are processed before presentation

One application of utilizing such a sensor system as illustrated in Figure 2.3, is shown in Figure 2.4, Where a number of these FBG's are attached onto the hull of a ship in order to measure mechanical stresses.

According to the blocks in the inset in Figure 2.4, this thesis main work are concentrated on the digital signal processing and logging part.

2. Preliminary design of fiber optic sensor system for the Composite Hull Embedded Sensor System, CHESS. A NRL (Naval Research Laboratory, U.S.A.) and NDRE cooperative R&D project.

3 WAVELET THEORY

In this chapter we will give an overview of the concept of wavelets. First we define the analyzing function, then the definition of the wavelet transform is stated. A detailed example with an interpretation of the transform follows. To achieve a fast algorithm for computing the transform, multiresolution analysis is used to show how the transform can be implemented as a filter bank. Then the properties of the wavelets are presented. At the end the use of wavelet package and M–band filter banks is discussed before the chapter closes with the practical implementation of discrete time series.

No unified usage of symbols and notation has been established in the literature. In this work we have chosen a notation which we have found most convenient.

3.1 Introduction to the Wavelet Transform

The idea behind the wavelet transform is to represent a signal *f(t)* as a superposition of wavelet functions. The word *wavelet* is a commonly used term for *a small wave*[3]. For a historical background, I recommend (5), (6) and especially (7). We want all wavelets to be expressed from a basis[4] wavelet, called ψ in this text.

3.1.1 The Continuous Wavelet Transform

A general wavelet obtained from the mother wavelet, $\psi \in L^2(\Re)$, is given by:

$$\psi_{a,b}(t) = \frac{1}{\sqrt{a}}\psi\left(\frac{t-b}{a}\right) \qquad ,a \in \Re_+, b \in \Re. \tag{3.1}$$

The parameter a ($a \neq 0$) describe the scaling (dilation) of the mother wavelet $\psi(t)$, and b is used to localize the wavelet in time. The $1/\sqrt{a}$ factor is used to give each wavelet the same (unit) energy. To represent a function as a superposition of all $\psi_{a,b}$, we must find the inner product between the function *f(t)* and each one of the wavelets $\psi_{a,b}(t)$. These inner products are the wavelet transform, defined as

$$WT(a,b) = \left\langle \psi^*_{a,b}, f \right\rangle = \int_{-\infty}^{\infty} \psi^*_{a,b}(t) f(t) dt, \tag{3.2}$$

where * denotes complex conjugation. For all transforms we are interested in the existence of the inverse transform. There are some conditions the basis wavelet function must satisfy (8)(9)(10)(11) to achieve reconstruction. The first condition implies finite energy (3.3),

$$\int_{-\infty}^{\infty} |\psi(t)|^2 dt < \infty, \tag{3.3}$$

3. Ondelettes: First used by Grossmann (theoretical physicist) and Morlet (geophysical engineer), Meyer (mathematician) published the book *Ondelettes* in 1990.

4. Also called the mother wavelet, analyzing wavelet or basic wavelet in literature.

and the second, called the admissibility condition, ensures finite redundancy C_ψ (3.4). When the redundancy[5] equals 1, all the wavelets form an orthonormal basis.

$$\int_0^\infty \frac{|\Psi(\omega)|^2}{\omega} d\omega = C_\psi < \infty, \tag{3.4}$$

where Ψ is the Fourier transform of the wavelet function. Generally, the admissibility condition is satisfied if the function ψ is reasonably smooth and (3.5) is fulfilled.

$$\Psi(0) = \int_{-\infty}^{\infty} \psi(t)dt = 0. \tag{3.5}$$

With these conditions satisfied we can reconstruct[6] the signal *f(t)* from (3.2) as follows:

$$f(t) = \frac{1}{C_\psi} \int_{-\infty}^{\infty} \int_0^\infty WT(a,b)\psi_{a,b}(t)\frac{dadb}{a^2}. \tag{3.6}$$

When the parameters *a* and *b* are continuous, then *WT(a,b)* is called *the continuous wavelet transform* (CWT).

Example

To get a better understanding of what a wavelet transform is, this example will illustrate the CWT of two different functions (or signals) *f(t)*, with respect to two different wavelet bases. One of the bases will be a non–smooth function and the other one smooth. These are called the Haar basis and the Morlet basis, respectively.

First we look at the wavelet transform of the signal $f_s(t)$, which is a smooth function that starts at time t_1. As a first basis we choose the Haar wavelet.

$$\psi(t) = \begin{cases} 1 & ,0 \le t < \frac{1}{2} \\ -1 & ,\frac{1}{2} \le t < 1 \\ 0 & ,otherwise \end{cases} \qquad f_s(t) = \begin{cases} sin(\omega t) & ,t \ge t_1 \\ 0 & ,otherwise \end{cases}.$$

This wavelet basis was discovered by Haar around 1910, and is the simplest basis that is known. Figure 3.1 shows a segment of the CWT of $f_s(t)$ with $T = 2$ ($T = 2\pi/\omega$) and $t_1 = -1$. The inset in the image plot shows the analyzing wavelet.

5. For continuous scaling and translation parameters the redundancy will never equal 1 which indicate no redundancy.

6. Proof will be found in (8), page 24–25.

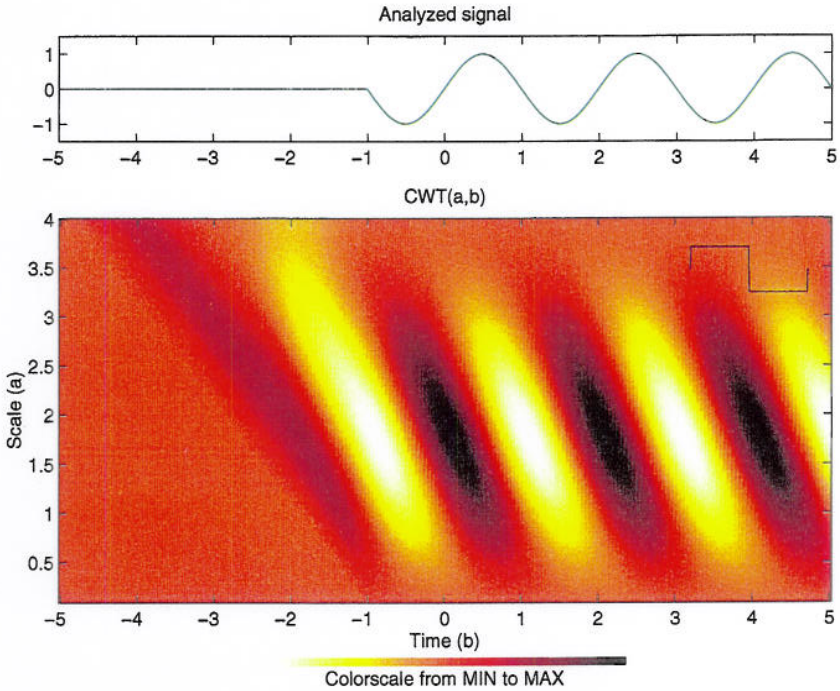

Figure 3.1 CWT of the partial sinus signal $f_s(t)$ with respect to the Haar wavelet

The next chosen wavelet basis is the Morlet wavelet[7].

$$\psi(t) = \frac{1}{2\pi} e^{ict} e^{-\frac{1}{2}t^2} \quad , c = \pi \sqrt{\frac{2}{\ln 2}}.$$

The CWT shown in Figure 3.2 is calculated with the same T and t_1, and it is the absolute value that is plotted since the wavelet is complex. In both cases the parameter a varies from 0,1 to 4.

7. The wavelet is plotted in Appendix A together with all the other wavelets in the wavelet toolbox from Matlab.

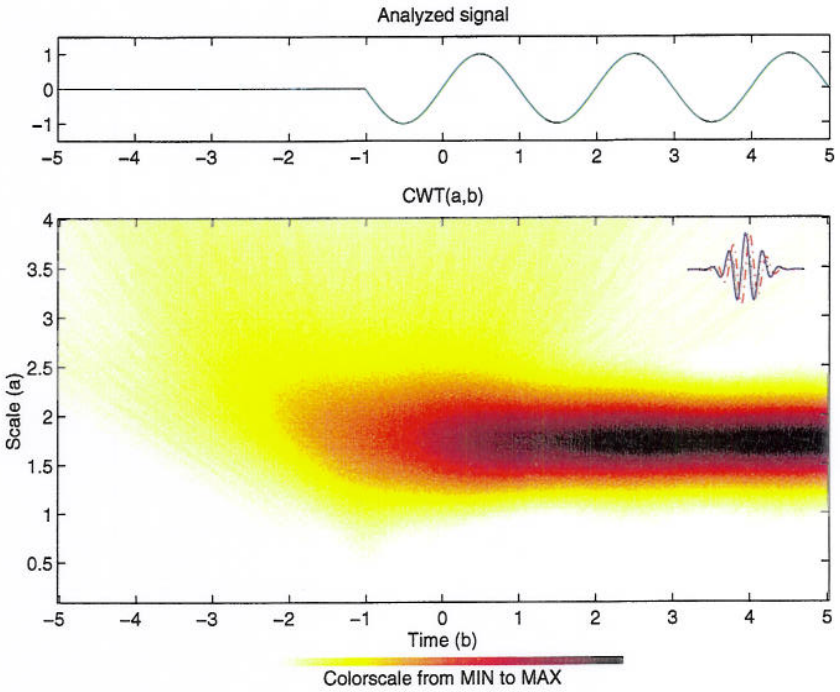

Figure 3.2 CWT of the partial sinus signal $f_s(t)$ with respect to the Morlet wavelet

Now, since one of the chosen bases is non–smooth we'll see how the two bases acts on a non smooth function, in this example the unit step function $f_u(t)$.

$$f_u(t) = u(t - t_1) = \begin{cases} 1 & ,t \geq t_1 \\ 0 & ,otherwise \end{cases}$$

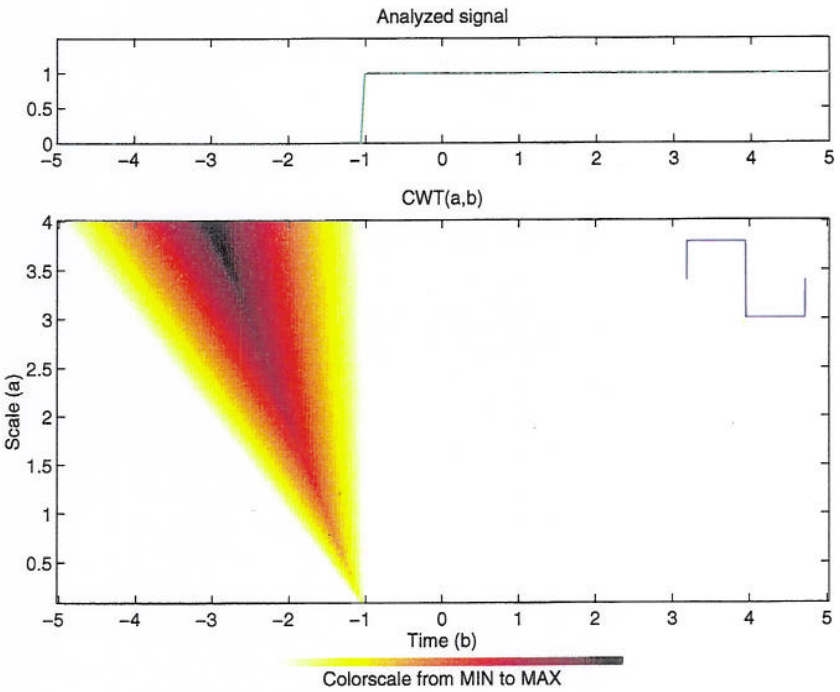

Figure 3.3 CWT of the unit step signal $f_u(t)$ with respect to the Haar wavelet

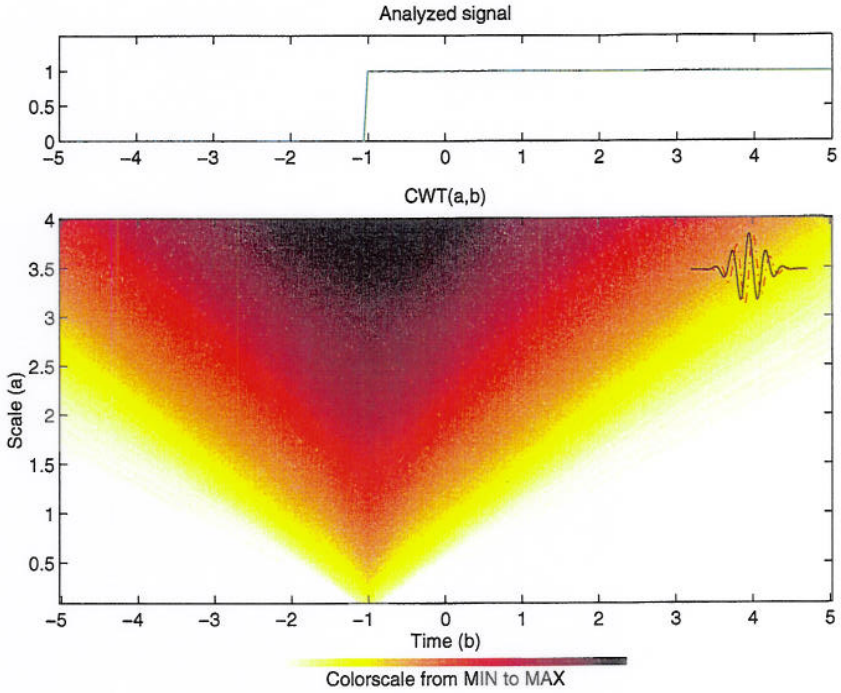

Figure 3.4 CWT of the unit step signal $f_u(t)$ with respect to the Morlet wavelet

This example illustrates the fact that knowledge of the signal is needed in order to choose the bast wavelet basis. Usually one would like to represent the signal with as few coefficients as possible (for large coding gain, i.e. for compressing pictures). Other times it is desirable to have a easy recognizable pattern (for fast manual identification). The clue is to choose a basis that extracts the properties important for your specific analysis. ■

3.1.2 Interpretation of the CWT

One of the most difficult problems for a new–comer to wavelets is how to interpret the wavelet transform pictures. As a start it is useful to think that the wavelet is sliding along the function to be analyzed. For each new time (b) we must evaluate a infinite number of integrals between $f(t)$ and $\psi_{a,b}(t)$.

Example

The easiest example that is really good, is analyzing a sinus function with a Morlet wavelet. Since the Morlet wavelet has a complex part, we must analyze the real and the imaginary part separately. For a number of situations the integrals becomes zero. Then there is a maximum when the frequency of the sinus and the wavelet is the same, and because of symmetry very much of the representation is zero. This is shown in Figure 3.2. By analyzing the relationship between the frequency of the sinus function and the scaling of the wavelet, we get a maximum at

$$a_{\max} = \frac{T}{2}\sqrt{\frac{2}{\ln 2}},$$

where 1/T is the frequency of the function. In this particular situation we have derived that the inverse of scale is frequency, so instead of calling it time–scale analysis we can call it time–frequency analysis. In the example in Section 3.1.1 $T = 2$, which results in $a_{\max} \approx 1{,}7$, which matches the figure very good. In (10) can be found some more illustrative examples of different sinus functions analyzed with the Morlet wavelet. ■

In principle, all transforms can be analyzed like this. Note that some wavelets not are symmetric around zero, and therefore a diagonal pattern, like in Figure 3.1, occurs. It is of course not possible to "see" frequencies in all wavelet transforms, and for that reason we call the wavelet transform a time–scale analyzing tool.

If the reader is in contact with the new toolbox on wavelets from MathWorks, there might be some confusion about any results compared to mine. Mine figures are <u>not</u> generated using this toolbox, but by own designed routines in Matlab!

When using this toolbox for a CWT on the same signals that I have, the resulting images will as stated not be the same. As an example the pattern in Figure 3.1 will appear vertically instead of diagonally when using the toolbox. By analyzing functions by hand according to the definition of CWT (Equation (3.2)), one will be convinced that mine results is correct. The only way to achieve vertically pattern is to use a shifted version of $\psi(t)$ as mother wavelet. The shift must be made in such a way that center of support of the wavelet coincidence with the vertically axis, i.e. the point $t = 0$. For the Haar wavelet this means that it must be shifted $1/2$ unit to the left. By analyzing functions with this version of the wavelet by hand, the same pattern as in the toolbox will occur. Why this is done do I not know. This effect is not documented in the manual either. There they have the same definition of the CWT as in this text. A possible reason for doing this is that these images may give users a better intuitive illustration of what scales that is present at a given time. This is just an assumption of mine, and it might not be right. Only MathWorks can answer this question.

3.1.3 The Discrete Wavelet Transform

In the case of continuous time, the function *f(t)* is represented as a combination of wavelets. As long as the parameters *a* and *b* are continuous, then *f(t)* is clearly overrepresented. This is because the wavelets $\psi_{a,b}(t)$ do not form an orthogonal basis for the space L^2. When we operate with continuous values we will never get, or be able to construct, an orthogonal basis for L^2. The case of overrepresentation of *f(t)* is normally undesired, and is avoided by forming an orthogonal basis of $\psi_{j,k}(t)$ that covers L^2. To get an orthogonal basis, we must use discrete values for a and b. In (8), page 53, it is concluded that if we choose $a = a_0^{-j}$, $a_0 > 0$ (*exept* for $a_0 = 1$)[8] and $b = k\, b_0 a_0^{-j}$, $b_0 \neq 0$ then

$$\psi_{j,k}(t) = \sqrt{a^j}\,\psi(a_0^j t - k b_0) \qquad ,j,k \in \mathcal{Z}\ (\mathcal{Z} - \textit{all integers}) \tag{3.7}$$

8. In many books and articles the minus before *j* is removed (this does not matter since *j* take all integers – negative and positive).

forms an orthogonal basis for L^2.
We now get a wavelet transform with respect to an orthogonal basis. This transform (3.8) is called *the discrete wavelet transform* (DWT), and (3.9) is called *the inverse discrete wavelet transform* (IDWT).

$$DWT(j,k) = \int_{-\infty}^{\infty} \psi^*_{j,k}(t) f(t) dt \tag{3.8}$$

$$f(t) = \kappa_\psi \sum_{j=-\infty}^{\infty} \sum_{k=-\infty}^{\infty} DWT(j,k) \psi_{j,k}(t) \tag{3.9}$$

Note that we still operate with continuous time even if we call the transform discrete. When the wavelet basis is orthonormal the inverse redundancy factor κ_ψ equals 1. The DWT is now a sampled version of the CWT plot. For dyadic values ($a_0 = 2, b_0 = 1$), the sampled points are related as shown in Figure 3.5.

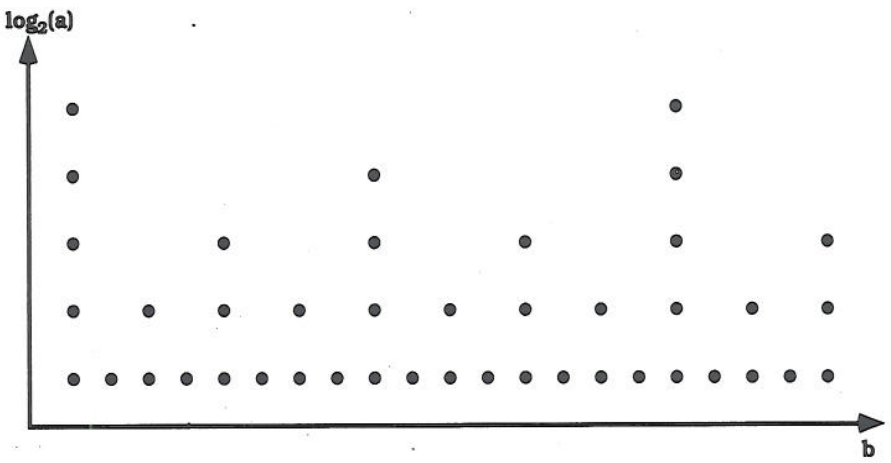

Figure 3.5 Dyadic (binary) sampling of the CWT

The next sections which cover multiresolution and filter banks, will give us the mathematical connection between the DWT and a filter bank (FB).
The three next sections and Section 3.6 are mainly based on (2).

3.2 Multiresolution

Both mathematical and practical interpretations of wavelets seem to be best served by using the concept of resolution (3) to define the effects of changing the scale. Multiresolution theory is based on functions that span spaces. In order to obtain a suitable division of L^2 space into smaller spaces, spanned by a finite number of wavelets, we must introduce the scaling function. This function is fundamental to the theory of multiresolution. As we shall see, the spaces spanned by wavelets are differentials of the spaces spanned by different scaling functions.

3.2.1 *The Scaling Function* $\phi(t)$

We will now define a new basis function $\phi(t)$, called *the scaling function*. Assume now that a set of shifted scaling functions $\phi_k(t) = \phi(t - k)$ will[9] span a space called V_0

$$V_0 = \underset{k}{Span}\{\phi_k(t)\}, \qquad k \in \mathcal{Z}, \tag{3.10}$$

where V_0 is a subspace of L^2. $\phi_k(t)$ will then form an orthogonal basis for V_0. The size of the subspace can be increased or decreased by changing the scale parameter of the scaling function. A family of functions is generated from the basis scaling function by scaling and shifting. Similar to the wavelet function $\psi(t)$, the different scaling functions are defined as

$$\phi_{j,k}(j) = \sqrt{2^j}\phi(2^j t - k), \qquad j \in \mathcal{Z}. \tag{3.11}$$

Then the functions $\phi_k(2^j t) = \phi_{j,k}(t)$ spans the space V_j.

$$V_j = \underset{k}{Span}\{\phi_k(2^j t)\}, \qquad k \in \mathcal{Z}. \tag{3.12}$$

If we decrease the parameter j, $\phi_k(2^j t)$ becomes wider and must be shifted in larger steps to form an orthogonal basis. Then they can only represent coarse information, and the space $\phi_k(2^j t)$ spans is smaller.
Now we formulate the basic requirement of multiresolution analysis (3) to cause a nesting of the spanned spaces by requiring

$$V_j \subset V_{j+1}, \quad j \in \mathcal{Z}, \tag{3.13}$$

with

$$V_{-\infty} = \{\emptyset\} \quad and \quad V_{\infty} = L^2. \tag{3.14}$$

The space that contains high resolution (or low scale) will then contain those of lower resolution (or high scale). This is illustrated in Figure 3.6.

9. Because of properties to be defined in Section 3.4.

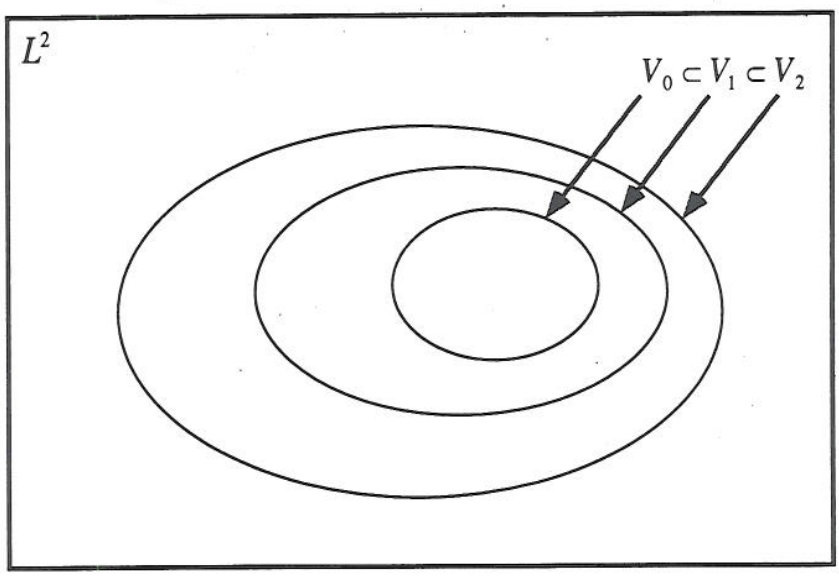

Figure 3.6 Scaling Function vector spaces in L^2

Because of the nesting (Equation (3.13)) and the definition of V_j (Equation (3.12)), the spaces have to satisfy a natural scaling condition

$$f(t) \in V_j \quad \Leftrightarrow \quad f(2t) \in V_{j+1}, \tag{3.15}$$

which ensures that elements in a space can be a linear combination of the elements in the next (or larger) space. This is achieved by requiring that

$$\phi(t) = \sum_n h(n)\sqrt{2}\phi(2t - n), \quad n \in \mathbb{Z}, \tag{3.16}$$

where the coefficients $h(n)$ are a sequence of numbers[10] (real or complex) called the scaling function coefficients. The factor $\sqrt{2}$ maintains the norm of the scaling function with the scale of two. If $\phi(t)$ is known we can calculate the scaling function coefficients $h(n)$, as long as the requirement of orthonormality

$$\int \phi_{j,k}(t)\phi_{j,l}(t)dt = \delta(k - l), \tag{3.17}$$

is satisfied, by multiplying to both sides of (3.16) by $\phi(2t - k)$ and integrating. This relationship is given by

$$h(n) = \sqrt{2}\int \phi(t)\phi(2t - n)dt. \tag{3.18}$$

The recursive equation (3.16) is fundamental to the theory, and is called *The Dilation Equation* (14).

3.2.2 The Wavelet Function $\psi(t)$

The important feature of a signal can better be described or parameterized, not by using $\phi_{j,k}$ to change the size of the subspace V_j, but by defining a different set of functions

10. Do not think of $h(n)$ as a digital filter yet, but as pure coefficients, i.e. linear combination. Later we will see that $h(n)$ in fact is a FIR filter.

$\psi_{j,k}$ that span the differences between the spaces spanned by the various scales of the scaling function. This new function $\psi(t)$ is called the wavelet function, and is the same function as in Section 3.1.

This new space which is the orthogonal complement of V_j in V_{j+1} is defined as W_j, which means that all members of V_j are orthogonal to all members of W_j. The inner product between these various basis functions are then given as follows:

$$\left\langle \phi_{j,k}, \psi_{j,l} \right\rangle = \int_{-\infty}^{\infty} \phi_{j,k}(t)\psi_{j,l}^{*}(t)dt = 0, \qquad j,k,l \in \mathcal{Z}. \tag{3.19}$$

Then the relationship between these subspaces can be seen from the following expressions. If

$$V_0 \subset V_1 \subset V_2 \subset \ldots . \subset L^2, \tag{3.20}$$

then the wavelet spanned subspace W_0 is defined such that

$$V_1 = V_0 \oplus W_0, \tag{3.21}$$

which extends to the general relationship

$$L^2 = V_0 \bigoplus_{j=0}^{\infty} W_j, \tag{3.22}$$

as illustrated if Figure 3.7.

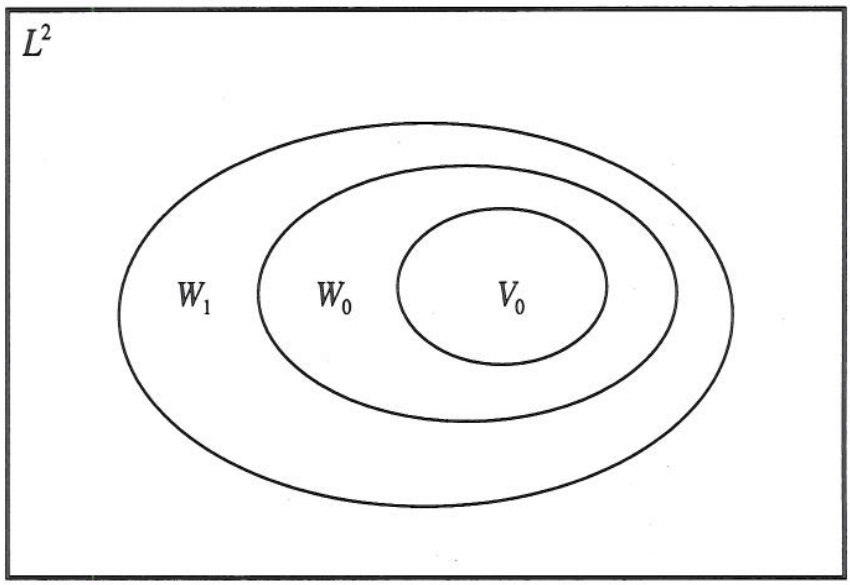

Figure 3.7 Wavelet Function vector spaces in L^2

Since the parameter $j \in \mathcal{Z}$, the scale of the initial space is arbitrary and can be chosen for a higher resolution (lower bound for $j > 0$) or for a lower resolution (lower bound for $j < 0$). This means that there is no need to start at V_0, but it gives an easier under-

standing of the multiresolution concept. For an example and more detail see (2), Chapter 2. In practice W_0 is usually chosen to represent the coarsest detail of interest in a signal. Note that the wavelet functions that spans W_0 is contained in the space spanned by the next narrower scaling function, $W_0 \subset V_1$, and as a result they can be described by a linear combination of these respective scaling functions

$$\psi(t) = \sum_n h_1(n)\sqrt{2}\phi(2t - n), \qquad n \in \mathcal{Z}, \tag{3.23}$$

for some set of coefficients $h_1(n)$. In the appendix of (2) it is shown that these wavelet function coefficients (modulo translations by multiples of two) and the scaling function coefficients are simply related, according to the equation

$$h_1(n) = (-1)^n h(1 - n). \tag{3.24}$$

An example for a finite even length–N *h(n)* could be

$$h_1(n) = (-1)^n h(N - 1 - n). \tag{3.25}$$

The function that is generated by Equation (3.23) is the wavelet basis function (or mother wavelet), and (3.23) is called *The Wavelet Equation* (14).

The result of the construction of the set of functions $\phi_{j,k}(t)$ and $\psi_{j,k}(t)$ that span L^2, is that any function $f(t) \in L^2$ can be written

$$f(t) = \sum_{k=-\infty}^{\infty} c(k)\,\phi_{0,k}(t) + \sum_{j=0}^{\infty}\sum_{k=-\infty}^{\infty} d_j(k)\,\psi_{j,k}(t), \tag{3.26}$$

or in more general terms if $f(t) \in V_{J_1}$

$$f(t) = \sum_{k=-\infty}^{\infty} c_{J_0}(k)\,\phi_{J_0,k}(t) + \sum_{j=J_0}^{J_1-1}\sum_{k=-\infty}^{\infty} d_j(k)\,\psi_{j,k}(t), \tag{3.27}$$

where the $c_j(k)$ is the scaling representation of the signal and $d_j(k)$ is the wavelet representation. In Equation (3.26) $J_0 = 0$ and $J_1 = \infty$, but these two values can be chosen arbitrary. The choice of J_0 and J_1 will be discussed later. For a pure wavelet representation we write

$$f(t) = \sum_{j=-\infty}^{\infty}\sum_{k=-\infty}^{\infty} d_j(k)\psi_{j,k}(t), \tag{3.28}$$

that is in fact the same definition as the reconstruction formula in Equation (3.9). These wavelet coefficients $d_j(k)$ completely describe the original signal $f(t)$ and can be used for analysis, description, approximation and filtering in a way similar to Fourier series coefficients.

3.3 Filter Bank realization

In this section we will study the relationship between DWT and filter banks (FB). First discussed are the connections between the recursive Equation (3.16), Equation (3.23)

and Mallat's algorithm (3)(12)(13). Then we will see that this algorithm from a signal processing point of view in fact is a FB.

3.3.1 *From Fine Scale to Coarse Scale – Analysis bank*

We start with the fundamental recursion Equation (3.16) where $t \rightarrow 2^j t - k$ (scaling and translating the time variable) so we get

$$\phi(2^j t - k) = \sum_n h(n)\sqrt{2}\phi(2^{j+1}t - 2k - n), \tag{3.29}$$

assuming that a unique solution exists given a set of $h(n)$. By changing the variables to $m = 2k + n$, Equation (3.29) becomes

$$\phi(2^j t - k) = \sum_m h(m - 2k)\sqrt{2}\phi(2^{j+1}t - m). \tag{3.30}$$

From Equation (3.12), and assuming that $f(t) \in V_{j+1}$, we can write $f(t)$ as a linear combination of the basis functions that span V_{j+1}. Then the function can be expressed by

$$f(t) = \sum_k c_{j+1}(k)\sqrt{2^{j+1}}\phi(2^{j+1}t - k), \tag{3.31}$$

that is, its scaling coefficients only and no wavelets coefficients. The general term of Equation (3.21),

$$V_{j+1} = V_j \oplus W_j, \tag{3.32}$$

leads to the new expression

$$f(t) = \sum_k c_j(k)\sqrt{2^j}\phi(2^j t - k) + \sum_k d_j(k)\sqrt{2^j}\psi(2^i t - k), \tag{3.33}$$

which also can be written

$$f(t) = \sum_k c_j(k)\sqrt{2^j}\phi_{j,k}(t) + \sum_k d_j(k)\sqrt{2^j}\psi_{j,k}(t). \tag{3.34}$$

This is consistent with multiresolution theory. Now, if $\phi_{j,k}(t)$ and $\psi_{j,k}(t)$ are orthonormal or a tight frame[11], the *j 'th* level scaling coefficients c_j are found by taking the inner products

$$c_j(k) = \langle f, \phi_{j,k} \rangle = \int f(t)\phi(2^j t - k)dt, \tag{3.35}$$

which, by substituting Equation(3.30), and interchanging the sum and integral, can be written as

11. A tight frame is an orthogonal version of a basis for a representation. A general frame (not tight) is an overspecified version of a basis set. Contrary to an orthogonal basis, a frame basis introduce redundancy in the representation, which gives a more robust representation.

$$c_j(k) = \sum_m h(m - 2k) \int f(t)\sqrt{2^{j+1}}\phi(2^{j+1}t - m)dt. \tag{3.36}$$

If we compare the last part of Equation (3.36) (the integral) with Equation (3.35), this is in fact the same expression at two succeeding levels. This leads us to the convolution formula

$$c_j(k) = \sum_m h(m - 2k)c_{j+1}(m). \tag{3.37}$$

The following corresponding relationship is obtained for the wavelet coefficients when deduced from the fundamental Equation (3.23).

$$d_j(k) = \sum_m h_1(m - 2k)c_{j+1}(m). \tag{3.38}$$

In signal processing terms these two convolution formulas can be interpreted as a two band analysis FB as illustrated in Figure 3.8, where $h_0 = h$. The right–hand boxes downsample, with a factor of two, the results form filtering c_{j+1} through the filters $h_0(-n)$ and $h_1(-n)$ (impulse responses) to achieve c_j and d_j.

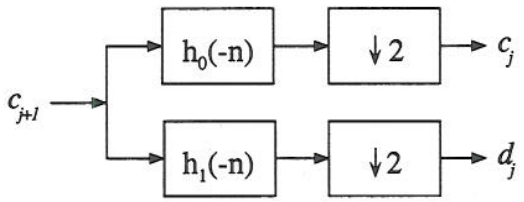

Figure 3.8 Two band analysis bank

3.3.2 *From Coarse Scale to Fine Scale – Synthesis bank*

We still expect that if $f(t) \in V_{j+1}$, then the function can be written in terms of the scaling function as

$$f(t) = \sum_k c_{j+1}(k)\sqrt{2^{j+1}}\phi(2^{j+1}t - k), \tag{3.39}$$

or in terms of the next scale (which also requires wavelets , based on Equation (3.32)) as

$$f(t) = \sum_k c_j(k)\sqrt{2^j}\phi(2^j t - k) + \sum_k d_j(k)\sqrt{2^j}\psi(2^j t - k). \tag{3.40}$$

Now, substituting the equations (3.16) and (3.23) into Equation (3.40) gives

$$f(t) = \sum_k c_j(k) \sum_n h(n)\sqrt{2^{j+1}}\phi(2^{j+1}t–2k–n) + \sum_k d_j(k) \sum_n h_1(n)\sqrt{2^{j+1}}\phi(2^{j+1}t–2k–n). \tag{3.41}$$

Because of the orthonormality condition (3.17), integrating (3.39) and (3.41) multiplied with $\phi(2^{j+1}t - k')$ results in the following expression

$$c_{j+1}(k) = \sum_m c_j(m)h(k - 2m) + \sum_m d_j(m)h_1(k - 2m), \tag{3.42}$$

which is the opposite operation to an analysis bank, namely called the two band synthesis bank. This FB structure is shown in Figure 3.9,

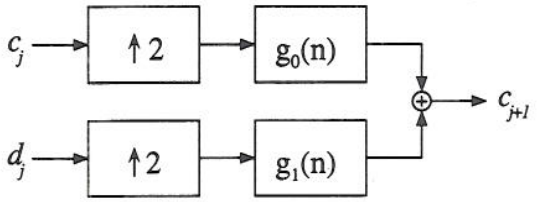

Figure 3.9 Two band synthesis bank

where $g_0(n) = h(n)$ and $g_1(n) = h_1(n)$. The left boxes upsample the incoming signals by a factor of two, meaning that a zero is put between each old sample.

We have now derived the direct connection between DWT and FB. When it comes to construction we, depending on the problem to solve, choose how many stages we need (want) in the FB realization. Figure 3.8 and 3.9 illustrate a one stage analysis and synthesis bank, respectively.

3.4 Properties of the Scaling and Wavelet function

Until now we have not said anything about the properties of $\phi(t)$ and $\psi(t)$. In this section we will look at these two basic functions to see when they exist and what their properties are. In Section (3.2) about multiresolution, we derived the two fundamental equations

$$\phi(t) = \sum_n h(n)\sqrt{2}\phi(2t - n), \quad n \in \mathbb{Z}, \tag{3.43}$$

and

$$\psi(t) = \sum_n h_1(n)\sqrt{2}\phi(2t - n), \quad n \in \mathbb{Z}. \tag{3.44}$$

3.4.1 Necessary conditions

It can be shown that if $\phi(t)$ is a solution to (3.43) then

$$\sum_n h(n) = \sqrt{2}. \tag{3.45}$$

The proof goes as follows: Integrate (3.43) on both sides and interchange the sum and integral. Since the integral of $\phi(t)$ is shift invariant and by a change of variable it can be shown from

$$\int \phi(t)dt = \frac{1}{\sqrt{2}} \sum_n h(n) \int \phi(x)dx, \tag{3.46}$$

that a necessary requirement for Equation (3.45) to hold is that

$$\int \phi(t)dt \neq 0. \tag{3.47}$$

This shows that not just any set of scaling function coefficients will support a solution to Equation (3.43). The coefficients must satisfy the linear Equation (3.45). Assume that $\phi(t)$ is a solution to (3.43) such that (3.47) holds. Then

$$\sum_n h(n)h(n - 2k) = \delta(k), \tag{3.48}$$

if the energy of $\phi(t)$

$$\int |\phi(t)|^2 dt = E < \infty, \tag{3.49}$$

and if the orthogonality condition

$$\int \phi(t)\phi(t - k)dt = E\delta(k), \tag{3.50}$$

is fulfilled.

Now the $\delta(k)$ is the Kronecker delta function ($\delta(k) = 1$ *only if* $k = 0$). This relationship does not depend on normalization of $\phi(t)$. If $\phi(t)$ is normalized, then $E=1$, and $\phi_{j,k}(t)$'s form an orthonormal basis. The result of this is that the coefficients $h(n)$ of the recursive Equation (3.43) themselves are orthonormal after downsampling[12] them by two. A corollary to Equation (3.48) is obtained for $k=0$, which states that the norm of $h(n)$ is automatically unity.

$$\sum_n |h(n)|^2 = 1. \tag{3.51}$$

It is shown (2) that a second corollary of (3.48) is

$$\sum_n h(2n) = \sum_n h(2n + 1) = \frac{1}{\sqrt{2}}. \tag{3.52}$$

We now have three restrictions[13] on the coefficients $h(n)$, namely Equations (3.45), (3.51) and (3.52), all of which are independent of any normalization of $\phi(t)$. It can also be derived that if $\phi(t)$ has compact support on $0 \leq t \leq N - 1$ then $h(n)$ also has compact support over the same interval. Now the support (or length) of $h(n)$ which is N

12. In some cases "decimating" is used in the literature.

13. (3.48) is also a restriction on the coefficients $h(n)$, but it is dependent on E.

must be an even number.
All stated conditions ((3.45), (3.48), (3.51) and (3.52)) limit the choice of $h(n)$ in the time domain. In the frequency domain two of these four restrictions correspond to a frequency counterpart, namely

$$\sum_n h(n) = \sqrt{2} \Leftrightarrow H(0) = \sqrt{2}, \tag{3.53}$$

$$\sum_n h(n)h(n - 2k) = \delta(k) \Leftrightarrow \left|H(\omega)\right|^2 + \left|H(\omega + \pi)\right|^2 = 2, \tag{3.54}$$

where $H(\omega)$ is the Discrete–Time Fourier Transform (DTFT) of $h(n)$ and N the length of $h(n)$ (Note that $H(\omega)$ is periodic in 2π, and is symmetric around $\omega = 0$). From the orthonormality condition on $\phi(t)$ ($E=1$) it follows that

$$\sum_l \left|\Phi(\omega + 2\pi l)\right|^2 = 1, \tag{3.55}$$

where $\Phi(\omega)$ is the Fourier transform of $\phi(t)$. If $h(n)$ is viewed as a digital filter, the orthogonality requirement (3.54) states that this FIR (Finite Impulse Response) filter is equivalent to a so–called Quadrature Mirror Filter (QMF) (31) (see Figure 3.10). As a corollary of the above frequency response requirements, we see that

$$H(\pi) = \sqrt{2} - H(2\pi) = \sqrt{2} - H(0) = 0, \tag{3.56}$$

which says that the response at the so–called Nyquist frequency ($\omega = \pi$) is necessarily zero. This indicates that $h(n)$ in fact is a lowpass filter.

When the conditions on $\phi(t)$ are fulfilled and Equation (3.44) defines the wavelet, the wavelet is orthogonal to the scaling function at the same scale. Then

$$\int \phi(t - n)\psi(t - m)dt = 0, \tag{3.57}$$

if and only if the wavelet function coefficients $h_1(n)$ are given by

$$h_1(n) = (-1)^{n+n_0}h(N_0 - n), \tag{3.58}$$

which is a more general term for (3.24), where n_0 is an arbitrary integer to set the sign of $h_1(n)$, and N_0 is an arbitrary odd integer chosen to conveniently position $h_1(n)$. When $n_0 = 0$ and $N_0 = N - 1$ (N – length of $h(n)$), this results in (3.25). This condition also leads to the relation

$$\sum_n h(n)h_1(n - 2k) = 0, \tag{3.59}$$

between the scaling function coefficients and the wavelet function coefficients.
By substituting (3.58) into (3.52) we get

$$\sum_n h_1(n) = 0. \tag{3.60}$$

Then by integrating Equation (3.44), a condition on $\psi(t)$ becomes

$$\int \psi(t) = 0, \tag{3.61}$$

and in the frequency domain Equation (3.60) results in

$$H_1(0) = 0. \tag{3.62}$$

Another result can be derived from the definition of the DTFT combined with the knowledge of the wavelet function coefficients $h_1(n)$,

$$H_1(\pi) = \sum_n h_1(n)(-1)^n = \sum_n h(1-n)(-1)^{2n} = \sqrt{2}. \tag{3.63}$$

As a counterpart to $h(n)$, we now have shown that $h_1(n)$ is a high–pass filter, that also fulfills the demands to be a QMF.

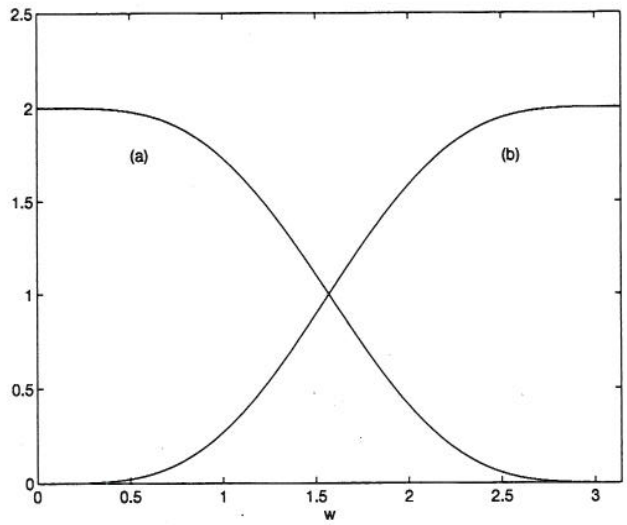

Figure 3.10 The two QMF frequency responses (a) $|H(\omega)|^2$ and (b) $|H_1(\omega)|^2$ corresponding to the db2 wavelet

In the frequency domain the following relationship arises between $H(\omega)$ and $H_1(\omega)$:

$$|H_1(\omega)|^2 = |H(\omega + \pi)|^2. \tag{3.64}$$

The results in this section have not included the effect of integer shifts of the scaling function or wavelet function coefficients $h(n)$ and $h_1(n)$. As noted in Section 3.2.1, the FIR filters are not causal. In a practical situation, these sequences may be arbitrary shifted to make the corresponding FIR filters causal.

In (15) there is presented an overview of the properties of the wavelets that is implemented in the Matlab toolbox. The most interesting by this overview is that it shows the

relationship between the existence of ϕ and the possibility of a discrete transform. There is also a connection between the FIR filters existence and the DWT[14]. Note also that not many of the wavelets have an explicit expression. The reason for this is that many of the wavelets is an iterated result of Equation (3.43) after designing the FIR filters to be QMFs. In the iteration process we start with $\phi(t)$ as the box function[15], and use the iterated version of Equation (3.43),

$$\phi^{(k+1)}(t) = \sqrt{2}\sum_n h(n)\phi^{(k)}(2t-n)\,, \qquad \phi^{(0)}(t) = \begin{cases} 1\,, & t \in [0,1] \\ 0\,, & otherwise \end{cases}. \tag{3.65}$$

When Equation (3.65) converge[16], we use the resulting scaling function to obtain the wavelet function from Equation (3.44).

One can distinguish between three main types of wavelets:

1. There exist no scaling function corresponding to the wavelet (*morl* and *mexh*).
2. The scaling function do exist, but no FIR filters exists. A fast algorithm does therefore neither exist (*meyr*).
3. Scaling function and FIR filters exist (*haar*, *dbN*, *symN*, *coifN* and *biorNr.Nd*).

Table 3.1 gives an overview of the properties to the wavelet families available in the new (Apr./May– 96) Matlab toolbox.
Appendix A plots all these wavelet functions with their corresponding scaling functions.

	morl	mexh	meyr	haar	dbN	symN	coifN	biorNr.Nd
"Crude"	✓	✓						
Infinitely regular	✓	✓	✓					
Compactly supported orthogonal				✓	✓	✓	✓	
Compactly supported biorthogonal								✓
Symmetry	✓	✓	✓	✓				✓
Asymmetry					✓			
Near symmetry						✓	✓	
Arbitrary number of vanishing moments					✓	✓	✓	✓
Vanishing moments for ϕ							✓	
Arbitrary regularity					✓	✓	✓	✓

14. Except for the Meyer wavelet. Fast algorithms can only be obtained for wavelets with existing FIR filters.

15. Box function: One if t is between zero and one, zero otherwise.

16. For a more detail study of the relationship between FIR filters and the convergence of (3.65), see (14).

Existence of ϕ			✓	✓	✓	✓	✓	✓
Orthogonal analysis			✓	✓	✓	✓	✓	
Biorthogonal analysis			✓	✓	✓	✓	✓	✓
Exact reconstruction			✓	✓	✓	✓	✓	✓
FIR filters				✓	✓	✓	✓	✓
Continuous transform	✓	✓	✓	✓	✓	✓	✓	✓
Discrete transform			✓	✓	✓	✓	✓	✓
Fast algorithm				✓	✓	✓	✓	✓
Explicit expression	✓	✓		✓				for splines

Table 3.1 Overview of Wavelet Families and Associated Properties. Source: (15)

In the table above the term biorthogonal analysis is introduced. Until now we have only studied orthogonal wavelets and filters. In this text biorthogonal wavelets will not be explained in detail. The only difference between orthogonal and biorthogonal wavelets is that there are two separate wavelets in biorthogonal analysis, one for decomposition and one for reconstruction. These two wavelets are now biorthogonal. Figure 3.11 indicate the difference between biorthogonal and orthogonal multiresolution.

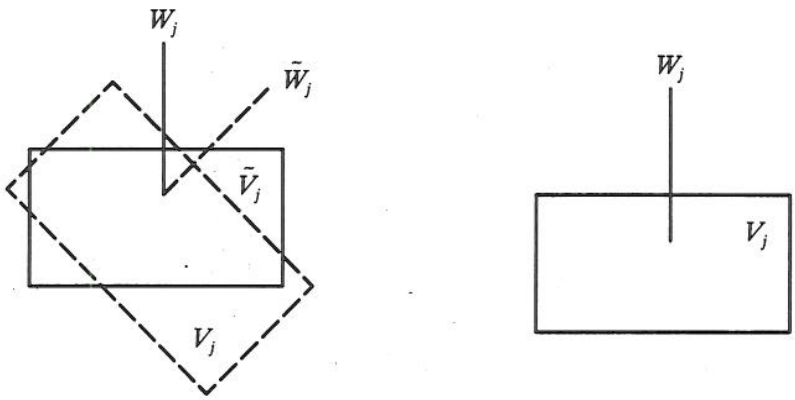

Figure 3.11 Visualization of biorthogonal vs. orthogonal multiresolution. Source: (14)

For a deeper study of the concept of biorthogonality, Section 6.5 in (14) is highly recommended.

3.5 Wavelet Packets / M – band FB

If the dyadic sampling grid in Figure 3.5 is inconvenient for our problem, it is possible to sample the time–scale plane almost as we want. This can be done by extending the two band wavelet FB to a multiband filter bank (M–band FB), or by using wavelet packets. These two realizations can in fact be equal, with respect to sampling grid, but just in some special cases. We have seen in the present how a wavelet decomposition structure looks like, and a general analysis bank is shown in Figure 3.12.

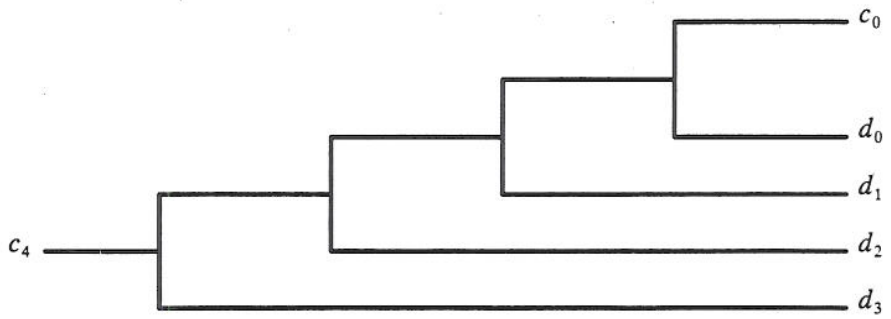

Figure 3.12 4–stage 2–band analysis bank

A wavelet packet structure is constructed with respect to which sampling grid is best suited for the problem. Assume as an example that for a certain scale you want a more dense grid so a detection is made more accurate. This can be done by analyzing the wavelet coefficients as shown in Figure 3.13.

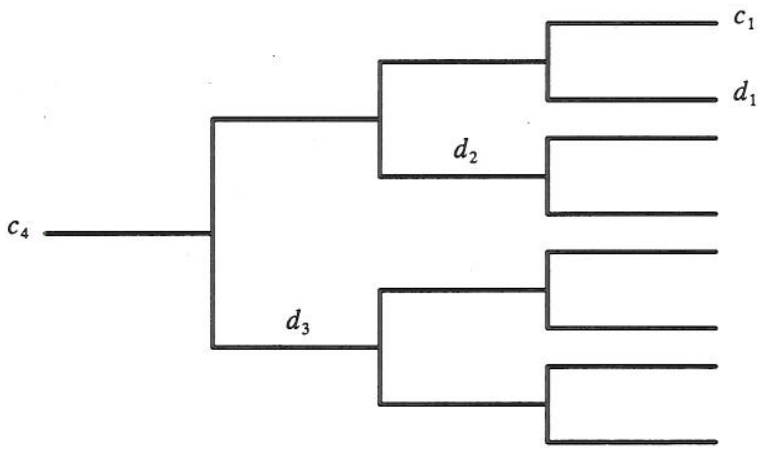

Figure 3.13 Example of a full wavelet packet analysis bank

An other method to achieve a different sample grid is the M–band FB. The theoretical background for this is built on the multiresolution method discussed earlier. The main clue is to split each wavelet vector space W_j into smaller spaces W_{jl}. For $M=4$ the decomposition of the vector space is as shown in Figure 3.14.

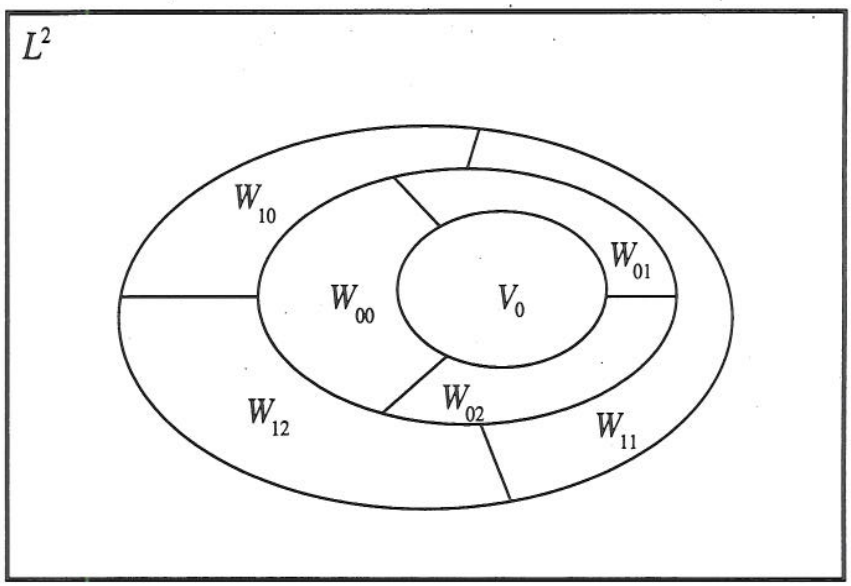

Figure 3.14 4–band wavelet system vector spaces in L^2

For the M–band wavelet systems the basic recursion Equation (3.16) changes to

$$\phi(t) = \sum_n h(n)\sqrt{M}\phi(Mt - n), \quad n \in \mathcal{Z}, \tag{3.66}$$

and the basis functions that spans each of the W_{jl} are all still orthonormal. This theory is a generalization of the 2–band theory discussed in Section 3.2. The FB structure for the 4–band wavelet system is just an extension of the structure in Figure 3.12. As noted before, the FIR filters can be arbitrary shifted to become causal, therefore the minus sign is removed in the figure below.

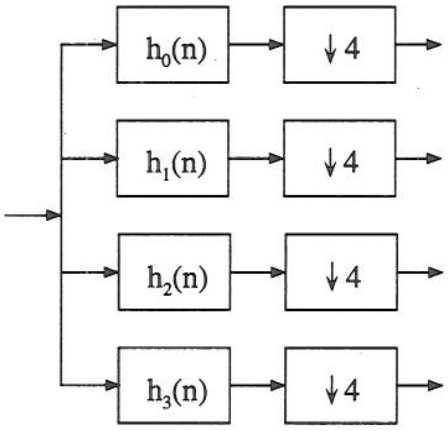

Figure 3.15 Four band analysis bank

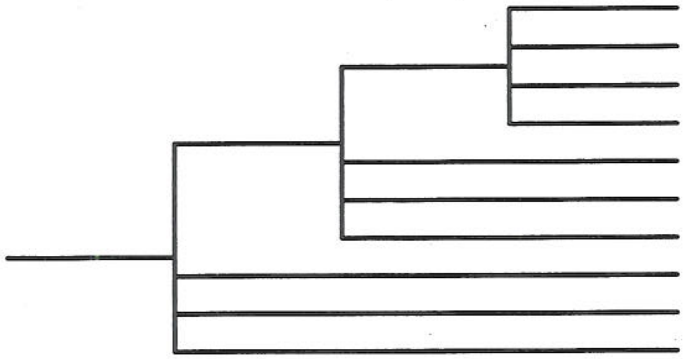

Figure 3.16 3–stage 4–band analysis bank.

For further readings on this subject, see (2)

3.6 Discrete Time Wavelet Transform

Until now we have presented a transform of continuous functions (or signals). In most cases, transforms are calculated by a computer. As a computer only can operate on discrete time series it is required that the signal we want to analyze must be sampled. When sampling a signal, there is a minimum requirement to maintain frequency information; namely the Nyquist criterion. To determine the sample frequency we must have some information about the signal. Normally, typical signal characteristics are known, sensors have a limited bandwidth, and the noise can more or less be determined. Even if much information are available, to avoid aliasing, an analog lowpass filter is typically used before the A/D–converter.

As discussed in the multiresolution Section (3.2) the signal can be represented as follows

$$f(t) = \sum_{k=-\infty}^{\infty} c_{J_1}(k)\,\phi_{J_1,k}(t), \tag{3.67}$$

if $f(t) \in V_{J_1}$. This is the finest scale in the signal, i.e. $f(t)$ can be perfectly reconstructed from these coefficients alone. These coefficients

$$c_{J_1}(k) = \left\langle f, \phi_{J_1,k} \right\rangle, \tag{3.68}$$

are to be input to the analysis filter bank. To achieve this we need the connection between the sampled signal and the coefficients $c_{J_1}(k)$. For J_1 large enough, $\phi_{J_1,k}(t)$ can be approximated by a Dirac impulse at its center of mass (first moment) since $\int \phi(t)dt = 1$. For large J_1 this gives

$$c_{J_1}(k) = \sqrt{2^{J_1}} \int f(t)\phi(2^{J_1}t - k)dt = \sqrt{2^{J_1}} \int f(t + 2^{-J_1}k)\phi(2^{J_1}t)dt, \tag{3.69}$$

which from

$$2^j \int f(t)\phi(2^j t)dt \approx \int f(t)\delta(t - 2^{-j}m_0)dt = f(t - 2^{-j}m_0), \tag{3.70}$$

where m_0 is the first moment of $\phi(t)$, results in the approximation

$$c_{J_1}(k) \approx \sqrt{2^{-J_1}} f(2^{-J_1}(m_0 + k)). \tag{3.71}$$

This method for discretization of the signal is presented in (2). There are just a few refences that discuss this topic (2)(16)(17). Burrus *et. al.* (2) claims with support from (16), that for all 2–regular wavelets (i.e. wavelets with two vanishing moments[17], regular[18] wavelets other than the Haar wavelet – even in the M–band case where one replaces 2 by M in (3.71), $m_0 = 0$) one can show that the samples of the functions themselves form a third order approximation to the scaling function coefficients of the signal. That is, if $f(t)$ is a quadratic polynomial, then

$$c_{J_1}(k) \approx \sqrt{2^{-J_1}} f(2^{-J_1}k). \tag{3.72}$$

Thus, in practice, the finest scale J_1 is determined by the sample rate. By rescaling the function and amplifying it appropriately one can assume that the samples of $f(t)$, $x(n)$, are equal to the scaling function coefficients $c_{J_1}(n)$. This is the way it is done in the new (Apr./May –96) Matlab wavelet toolbox from *The MathWorks Inc.* There the sampled signal $x(n)$ is directly run through the FB. They also assume that the sampling frequency is 1 Hz! Therefore one must, when using this toolbox, rescale the time and scale axes to achieve the exact transform.

Equation (3.72) states that analyzed signals $f(t)$ after being discretizied to $x(n)$ give the following relationship between scale and frequency:

$$2^{-J_1} = T_s \Rightarrow F_s = 2^{J_1}, \tag{3.73}$$

where T_s is the sampling period and F_s is the sampling frequency of $x(n)$. Now $x(n)$ must be multiplied by the factor

$$\sqrt{2^{-J_1}} = \frac{1}{\sqrt{F_s}}, \tag{3.74}$$

before any analyzing in the filter bank. The output of the lowermost branch according to Figure 3.12 is now denoted d_{J_1-1}. At this branch the scale is

$$a_{\min} = 2^{-(J_1-1)} = \frac{2}{F_s}. \tag{3.75}$$

Now a will increase in dyadic intervals, when j is decreased. The uppermost branch is denoted with the index $j = J_0$, according to Equation (3.27). For a three stage filter bank, the grid is placed according to the j and k axes as shown in Figure 3.17.

17. K–vanishing moments: All the k'th moments, from k=0 to k=K–1, of the wavelet function is zero.

18. K–regular: H(z) has K zeros for z = –1.

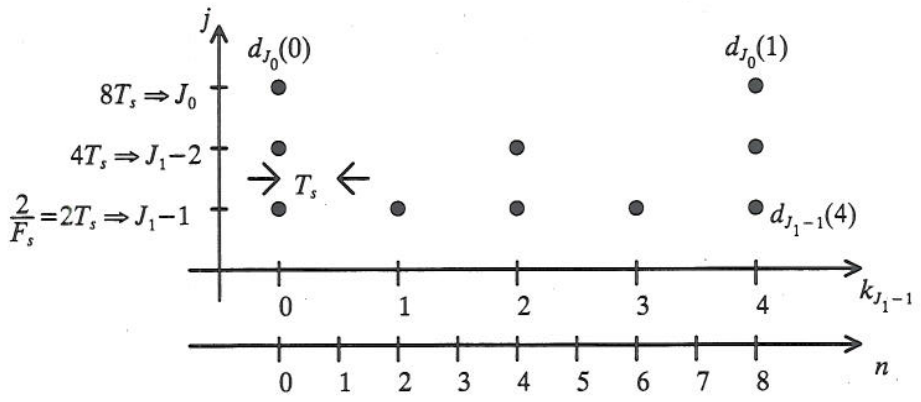

Figure 3.17 Relationship between sampling frequency and grid pattern for the DWT

The space between the indexes k_{J_1-1} will change when j is changed. This means that the k_{J_1-1} axis just is valid for the d_{J_1-1} coefficients.

4 TRANSIENT DETECTION

This chapter will consist of two main topics. First, methods for making the wavelet transform translation invariant, and second, making use of these methods for transient detection. However, before this, a short comparison between the wavelet transform and correlation is made. After introducing methods to avoid shift variance, there will be a brief discussion on detector performance before the detectors are presented.

4.1 Correlation compared to the Wavelet Transform

As stated in the previous chapter, the wavelet transform of a signal (or function) is defined as

$$WT(a,b) = \frac{1}{\sqrt{a}} \int_{-\infty}^{\infty} \psi^*\left(\frac{t-b}{a}\right) f(t)dt. \tag{4.1}$$

If we compare this equation with the equation for the correlation coefficient between two signals (continuous time (18)),

$$\rho_{\sigma_\psi \sigma_f}(\tau) = \frac{1}{\sigma_\psi \sigma_f T} \int_0^T \psi(t+\tau) f(t)dt - \bar{f}\bar{\psi}, \tag{4.2}$$

we note that there are only small differences. $\bar{\psi}$ and $\bar{f}$ are mean values, σ_ψ and σ_f are standard deviation and T is the observation window. Since the mean of ψ is zero (according to Equation (3.61)), we can remove $\bar{\psi}\bar{f}$.

If the analyzing wavelet has a large correlation coefficient with the reference signal we want to localize, a pure wavelet detector that will perform the detection with similar performance as techniques based on matched filters. However, with a wavelet technique we can obtain a detector which requires less computation time. Of course there are not many cases where this is an option.

As an example of correlation between a signal and wavelet, we design the synthetic transient

$$s(t,\omega,\lambda,A) = A\begin{cases} e^{-\lambda\left(t-\frac{T}{4}\right)}cos(\omega t)\,, t \geq 0 \\ \dfrac{cos(2\omega t)+1}{2} \quad , -\dfrac{T}{4} \leq t < 0 \end{cases}, \tag{4.3}$$

where ω is the oscillation frequency ($T = 2\pi/\omega$), λ the damping coefficient, and A the maximum amplitude. In Figure 4.1 a version of this transient is plotted as the smooth curve. Now, assume that ψ has compact support on the interval $[t_1, t_2]$. Then it is possible to rewrite Equation (4.2). Introducing a for scaling and energy conservation, we get

$$\rho(a,b) = \sqrt{a}\int_{t_1}^{t_2} \psi(t)\, f(at+b)dt.$$

In practice the two functions ψ and f are discretized on the interval $[t_1, t_2]$. Therefore we generated a vector with length of *768* for each function[19]. Then we compute the correlation coefficient between these two vectors for every a and b in Matlab. The correlation is not dependent on any factors multiplied by the functions, it is only dependent on the relative shape between the functions. Figure 4.1 shows the basis function ψ with the transient that gives the highest correlation ($\rho_{\max} = 0.9405$). The damping coefficient λ is optimized ($\lambda_{opt} = 1.179$), and $a = 1.205$ and $b = -1.175$ (T = 1.5). Among the wavelets in appendix A, db2 is the wavelet that gives the highest correlation.

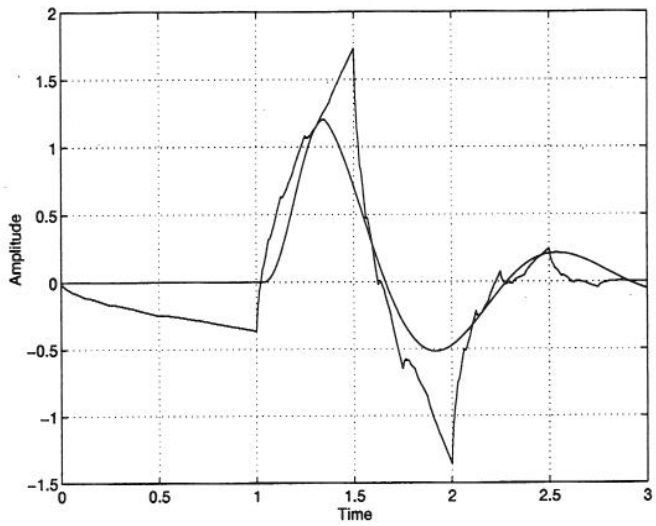

Figure 4.1 The transient (smooth curve) and db2 wavelet at maximum correlation

This example shows that there can be a very high correlation between a wavelet and a transient. This is one of the reason why it is interesting to use WT for transient detection.

4.2 Translation Invariant Transform (TI)

As discussed in Section 3.5, we may want another sampling grid of the WT than the dyadic one. No matter how we choose this grid, there is a substantial risk for the representation to be translation (shift) variant. As we know, two different signals will have different wavelet representations. Even if these two signals just differ by a time shift, we may risk that the concentration, waveform, or other properties of the coefficients is quite different. To avoid this we want the representation to be translation invariant.

4.2.1 Method 1: Cost function dependent algorithm

Two cost function dependent algorithms to avoid shift variance have been proposed, one by Mallat *et. al.*, and one by Beylkin (19). In (19), an extended version of the last

19. Vector length, resulting from the WAVEFUN command in Matlab with 256 iterations of Equation (3.65).

one is described. Below, this one will be explained in detail. Mallat's proposal to solve this problem will be quoted directly from (19):

"They first calculate the decomposition of the wavelet basis functions at each scale without down–sampling. This procedure retains all the samples output by the highpass filters (eliminates the rate–change operators in the filter bank); then, at every scale, only those coefficients that are local extrema are retained. An iterative reconstruction algorithm was proposed to recover the signal from the local extrema representation of its wavelet transform".

In the following explanation, the theory is based on the presentation of the translation invariant transform in (19) and (20).

In general, this translation invariant transform consist of two main procedures. First, we compute the WT of all circular shifts of a N–length signal. For each single WT representation we compute the corresponding cost function, and then uses the representation that minimizes this function. Many different cost functions are useful, but the most frequently used function is the vector entropy[20]

$$\mu_e(\{x(n)\}) = -\sum_n \frac{|x(n)|}{\|\underline{x}\|_2}^2 \log_2 \frac{|x(n)|}{\|\underline{x}\|_2}^2, \tag{4.4}$$

where $\{x(n)\}$ is a discrete sequence, and $\|\underline{x}\|_2$ is the norm of the vector $\underline{x}$. Since μ_e is not additive ((20)) we use the additive cost function

$$C(\underline{x}) = -\sum_n |x(n)|^2 \log_2 |x(n)|^2, \tag{4.5}$$

instead. An additive cost function must satisfy the following properties:

$$C(\underline{0}) = 0 \ , \ C(\underline{x}) = \sum_n C(x(n)). \tag{4.6}$$

The "negative" energy measurement

$$\tilde{E}(\underline{x}) = -\sum_n x^2(n), \tag{4.7}$$

will also satisfy the properties in Equation (4.6). Hence, to reduce the computing complexity, this energy measure can also be chosen.

As we will see in the following, there is no need for computing the WT of all circular shifts of the N–length signal. In fact it is the degree of downsampling in one stage that decides how many WT we need to compute. For a 2–band wavelet structure we only need two WT computations. Then the best representation is passed on to the next stage (level) in the decomposition tree. As an example we will study the cost function for all circular shifts on each level of a 4–stage 2–band structure. This structure is similar to figure 3.12.

20. A measure of the concentration of the energy of the coefficients, (19).

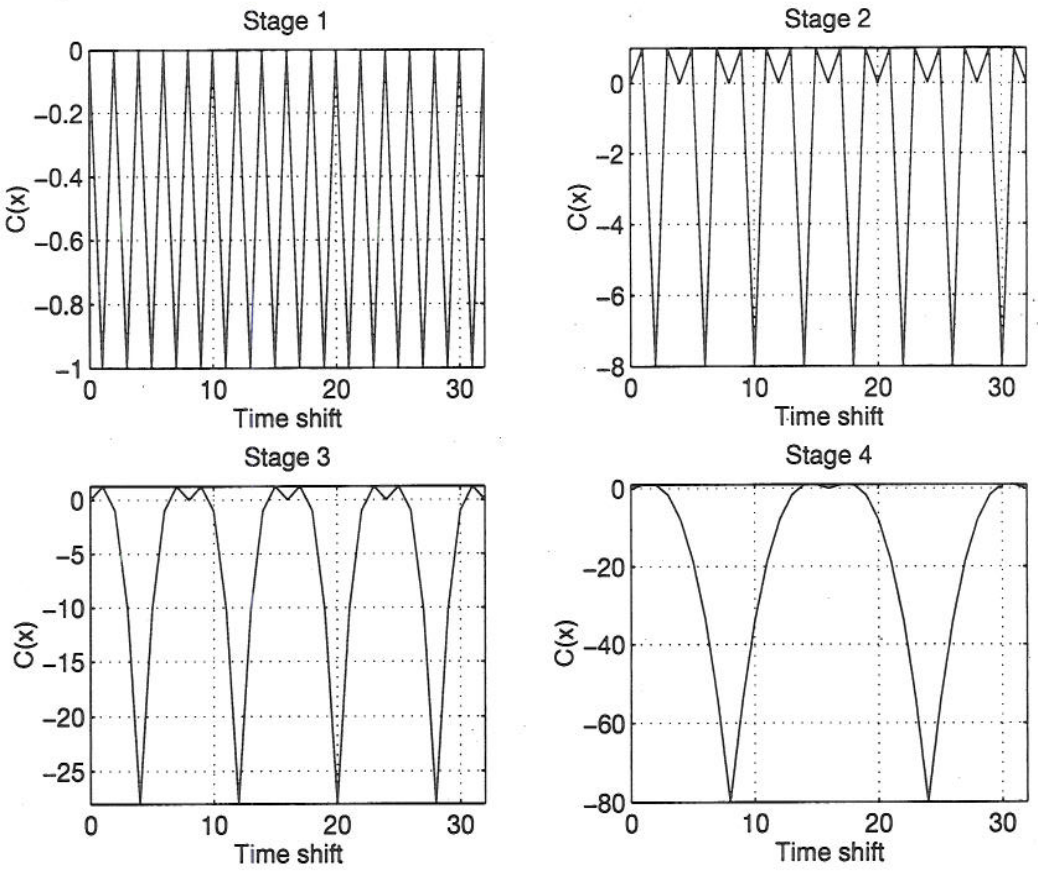

Figure 4.2 Cost function for all circular shifts of $\underline{x}$ on each stage

The $\underline{x}$ vector in this example has a length of *128*, and it is shaped like a Haar function. In the FB the Haar filters (the filters corresponding to the Haar wavelet) are used. We see that in the first stage the WT representation only need to be computed twice to obtain the minimum cost. The interesting with these plots for stage 2–4, is that their period is direct dependent of the downsample factor. When we are on stage S, the period of the cost function is 2^S. In general[21], the maximum number of shifts to be made in each stage, to find the minimum representation for the cost function, is equal to the downsample factor at that stage. So, for a single stage M–band structure it is necessary to compute M different WT.

When we are using this translation invariant transform, the algorithm is more complex. The complexity refer to the number of multiplications executed by the algorithm. A simple WT has complexity $\mathcal{O}(n)$, while the total complexity for this TI algorithm is $\mathcal{O}(n \log_2 n)$. Now an argument regarding computable complexity of the TI transform vs. the Fourier transform vanish. Even if this is not the most important argument for choosing wavelet analysis, it is a factor that must be taken into consideration when performing time–frequency analysis[22].
If the signal is oversampled, the variations between neighbor samples will decrease. Then a shift of the signal does not results in such a large difference in the wavelet representation. Clearly, with higher sample rate there is a stronger restriction on the number

21. Independent of the decomposition structure.

22. Remember that scale is the inverse of frequency.

of operations that can be implemented to achieve a real time system. If the upper boundary of the sample rate is substantially larger than the maximum frequency in the analyzed signal, there is no need for a translation invariant transform. However, in all cases there will be a trade off between the sampling frequency and the complexity of the implemented algorithms.

4.2.2 *Method 2: Downsampler ignoring algorithm*

In transient detection, and most likely in other applications using the wavelet transform, translation variance is an undesired effect. When analyzing a discrete signal, the sampling frequency is chosen in such a manner that there are only small changes from sample to sample. This result in minor changes in the wavelet transform if the signal is shifted one sample either way. Therefore, by sampling the CWT in horizontal direction, or in time, according to the sampling period, the representation is as translation invariant as possible. The purpose with this section is to make an algorithm that achieves this requirement. Now, assuming that the analyzed signal $x(n)$ is run through a filter bank realization. Then a grid pattern just like in Figure 3.5 occur. The space between two gridpoint at the lowest level is $2T_s$, where T_s is the sampling period of $x(n)$. Now, delaying the signal an arbitrary number of samples before running through the filter bank. First, let this delay be equal to T_s. In the first stage ($a_{\min}$) in the grid, all points will now be moved right between two old ones. The space between all these points (old and new) will now equals T_s, according to Figure 4.3.

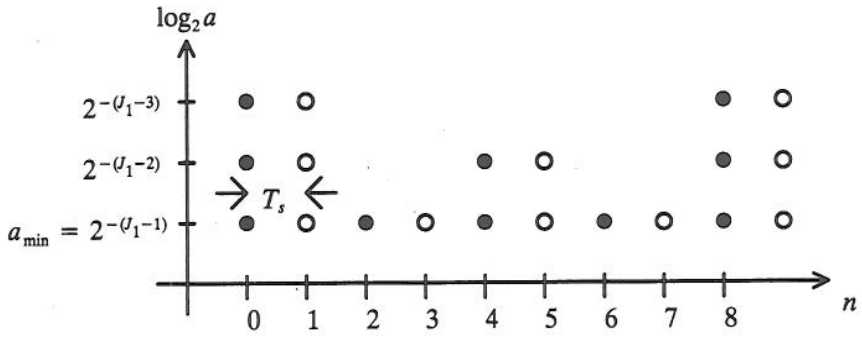

Figure 4.3 Original (black grid) and one shifted (white grid) version of the DWT

If we delay $x(n)$ one more T_s, the grid will be more complete in a homogenous sense in the horizontal direction. Now, after a certain number of delays, the grid will be complete. At this time we will not discuss the fact (or effect) that many of these new gridpoints coincide with old ones. To achieve a homogeneous grid, the structure in Figure 4.4 must be implemented.

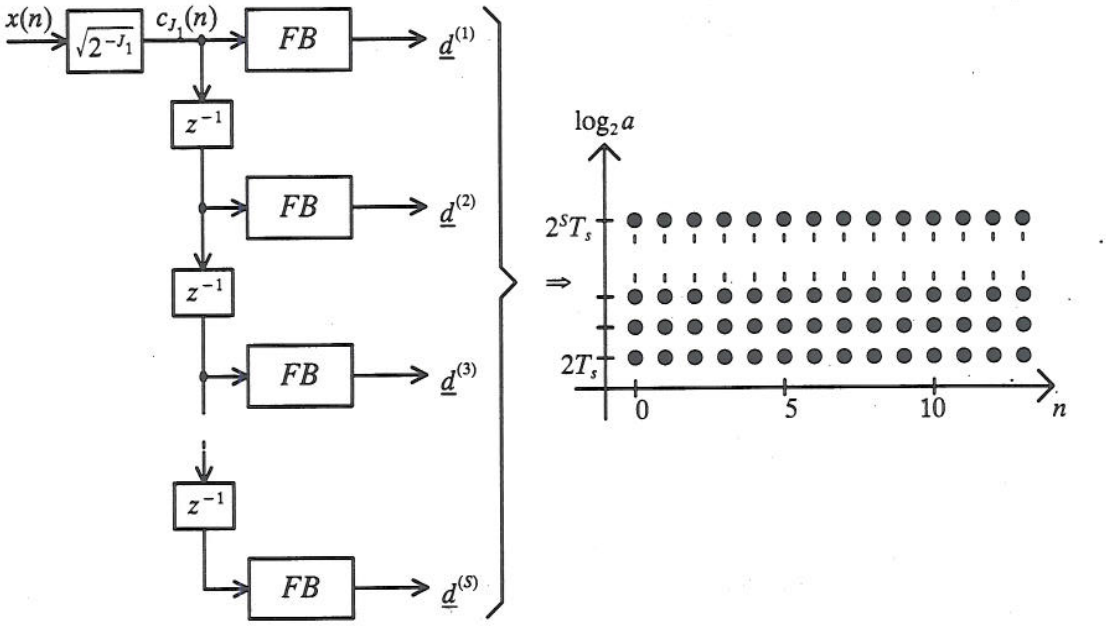

Figure 4.4 "Making" a homogeneous grid in time direction

If now this grid could be computed in an efficient way, a useful translation invariant representation for detection problems is developed. In the following one such "fast" algorithm will be derived.

As the Figure 3.12 try to illustrate, filter banks are structures with many branches that consist of one FIR filter followed by a downsampler. This means that on the way from $c_{J_1}(k)$ to $d_j(k)$, the signal must pass through a number of filters and downsamplers in cascade. The simplest case is for $j = J_1-1$, when we only have one filter and one downsampler.

By applying one of the Noble identities on each branch leading from $c_{J_1}(k)$ to the d_j coefficients, it is possible to move all downsamplers in each branch to the right in the structure. All filters will then be gathered at the left. This interchange of a filter with a downsampler results in a new filter according to the first Noble identity.

Figure 4.5 The first Noble identity

As a result of this, each filter bank will now have a new structure, shown i Figure 4.6. Figure 11.3–6 in (21) shows this equivalent for a three level (or stage) filter bank structure. The filter $H_1(z)$ is the same as $h_1(n)$ in Figure 3.8.

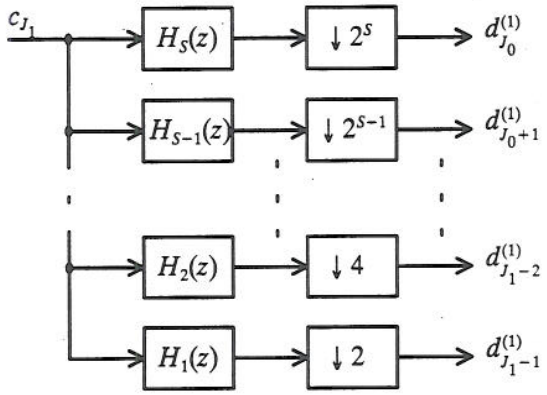

Figure 4.6 Filter bank realization after using the 1st Noble identity to gather the downsamplers to the right

For each of the filter banks in Figure 4.4, this structure will appear. Because all our filters are of the FIR type, they can be interchanged with a delay element without changing the system. Now, several identical (S to be exact) filters in parallel, with different structures on its outputs, can be put together and the ramification may be moved to after the filters. The result is illustrated in Figure 4.7.

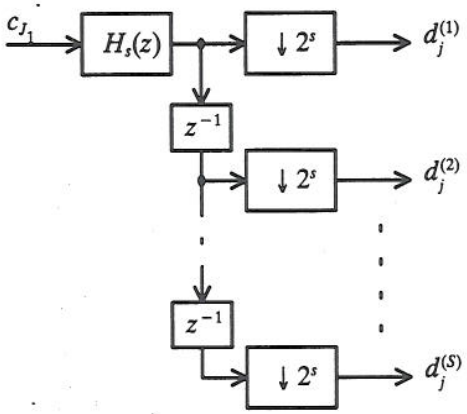

Figure 4.7 Structure after interchanging delays and filters, and moving the ramification point

Up to this point operations done on the structure has been mathematically correct. The next manipulation is not legal, but I will try to convince the reader with a proof that it is possible to do this to achieve the homogeneous grid.

For the branch according to $H_s(z)$ we upsample the first 2^s subbranches, with the same factor as for downsampling, and then sum the results. This is not perfectly legal because we have left out some subbranches, and also introduced upsampling that was not present at an earlier stage.

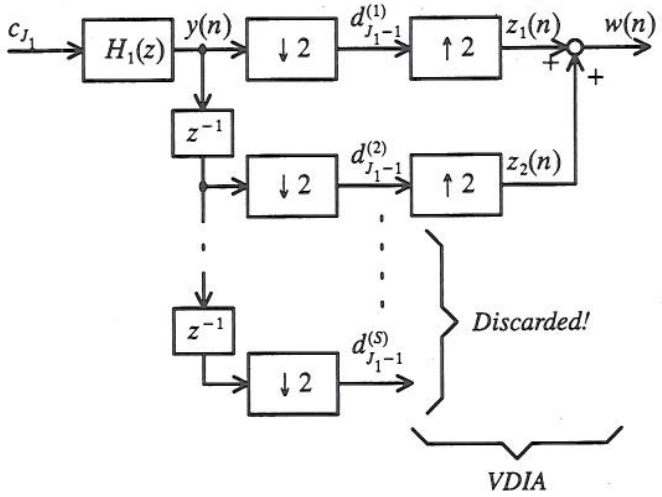

Figure 4.8 Example of Virtual Index Dependent Addition (VIDA) of subbranches. Shown for the 1st branch

Figure 4.8 shows this effect for the subbranches under $H_1(z)$. The upsamplers are just used to make the use of addition correct. Then it can be shown that the output $w(n)$ is equal to $y(n)$. The reason why the operation is named VIDA, is that we virtually add the $d^{(1)}_{J_1-1}$ vector with $d^{(2)}_{J_1-1}$ vector with respect to the index n. After downsampling, the index n can not be used on these to vectors if we follow the mathematical rules.

In Figure 4.9 the content of the vectors are shown. Note that the empty places for $d^{(i)}_{J_1-1}$ vectors are not defined. This is the reason why we use upsamplers.

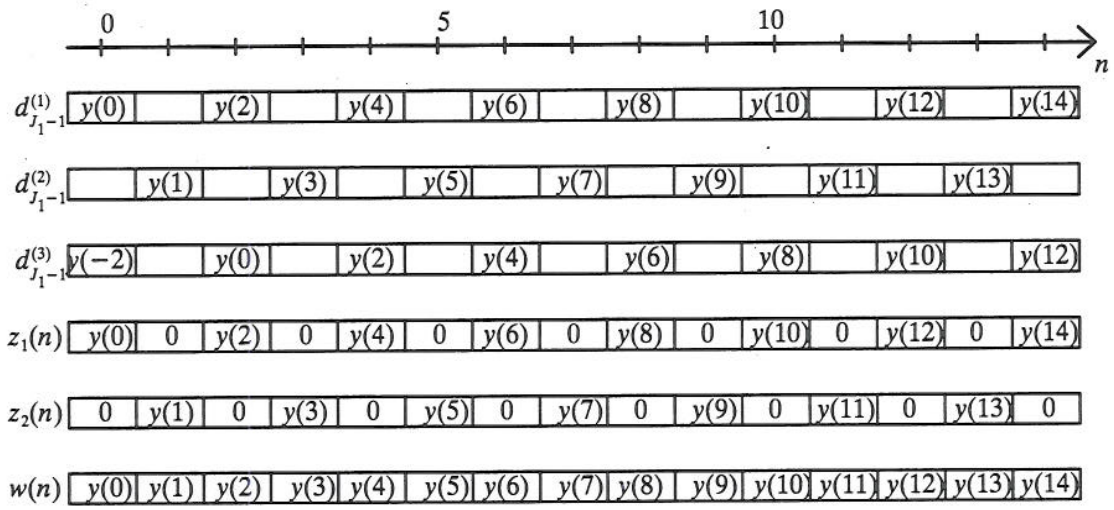

Figure 4.9 Vector contents shown relative to the index n

If this method is applied to the subbranches after every filter, the resulting structure will only consist of filters.

The outputs of this simplified structure will now produce a new sample out on each branch for each new sample in. This means that the grid in time direction is homogeneous.

Proof

To prove that this simplicity is valid, we shall compare the results of the CWT of a Dirac delta function to our system response to a Kronecker delta.

First we derive the wavelet transform of the Dirac delta function. To do this we use Equation (4.1). This gives

$$WT_{\delta}(a,b) = \frac{1}{\sqrt{a}}\int \psi^*\left(\frac{t-b}{a}\right)\delta(t)dt = \frac{1}{\sqrt{a}}\psi^*\left(-\frac{b}{a}\right). \tag{4.8}$$

This shows us that the CWT of a delta pulse is the complex conjugated to ψ flipped around the vertical axis. For a certain value of a, a scaled (and flipped) version of the wavelet (assuming that it is not complex) will appear.

If our new sampling grid is supposed to be right, it must return a sampled version of the previous CWT when a Kronecker delta is used as an input. In the time direction the sample interval is constant for an arbitrary value of a (or j). Since a decides the support of the CWT along b, this lead to the fact that for high values of a, the number of samples within the support increases. As a simple example we can study this effect on the Haar wavelet for a single value of a.

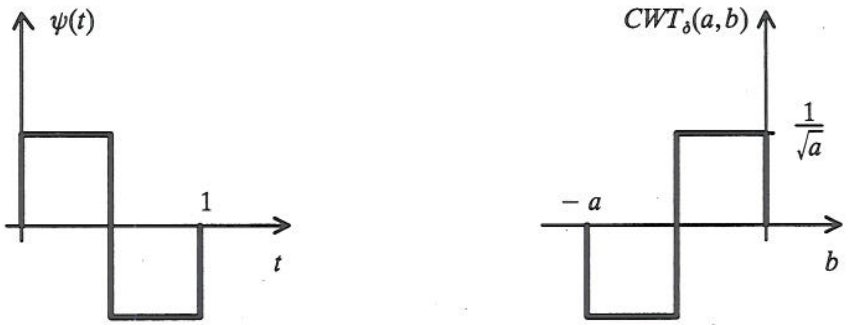

Figure 4.10 Haar mother wavelet (left) and the CWT of a delta pulse with respect to the Haar wavelet for a given a (right)

For simplicity we use F_s=1Hz which leads to $a_{\min}$=2 according to Equation (3.75). Now the $CWT_{\delta}(2,b)$ will have [–2, 0] as support. Since we now sample every second (T_s=1 sec), there are two samples that are different from zero. These values are $-1/\sqrt{2}$ for b=–2 and $1/\sqrt{2}$ for b=–1. The definition to the Haar mother wavelet is stated in the example in Section 3.1. By increasing j by one (gives a=4), we get four samples different form zero within the support. For a large number of j, the samples will construct the original shape of the analyzing wavelet.

If we take a look at the filter coefficients for all our filters, which are the same as the impulse response, they give the same results. For the filter $H_1(z)$ the coefficients is $\left\{-1/\sqrt{2}, 1/\sqrt{2}\right\}$. The filter coefficients according to the db2 wavelet (see Appendix A), for the four first stages is plotted are the figure below.

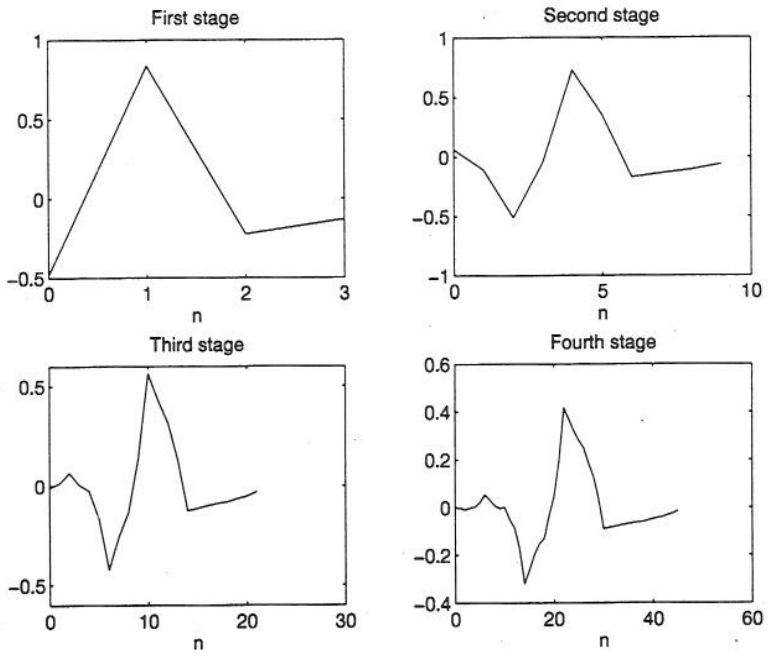

Figure 4.11 The first four stage impulse responses when using the db2 wavelet as basis

When comparing these plots to the original wavelet, there is no doubt about that our algorithm is correct. ■

At the end it is important to say that our filters are anti causal, which means that there will be no action on the outputs before something arrive on the input. By definition CWT is a causal operation on a signal, and therefore by comparing results from CWT and our algorithm, time localization will not be equal! Equality may be achieved by making all our filters causal.

A consequence of this algorithm is that the downsamplers may not be thrown away, but only by changing the factor, the grid in time direction may be constructed to achieve a desired pattern or resolution. This resolution does not need to be equal for different levels or stages. By inspecting each horizontal row separately, they will now have different degrees of redundancy. To get the right wavelet representation, the outputs from each branch must be divided by its respective redundancy factor. This factor is equal to the degree of overrepresentation in each branch. For the branch according to $H_1(z)$ the redundancy is 2, because we use twice as many representation points as needed to describe the analyzed signal when taking away the downsampler.

4.3 Detector Performance

The best WT based detector result will appear if the basis function ψ matches the transient exactly. Then we have a so–called matched filter (MF) detector. This detector performance depends on the degree of correlation between the basis function and the transient (20). Of course, normally the shape of the transient is unknown. Therefore, the resulting detector performance depends on the prior information we have about the transient signal (or about a typical transient). If we have absolutely no prior information, an

energy detector (ED) serves as a lower limit of acceptable performance. The MF detector serves as an upper limit for the performance (22). The performance is plotted as a ROC[23] curve. The ROC curves are normally produced through the so–called Monte–Carlo[24] simulations (20), with synthetic generated signals.

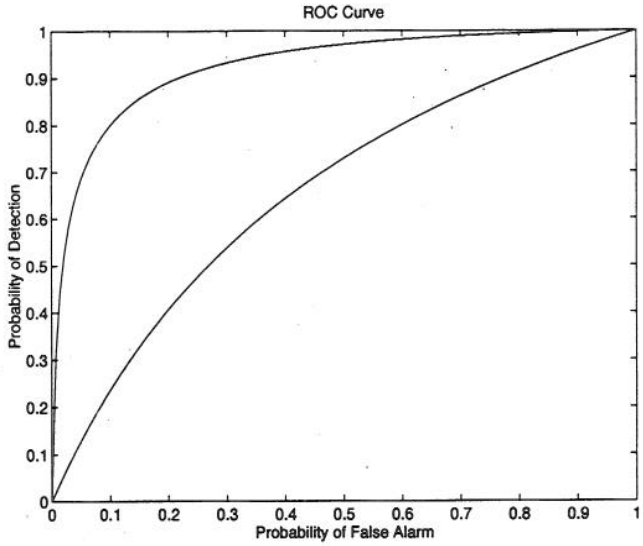

Figure 4.12 General ROC curve relationship between the MF (upper) and the ED (lower) detector

When trying to detect a transient it is, as discussed above, desirable to use a basis function that is as equal to a transient as possible. Of course, we can choose any basis function (with finite support) and get a wavelet representation of the signal. But it is only possible to reconstruct the signal if the basis function ψ satisfy the conditions introduced in Section 3.1. This representation will be highly redundant and not very efficient to compute. If we instead choose the basis function in such a way that ψ becomes a wavelet with properties so that a fast algorithm (i.e. FB computation) can be implemented, we can get a much more optimized efficiency. This is an important factor in real time systems.

4.4 The Detector

Now, two different transient detection algorithms will be presented. The first is detection on the basis of a signals wavelet representation. This method is used in some of the references, and good results are achieved. As a translation invariant algorithm, method 1 described earlier is exclusively used. The second detector is based on the matched filter (MF) algorithm. Now the wavelet transform (WT) is an important part of the algorithm. No literature is found on this detector, and the presented connection between the MF technique and the WT is a result of the authors own deep study of this problem. Method 2 for achieving shift invariant representation is also a product of this study.

23. Reciver Operating Characteristics: Probability of detection vs. probability of false alarm.

24. Observation of a systems behavior in action instead of analyzing a mathematical model of the system (52).

4.4.1 *Detection using the wavelet transform directly*

For detection purposes in signals we must first decide if the waveform to be detected is contained in the signal. This decision problem can be stated as the hypothesis[25]

$$\begin{aligned} \mathcal{H}_0: &\quad x(t) = n(t) \\ \mathcal{H}_1: &\quad x(t) = A \cdot s\left(\frac{t-\tau_0}{a_0}\right) + n(t) \end{aligned}, \tag{4.9}$$

where the waveform $s(t)$ is typically known[26], and $n(t)$ is Gaussian noise. The parameters A, τ_0 and a_0 are unknown.
If we are searching for some specific waveforms, then several pairs of A, τ_0 and a_0 are known. Then the optimal detector is based on correlation between $x(t)$ and $s\left((t-\tau_0)/a_0\right)$. A detector may now be defined as

$$\max_{a,\tau} \int_{-T/2}^{T/2} x(t) s^*\left(\frac{t-\tau}{a}\right) dt \underset{\mathcal{H}_0}{\overset{\mathcal{H}_1}{\gtrless}} \xi(A), \tag{4.10}$$

where ξ is a threshold that is pre–determined and T is the observation interval. Equation (4.10) states that the received signal $x(t)$ passes through an infinite number of matched filters, and the filter with the maximum output is chosen. This maximum is compared to the threshold ξ, and a decision with respect to the hypothesis is made. The search for the maximum is actually performed on the two dimensional plane (a, τ). Further details on this detection theory can be found in (25).

The similarity of Equations (4.1) and (4.10) indicates strong connection between the wavelet transform and correlation, as discussed in detail in Section 4.1. We can now redefine Equation (4.10) so that the wavelet transform can be used instead.

$$\max_{a,b} WT(a,b) \underset{\mathcal{H}_0}{\overset{\mathcal{H}_1}{\gtrless}} \xi\left(\sqrt{a}\,A\right), \tag{4.11}$$

where $\psi(t) = s(t)$ and $f(t) = x(t)$ according to Equation (4.1). In Figure 4.13 the block diagram for Equation (4.11) is illustrated.

25. This is proposed in (22)–(25).

26. This knowlegde gives the detector performance as discussed in Section 4.3.

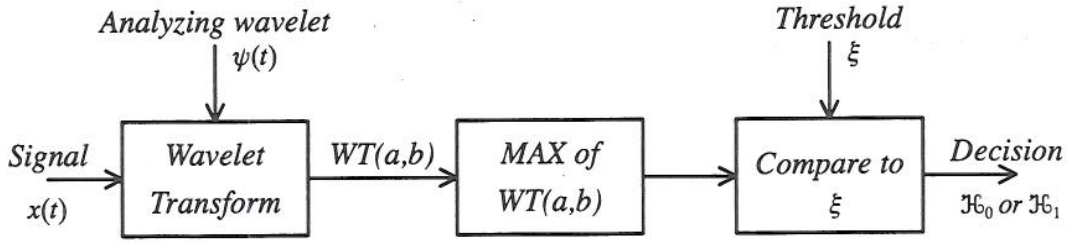

Figure 4.13 Block diagram of a WT based detector

Now there are two things that must be determined before we can start to use the detector, namely the threshold ξ and the wavelet function ψ. The ψ is easiest to determine, because we want as large correlation as possible between the wavelet and the waveform that we are searching for. After this choice, the threshold ξ must be appointed. The size of this depend on the information we want to extract from the analyzed signal. The signal to noise ratio (SNR) is an important factor in relation to the credibility of the extracted information.

As probably noted, the wavelet transform above is the continuous one. In the previous chapter we introduced the discrete wavelet transform DWT. There we showed that this transform can be realized as a filter bank to get a fast algorithm to compute the representation coefficients. Instead of using the continuous transform as in Equation (4.11), we use the discrete transform to get

$$\max_{j,k} DWT(j,k) \underset{\mathcal{H}_0}{\overset{\mathcal{H}_1}{\gtrless}} \xi\left(\sqrt{a}\,A\right). \tag{4.12}$$

The key assumption in the derivation of Equation (4.11), and then (4.12), is the *a priori* knowledge of the waveshape to typical transients in the analyzed signal (22). As mentioned before, in Section 4.3, the relative difference between a transient and the wavelet is an important factor for the detector performance.

It is possible to use several versions, i.e. Section 3.5, of the wavelet transform for transient detection. In (20) there is used the four following versions for detection purposes:

- Ordinary 2–band WT, i.e. Figure 3.12.
- Full 2–band WP, i.e. Figure 3.13.
- 2–band TI transform introduced in Section 4.2.
- M–band TI (MTI) transform, i.e. Figure 3.16 (*M=4*).

As an analyzing wavelet, the db2 basis was chosen[27]. For the MTI case an extended version of the db2, corresponding to *M=4*, was used. Then it is shown that the energy distribution in the time–scale plane is more concentrated as we go down the given list.

27. Also denoted D4 in the litterature because the corresponding filters have order four.

The conclusion with respect to the detector performance, measured[28] by the ROC curve, is that highest energy concentration results in the best detector. With other words, the detector performance ranking is given by reversing the list, although the TI and MTI have, in this case, almost equal performance.

4.4.2 *MF detector making use of the wavelet transform*

As discussed in Section 4.3 about detector performance, the best detector for finding known signal shapes in analyzed signals is the matched filter (MF) technique. This technique is based on correlation (26), and the output from this algorithm is

$$y(t+T) = \int_0^T s(\tau)x(t+\tau)d\tau, \tag{4.13}$$

where T is the length of the known wave shape $s(t)$ and $x(t)$ is the analyzed signal. The input signal is normally noisy, and for white Gaussian noise the MF algorithm is optimal for detection purposes. To derive the algorithm using WT, another notation will now be used. This notation is based on *bra* and *ket* vectors found in (27) and (28) and first used in Equation (3.2). Now the output from the MF is expressed

$$y(t+T) = \langle s, x \rangle. \tag{4.14}$$

By introducing the identity operator

$$I = \sum_{j,k} |\psi^*_{j,k}\rangle\langle\psi^*_{j,k}| = 1, \tag{4.15}$$

Equation (4.14) can be written as

$$\langle s, x \rangle = \langle s | \left[\sum_{j,k} |\psi^*_{j,k}\rangle\langle\psi^*_{j,k}| \right] | x \rangle = \sum_{j,k} \langle s, \psi^*_{j,k}\rangle\langle\psi^*_{j,k}, x\rangle, \tag{4.16}$$

where the $\psi^*_{j,k}$ functions span L^2. When inspecting Equation (4.16) we clearly see that the two inner products $\langle s, \psi^*_{j,k}\rangle$ and $\langle \psi^*_{j,k}, x\rangle$ are the discrete wavelet transforms of $s(t)$ and $x(t)$, respectively. A requirement for achieving this result, is that the $\psi^*_{j,k}$'s are orthonormal. The wavelet transform of $s(t)$ is constant since it is a known signal shape. The transform of $x(t)$ will be updated for every new sample $x(n)$.

Now, let the WT of $s(t)$ be a matrix $\tilde{S}$ with length according to the observation window T, and height according to the numbers of stages in the filter bank. To avoid any distortion, the size of $\tilde{S}$ must be chosen so that it contain all non zero wavelet coefficients. Let the wavelet representation matrix of $x(t)$, $\tilde{X}$ be of same size as $\tilde{S}$. For each new sam-

28. Obtained by 2 Monte–Carlo simulations each of *2000* tests with SNR = –7 dB.

ple[29], the content in $\tilde{X}$ will be shifted one place to the left, and the rightmost column obtain the new wavelet coefficients. These two matrices are multiplied element by element, and all these products are added together. This sum is the output of our algorithm at a given time. The output must now be compared to a pre–determined threshold ξ, and then a decision about the presence of any wave shape is made. Figure 4.14 tries to illustrate this.

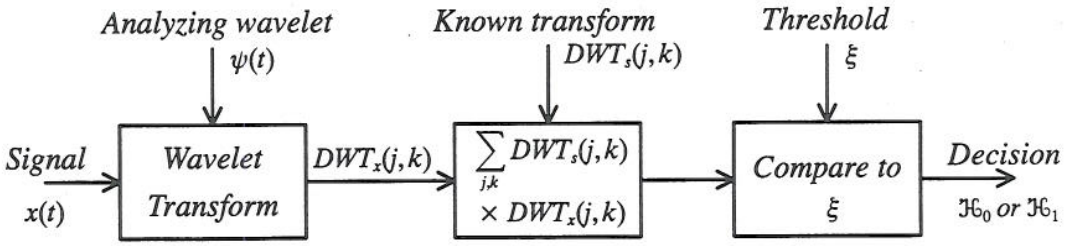

Figure 4.14 Block diagram of the WT based MF detector

When using the detector presented above, there are some important considerations that must be taken. The block diagram in Figure 4.14 is just true for a dyadic division of the time–scale plane, so when using the method 2 translation invariant algorithm, one must take into consideration the different redundancy in each stage. If not using the TI algorithm, the $\tilde{X}$ matrix will only be updated when all the stages have produced at least one new output. By doing this one can decide how often, and how accurate, the time localization of an arrived signal will be. In this text this option will not be further discussed.

Example

To show that this detector is a real MF detector, we shall compare its performance with the correlation version in Equation (4.13). First we generate a synthetic transient $s(t)$ using Equation (4.3) with oscillation frequency π and damping coefficient 1. Observation length is 9 seconds. Then $x(t)$ is made with one identical transient starting after 15 seconds. When the sampling frequency is 16 Hz, it means that after 240 samples we will have a match. For the WT based detector the number of stages in the filter bank is 10.

29. Assuming that method 2 for translation invariant representation is used. If not, this procedure is executed every time a new sample is available at the output of the branch containing the coarsest information. In other words, the branch that has slowest rate for updating.

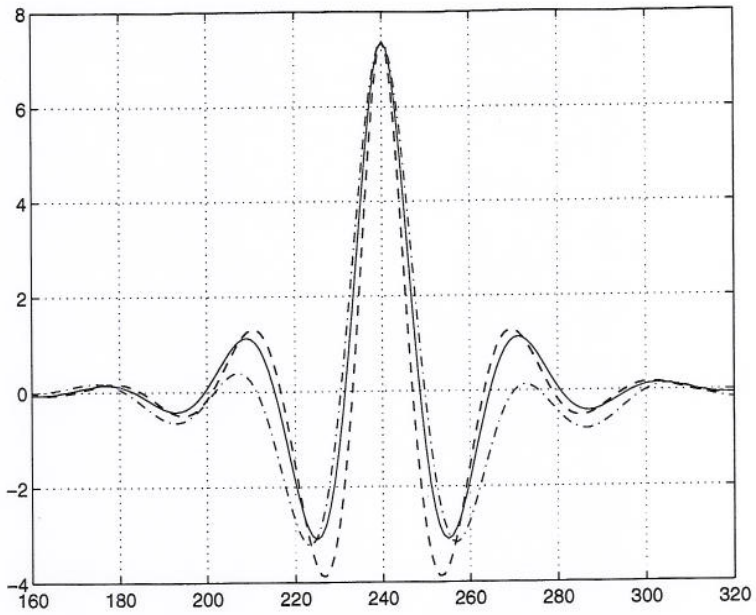

Figure 4.15 Comparison of detector quality of the correlator based MF (green) and WT based MF with correction for redundancy (blue) and without correction for redundancy (red). The amplitude for the WT based curves are manipulated to make the comparison better

By looking at the time localization, all three curves give the desired result. The correlator based detector has the desired shape that the two other ones also are supposed to have. Deviation from the ideal curve may be caused by many factors. In this example the absence of the redundancy factors give the largest distortion. The observation window will also cause a slight distortion. ■

If the analyzed signal contain many uncorrelated events at different scales (or frequencies), an individual search may give more efficient algorithms. This means that the wavelet representation grid can be different for each located event.

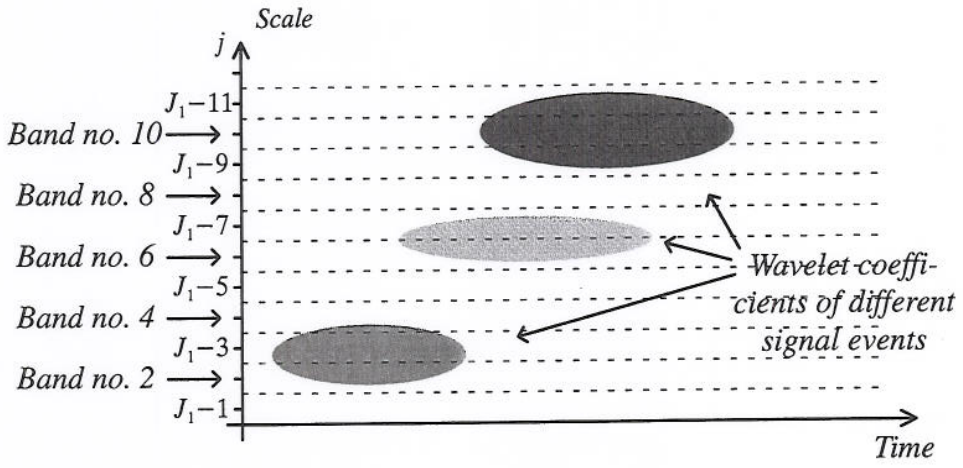

Figure 4.16 Schematic representation of wavelet transforms of three different events. The shaded areas represent the relative distribution of wavelet coefficients

By applying this technique to Figure 4.16, the lowest located event need only the four first band for detection. The middle event need 3–4 bands to be located. Since this event

have lower frequency components, distance between grid points can be increased. The third and last event need only band 9–11 to be found, and distance between grid points can be increased more. This method is used in the next chapter, where no interesting information is contained in the first four bands.

In the next chapter some experiments on real data are made. There the goodness of the WT based MF detector will be tested on noisy signals.

4.5 Transient Characterization

Until now our only concern has been detection of transients. The characteristics of a transient is also important information in structure monitoring. When the oscillation or damping coefficient of transients change, it may be as a result of a damage in the hull. Then changes in typical characteristics of the transients can be sufficient for a warning.

When a transient is detected, the information provided by the similar or equality factor can be enough to make estimations of ω and λ. If the SNR is to small (to much noise), the detector output can be distorted so much that it is not possible to use it for characterization of transients. Then a reconstruction of signals must be used along with some algorithms for removing the noise. After removing the noise, the signal segments containing transients can be analyzed once more, or analyzed using special algorithms for characterization directly. A combination of these two methods will probably give an optimal estimation.

In this text just a brief discussion on this topic will be held. This discussion will be superficial, and just an simple algorithm using the similarity curve is presented.

Assume now that $x(n)$ is sliding along $s(n)$. When a maximum value is returned from our detection algorithm, there is a match. For transients with a phase shift of $1/2$ period of the oscillation frequency, a minimum will occur. Now measure the time between maximum and minimum. This time will normally be equal to half the period of the unknown transient. The accuracy of this measure may be distorted by noise. If the transient have no damping at all, the maximum and proceeding minimum amplitudes will have same absolute value. A change in this amplitude can be a measure of how big damping coefficient any transient have.

Of course this algorithm alone, especially in noisy environment, is not sufficient for a good estimation of ω and λ. Together with other more specialized algorithms, this method for characterization of transients is powerful. In this thesis any study on this subject is left out because of other theoretical topics are prioritized.

5 EXPERIMENTS AND APPLIED THEORY

5.1 Short wavelet analysis on some real data

In this chapter we will apply the wavelet theory on some real data. These data are provided to us by Det Norske Veritas AS (DNV), and are measurements from a test vessel, named "Njord", made by Kværner Mandal AS.

5.1.1 Origin of the data

The data come from test measurements done on a test vessel made by Kværner Mandal AS, and the measurements were carried out by DNV (29). The test took place during the first half of 1993 on the coast of Mandal, and our provided data is recorded on the 3rd of June. Each signal has duration of approximately 3 minutes.

The boat is a high–speed vessel of surface effect ship (SES) or air cushion catamaran type. The test vessel was built in scale 1:3.2, with single skin construction. The use of materials was asymmetric, meaning that one side is constructed with glass fibre reinforced polyester matrix and the other side with glass/Kevlar™ [30] hybrid reinforced polyester matrix.

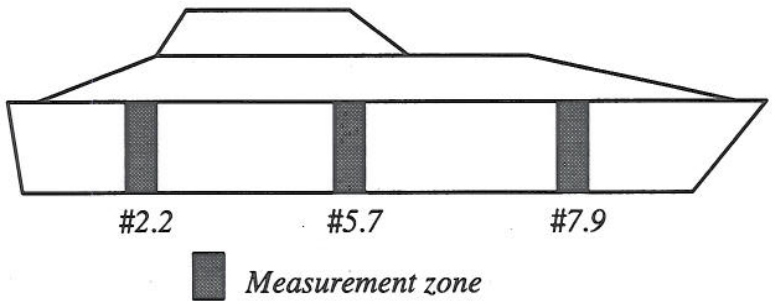

Figure 5.1 Measurement zones (frame no.) on the vessel. Source: (29)

Almost all sensors are located in one of the measurement zones indicated in Figure 5.1, and the location list of sensors is as follows:

- Global vertical acceleration at the longitudinal center of gravity (LCG).
- Global strain on the midship transverse frame.
- Strain on longitudinals (aft, midship and bow).
- Local strain on the wet deck panels (aft, midship and bow).
- Local strain on side hull inner/outer panels (aft, midship and bow).

For strain measurement, strain gauges from TML[31] was used, and an accelerometer[32] for measurement of the acceleration. A total of 61 strain gauges were mounted inside

30. Kevlar is a trademark of Du Pont's high strength para–aramid fiber.

the hull during construction. Figure 5.2 shows a crossection of the hull and the location of some of the strain gauges.

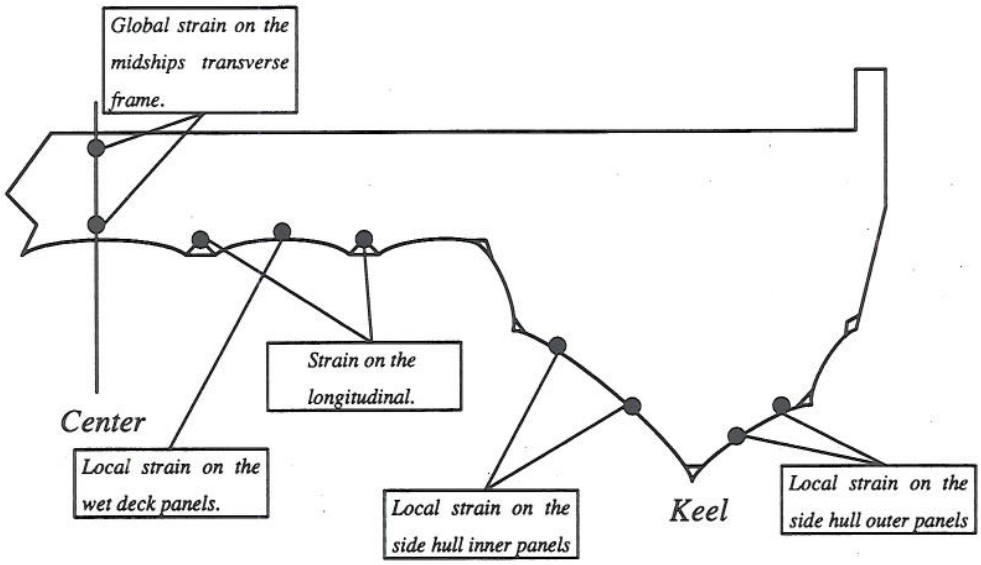

Figure 5.2 Crossection of the hull, location of strain gauges. Source: (29)

For each sequence of measurements, the signal from 16 sensors were amplified and stored on a DAT–tape with the tape recorder RD–200T from TEAC. The sensor number is the same as the channel number, which appears in the text. Figure 5.3 shows the signal flow on the vessel during testing. No analyzing of the data was performed on board. The tape recorder stored the signals with a bandwidth of 2.5 kHz.

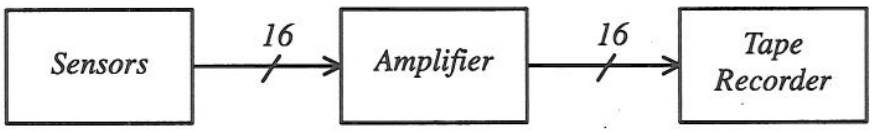

Figure 5.3 Data acquisition system on board

We used a personal computer (PC) with a 16 bit analog to digital converter board to digitize and transfer the data to a harddisk. The analog outputs from the tape recorder, were digitized with sample rate 6 kHz before storage. Figure 5.4 illustrates this.

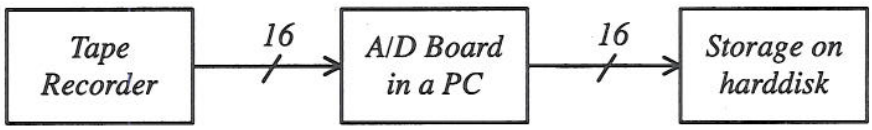

Figure 5.4 Our data processing

The duration of the signals from the 16 channels were approximately 3 minutes and 20 seconds. This corresponds to 1.2 Mill. samples pr. channel, 9.6 Mb pr file, representing each channel. We had three sequences of data recordings, which all together resulted in over 450 Mb of data!

31. Type: GFLA–6–70.

32. M1000 from Micro Movement.

Because of the short time available for analyzing the provided data, only a few examples of data manipulation using wavelets are presented.

5.1.2 *Wavelet filtering*

Since a large amount of data has been provided, it is a very time consuming job to look for typical transients by hand. Therefore only one of the most characteristic transients will be used in the experiment with transient detection in this work. In this section we study the selected transient, and subtract noise by wavelet filtering, and in the next section we will demonstrate transient detection.

Figure 5.5 shows the transient that was chosen as a typical transient in the experiments. We can not claim that it is typical for the entire data set, since a visual search through the whole set was too time consuming. However, we see that the chosen transient has the properties that are characteristic for transients.

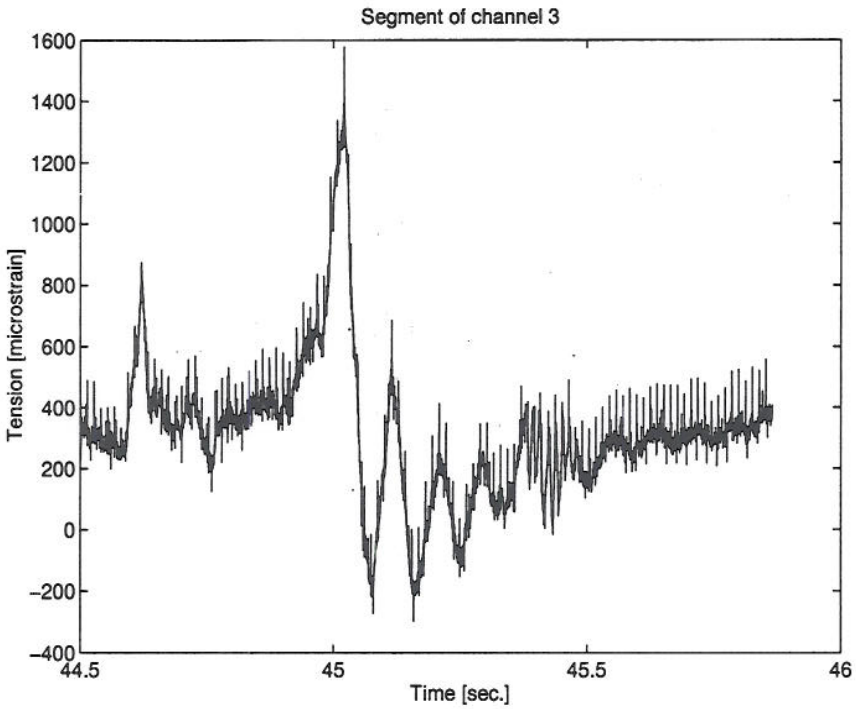

Figure 5.5 A segment of one of the channels

This recording is corrupted by a great deal of unwanted noise as shown in Figure 5.5. Now we will try to use the filter bank to reduce this noise. First we must try to find out in which band (or stage) the different elements in the signal are located. This is done by making a full decomposition of the signal and then generating a series of reconstructions where a single band is ignored at a time. By inspecting the reconstructed versions of the signal, an investigation of the effect each band has on the signal is performed.

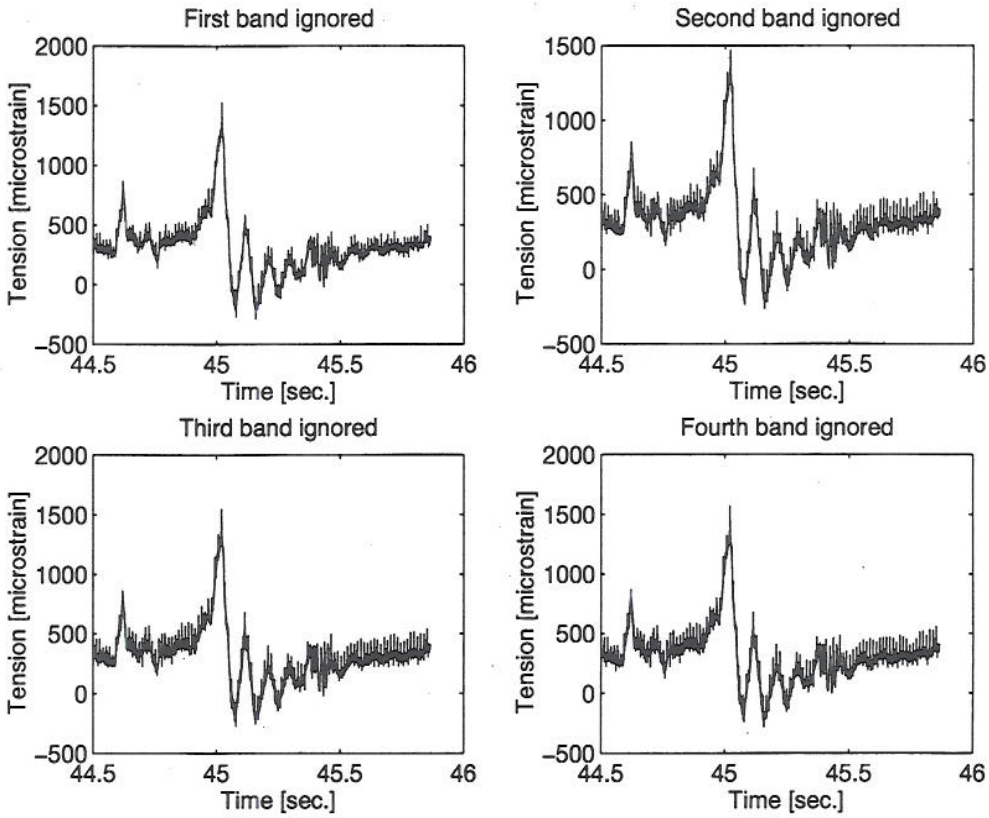

Figure 5.6 The effect of the first to fourth stage on the signal

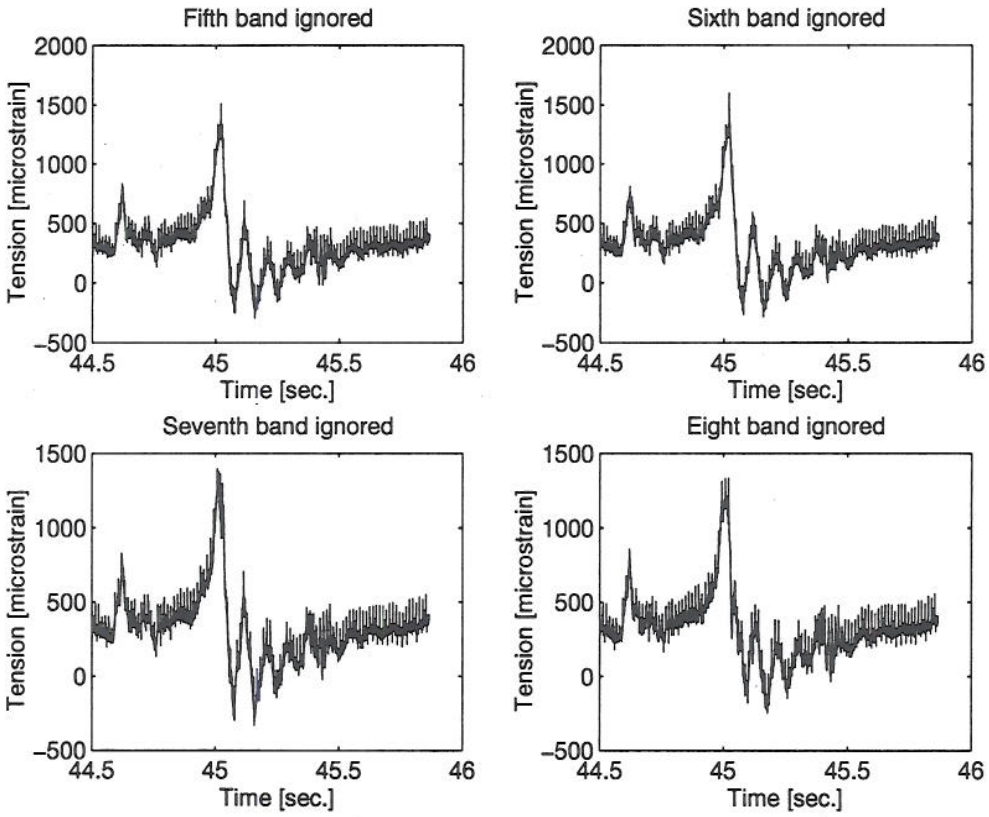

Figure 5.7 The effect of the fifth to eight stage on the signal

As shown in the figures, the first band contains most of the noise. Even if this noise has a period of approximately 80 Hz, most of it is removed by ignoring the first band. This

is probably because impulses have a very large bandwidth. The wave shape is not much distorted by removal of either of the first five bands. For the sixth band there is some distortion of the frequency component just below 45.5 seconds. For bands higher than this, the distortion is becoming more significant.

From these results we can draw the conclusion that is should be possible to remove the first 4–5 bands without significant loss of information. To show this we have removed the bands one by one from the first to the eight band in Figures 5.8 and 5.9.

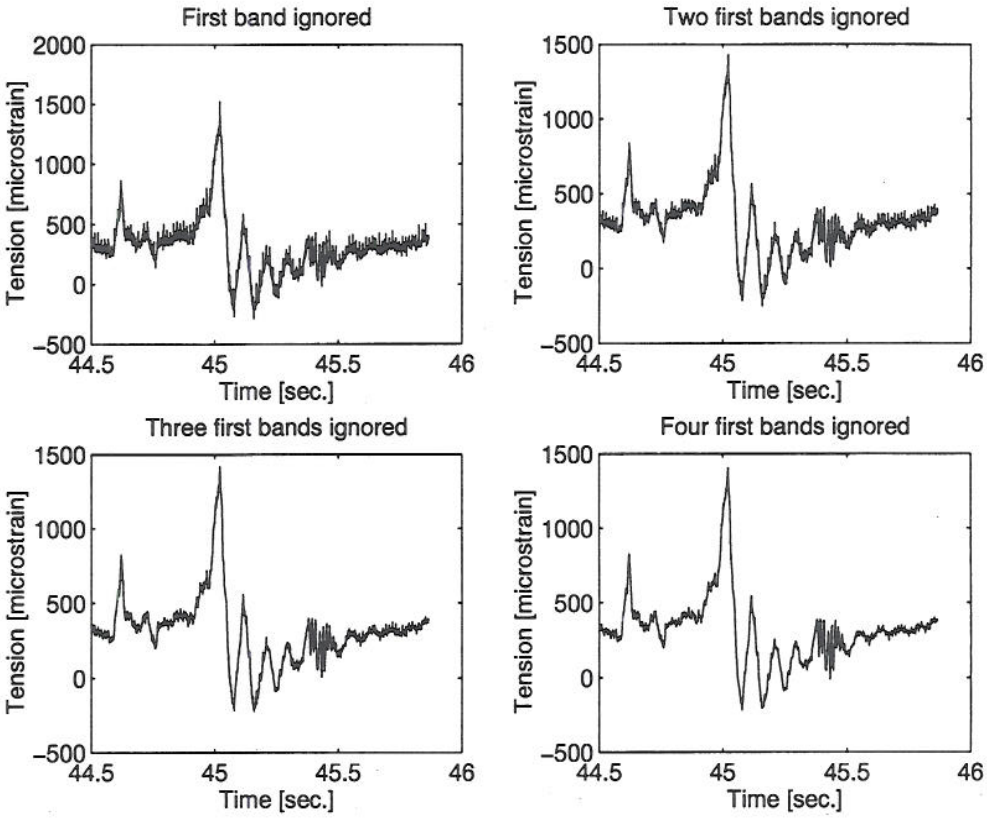

Figure 5.8 Signal after reconstruction when the first to the four first bands are removed

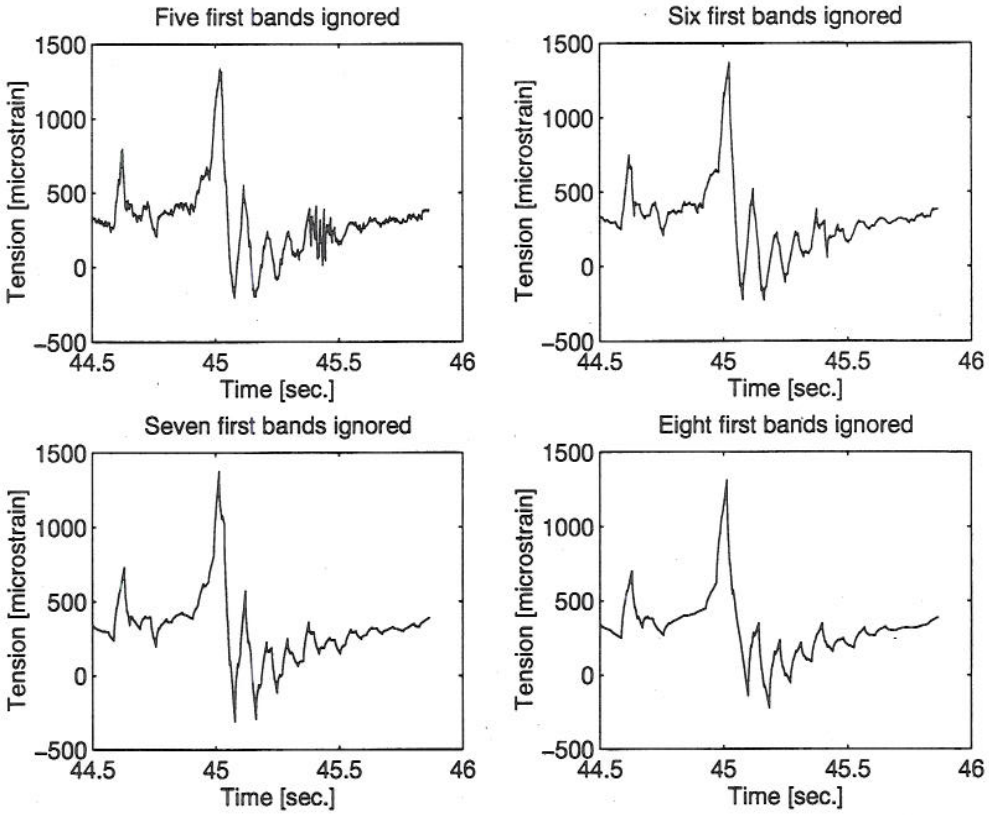

Figure 5.9 Signal after reconstruction when the five first to the eight first bands are removed

As stated no significant information is lost when the first five bands are canceled. Beyond those, the distortion is beginning to have an effect. With this knowledge, we filter away the first four bands before further analysis.

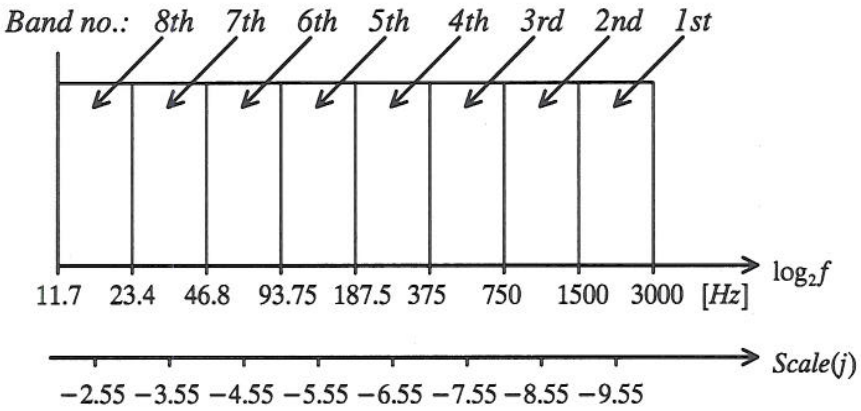

Figure 5.10 Frequency bounds for the first eight bands with their corresponding scale values

From Figure 5.10 we see that by removing the first four bands, frequencies higher than 190 Hz are filtered away. The main transient carrier in this segment of the signal has, by inspection, a frequency of approximately 12 Hz. By inspecting Figure 5.11 and 5.12, one will see that the scale parameter j not are an integer. Some values for j are shown in Figure 5.10. The reason why j not is an integer as assumed during the derivation of the multiresolution theory, is that we have a connection between J_1 and our sampling fre-

quency according to Equation (3.73). For practical use this is not a problem. The parameter j will only be an integer if the logarithm with base two of the sampling frequency is an integer. The only reason for using j at all is that the sampled signal should be multiplied by a factor according to Equation (3.72), and proper values should be given on the scale axis of the time–scale plot.

We have now extracted one transient shape that may be typical for its location on the vessel. It can be used in the WT based MF detector as the reference signal to search for similar events.

5.1.3 *Transient detection*

As an example of transient detection, the previous filtered transient will now be used as reference for detection on that same sensor element. Since we have filtered out the four first bands, the reference signal can be downsampled by a factor $2^4 = 16$ along with the analyzed signal[33]. This because the frequency components we search for must lie in the same bands in both signals. Now, our search for frequency components is limited.

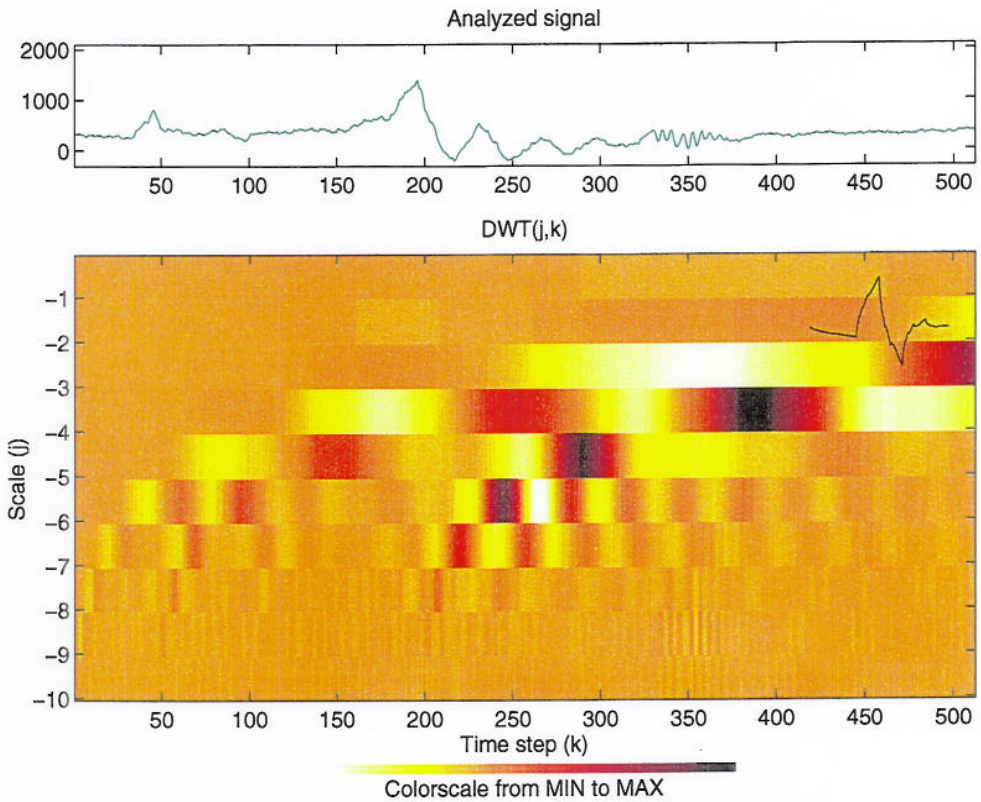

Figure 5.11 Discrete translation invariant wavelet transform of the filtered transient

Figure 5.11 shows that the DWT of our transient has a characteristic shape, where no frequency components of the transient are left out. Now, a larger segment of the sensor signal is extracted. By inspecting its wavelet transform, we notice that the selected area contains our reference transient together with another with almost identical shape. In the time–scale plane in Figure 5.12 both these two transients are located. When using the

33. Both signals are filtered before downsampling to avoid aliasing.

WT based MF technique for detection, both transients are detected. Figure 5.13 shows the detector output for these simulations.

This example illustrates that wavelets can be useful for both filtering and detection problems. We have now seen how a found and modified transient can be used as reference for detection of other transients from the same sensor element. By inspection of Figure 5.12, we clearly see that patterns similar to Figure 5.11 are found according to each located transient. The first detected transient is the same that we have used as a reference, and therefore the output form our detector is a high value as shown in Figure 5.13. The second detected transient has roughly identical shape, and the output is therefore almost as high as for the first transient. The performance of the detector in this example shows promising results.

During this example the db2 wavelet was used. No other chooses of wavelet functions were tried out.

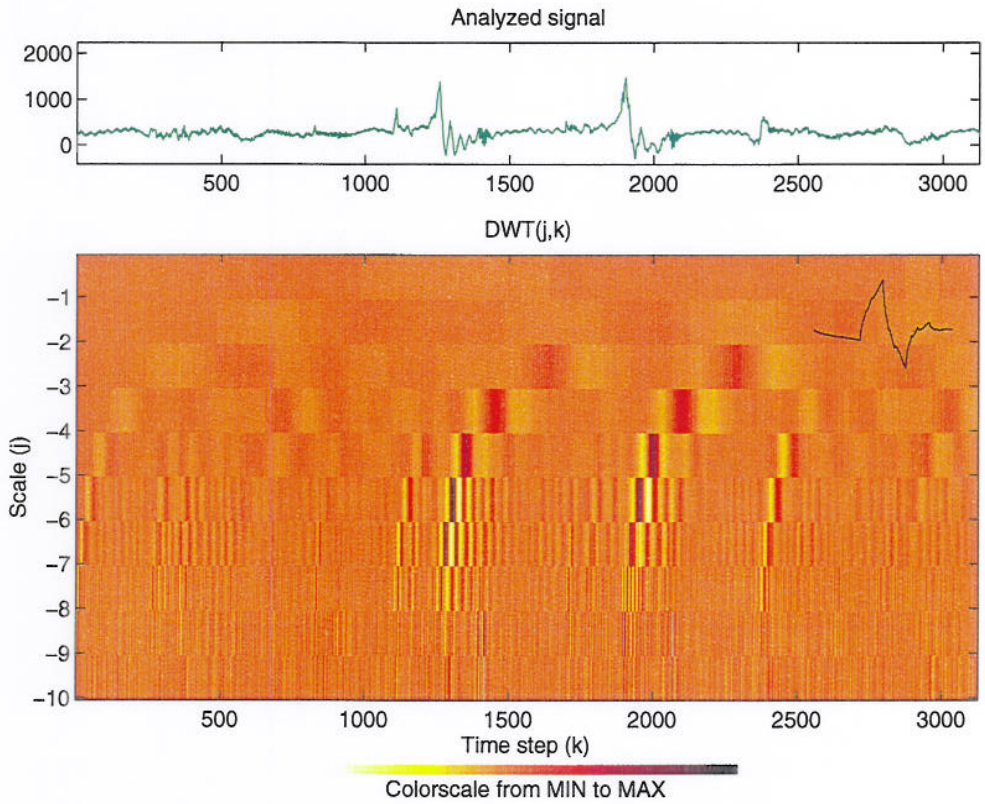

Figure 5.12 Wavelet transform of a large segment of the analyzed signal

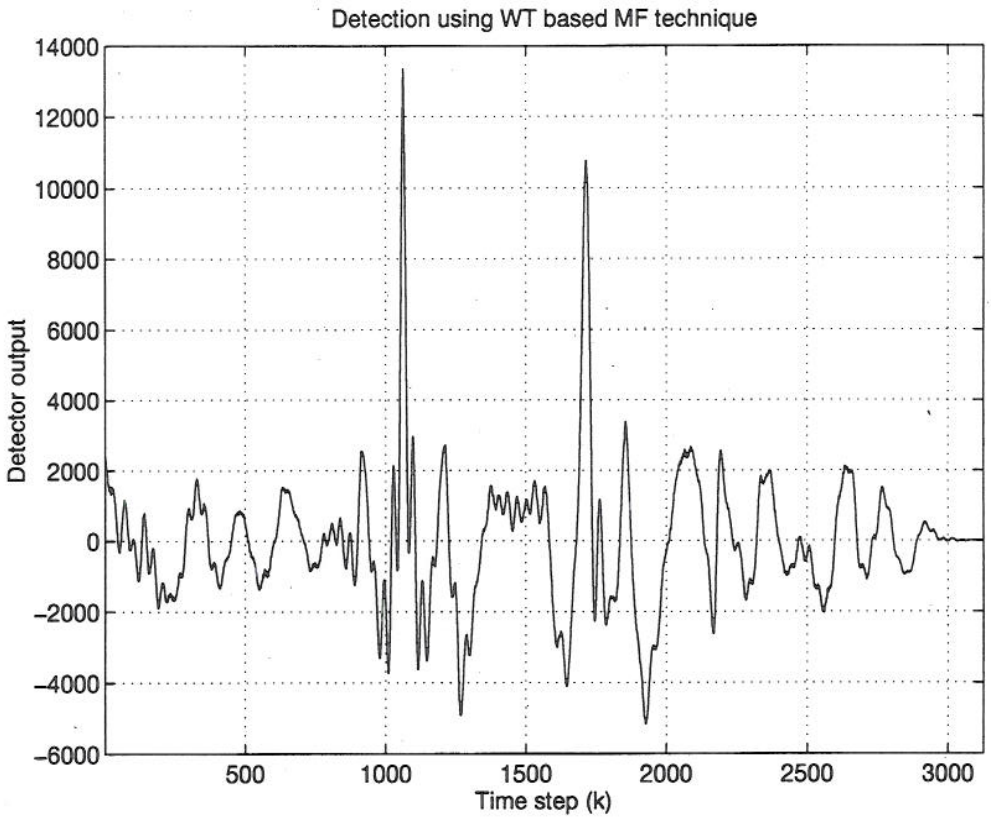

Figure 5.13 Output from the WT based MF detector. The two transients that is present in the signal are clearly detected

Since one of the proceeding detected transients are the reference signal, another segment of the channel are analyzed. This analysis is shown in Figure 5.14. In the transform plot one clearly recognize events similar to those in the first analyzed segment. It is interesting to note that one of these new transients (for time step 2000) almost have identical characteristics as our reference transient. Only the amplitude seems to be different. By close inspection of the detector output in Figure 5.15, the output for this specific transient is almost similar to the output when the reference signal is analyzed (see Figure 5.13).

This last analysis shows that even if the transients have less amplitude than the reference, an equality with respect to the other characteristics are enough to get detection.

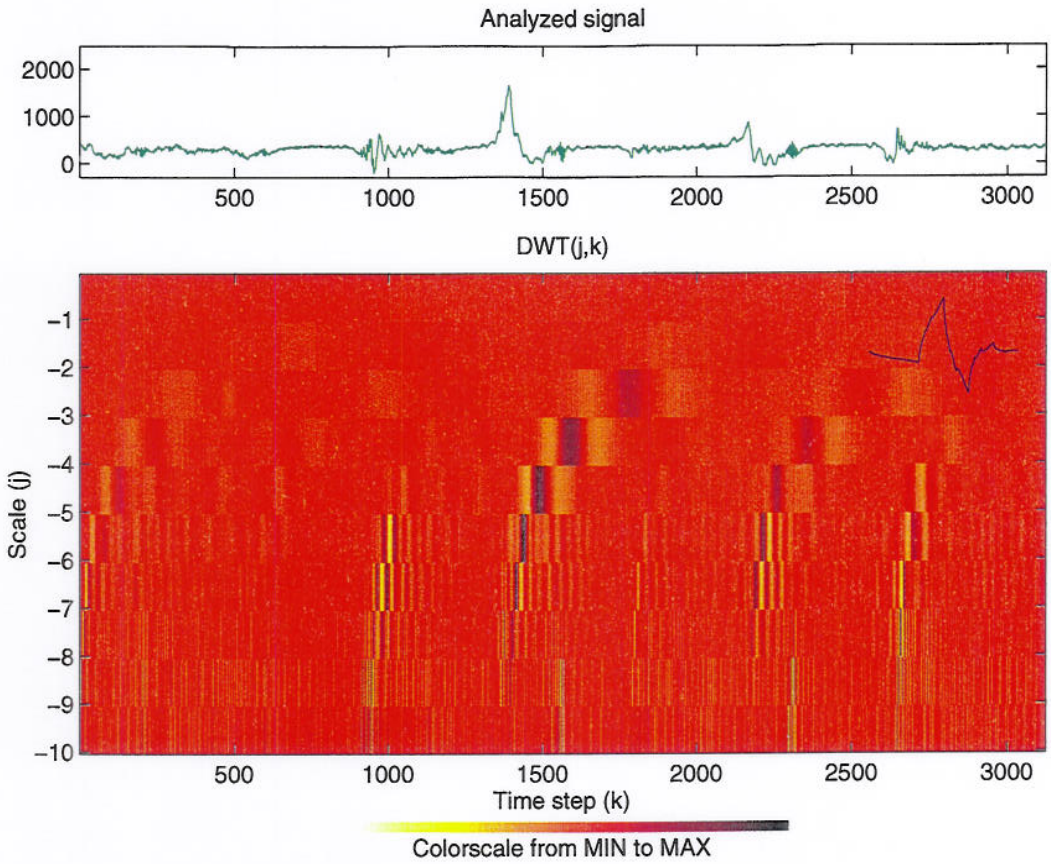

Figure 5.14 Wavelet transform of another large segment of the analyzed signal

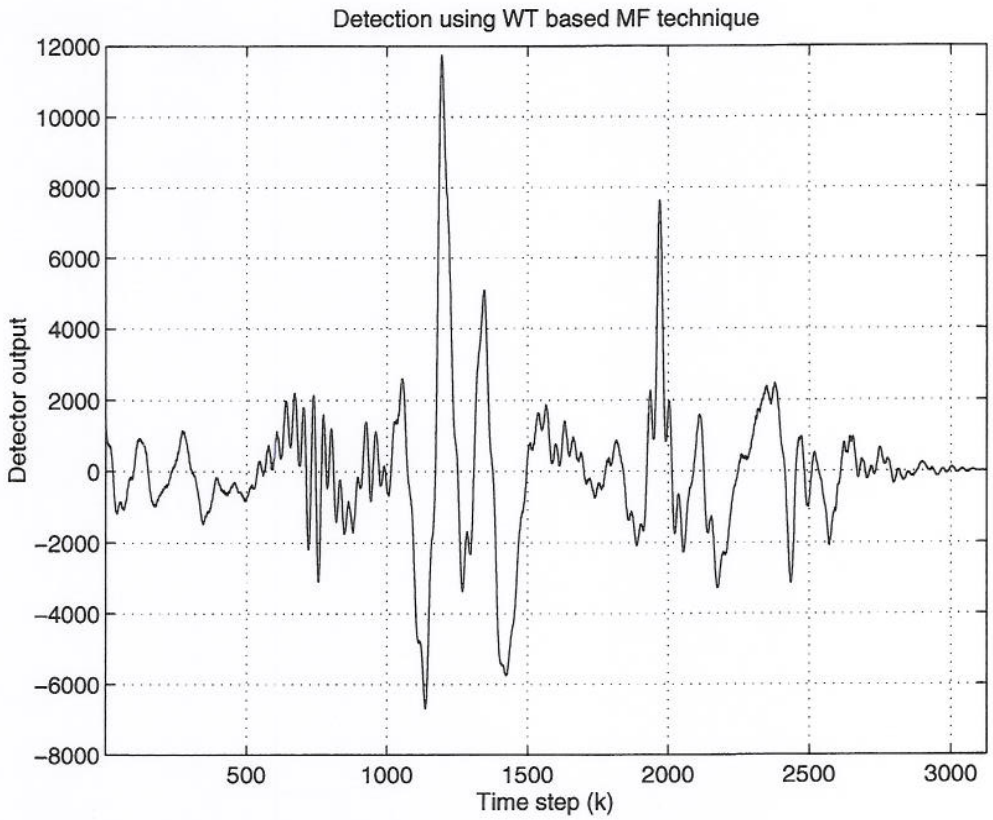

Figure 5.15 Output from the WT based MF detector. Two other transients are detected

6 OVERVIEW OF SIGNAL PROCESSING SYSTEM

A suggested schematic overview of the signal processing part of a realtime system for structural monitoring is shown in Figure 6.1. As indicated, this thesis are concentrated on the use of wavelet transform for this purpose. A thorough study of the wavelet concept have been the most central part of this thesis. Therefore a investigation of how to characterize the load and mechanical response of the hull is left out.

The storage capacity is important when deciding what data one want to keep. Probably will a system with many sensors, where a high sampling frequency is used, not be able to code and store raw data fast enough. The data will probably also need bigger storage capacity than can be provided. The number of sensors and sampling frequency will determine the required processing and storage capacity. In the technical feasibility study project, CHESS, it is planed to use in the order of 50–100 sensor elements simultaneously. In future operating systems, the number will be much larger (The quantity shown in Figure 2.4 is very exaggerated).

Wavelet analysis, or filter banks, can in most cases give very good improvement in data compression, and since the transform has an inverse, storage of wavelet analyzes data will give some advantages. Of course interesting events, such as transients, must be stored to be able to do analysis of structural influences by hand in the future. A continuous update of each sensor elements typical transient shapes is necessary to achieve good detector performance. These stored characteristics are a very important part of the detector system.

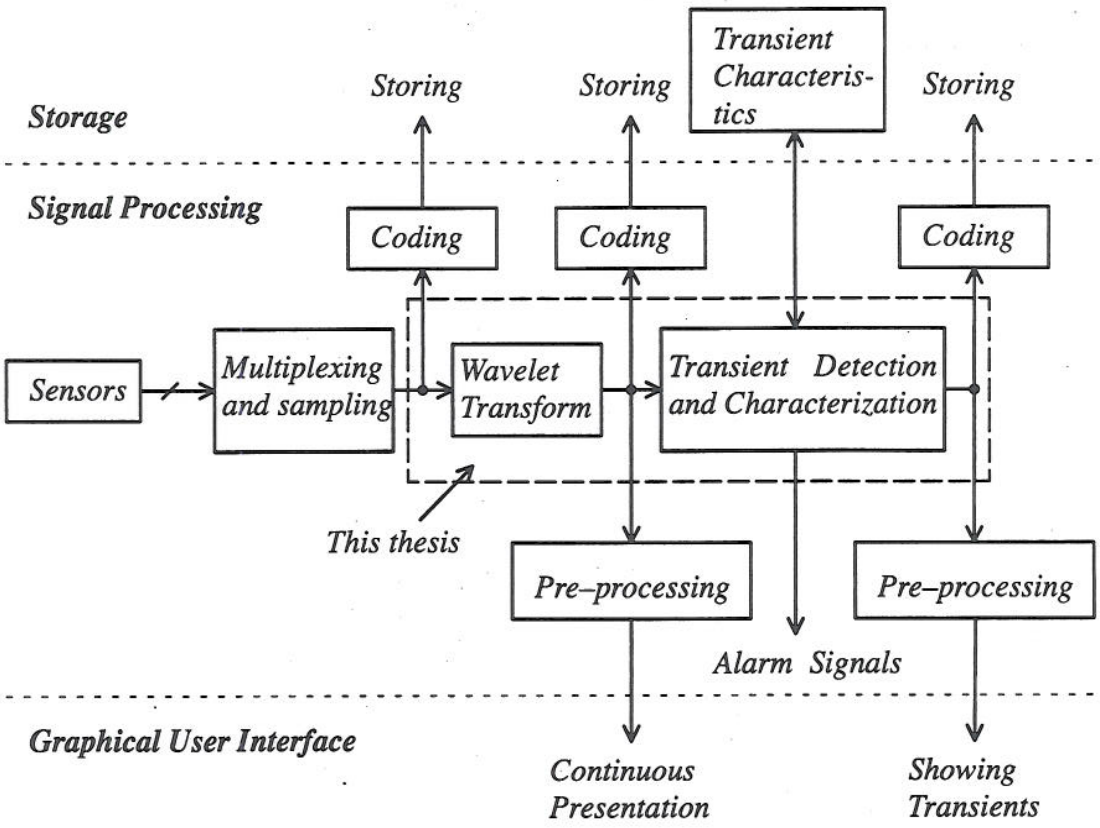

Figure 6.1 Overview sketch of proposed realtime signal processing system. The work done in this thesis is marked by the dashed line box

Before any graphical presentation of results to the user, some pre–processing must be done. This pre–processing are dependent of how the information shall be presented. An advanced graphical user interface (GUI) demands a more complex pre–processing. Any graphical illustrations must be designed so that the user fast and without doubt can understand the meaning of presented events on screen.

7 FURTHER WORK

As briefly discussed in Section 4.5, sophisticated algorithms for transient characterization will give good estimates of oscillation frequency and damping coefficients. Such algorithms may more or less make use of wavelets. To obtain good results, a careful study is required.

When using filter banks, removal of noise can be done statistically. For each band, statistical values are updated continuously. Only statistical deviations are stored, or start more complex algorithms for analyzing events, i.e. thresholds is introduced. This can be a very important part of a logging system, because much uninteresting data is discarded. As a result of this, storage capacity is increased. Statistics may also be used to look for deviations in transient characteristics. If so, it may be a indication of structural damage. This is maybe the most interesting use of statistics in hull monitoring.

Instead of calculating inner products according to Equation (3.68) to achieve the right coefficients for filter bank analysis of signals, sampled versions of the signals are frequently used directly. What the effect of this is for different sampling frequencies can in some cases be interesting. The effect is briefly discussed in (2), (16) and (17), and more complete conclusions may be derived.

In discrete wavelet representations redundancy can be introduced according to the discussion in Section 4.2.2. To get the algorithm for the WT based MF detector with as good performance as possible, one must correct wavelet coefficients with the right redundancy factor. A full deduction of the value of these factors in each band (or level) is highly important. One must remember that several orthonormal bases is used in each band to span the same function space. At the lowest level, two orthonormal bases span W_{J_1-1}. Intuitively, the redundancy factor in this case equals 2, but no proof of this is given in the literature. These factors should hopefully also be independent of the mother wavelet.
It seems like that the easiest way to derive this, is to use *bra* and *ket* vector notation. When one need higher resolution in scaling direction, wavelet packages are used. If using a full wavelet package, a homogeneous grid is achieved in this direction. By moving all downsamplers, it would be interesting to see if the representation is correct with respect to a completely homogeneous sampling in both directions of the time–scale plane.

System identification using power spectra of the input and output signal of a system is a traditional method (30). One uses frequency information for the identification. Identification of systems using wavelets is not a studied topic. Assuming that the system is enforced with an arbitrary signal. On basis of the wavelet representations of the input and output signals, a characterization of the system may be achieved. Now, assuming that this analyzed system is our fibre optic sensor. Using wavelet analysis, typical sensor noise may be characterized. This can result in a much more reliable measurements of the tension at each sensor location. Since the sensors have different location, they may also have different noise characteristics.

8 DISCUSSION AND CONCLUSION

During this work, wavelet theory which was used for detection purposes in signal processing, are presented. Hopefully, the reader should have gained a good understanding of basic wavelet theory, and hence a further study on the topic will maybe be easier.

In Chapter 3, an introduction to the wavelet transform is given. Interpretation of analytical results are discussed. When using the wavelet transform, it is necessary to be able to interpret, or read, the transform images. One should note that transform images not always is true according to the definition of the wavelet transform.

The multiresolution theory provide us with the possibility to use filter banks when implementing discrete wavelet transforms. This is a powerful tool which gives faster algorithms for time–frequency analysis compared with for example a traditional method such as the short time Fourier transform (STFT). Together with the excellent ability to analyze non–stationary signals, the fast algorithm are one of the best reason for choosing wavelet analysis in transient detection problems. In this case, the similarity with the matched filter method are also a contributing factor for studying wavelets.

Compared to the cost function dependent algorithm, the downsampler ignoring algorithm reduces the total complexity for the translation invariant wavelet representation. However, if data are supposed to be stored, the last algorithm needs more storage capacity. Therefore this algorithm is only optimal when using the wavelet coefficients together with the matched filter (MF) based wavelet transform (WT) detector. Then one assumes that only interesting events are stored. If one wish to store the WT of an analyzed signal, this is most efficiently solved by downsampling the representation after the detector.

When using filter banks for wavelet analysis, one must remember that filters normally are anti causal, in difference from the wavelet transform which is normally causal. The wavelet transform are only anti causal when the analyzing wavelet has compact support for negative values of the time variable. To achieve identical transform images according to the definition of the wavelet transform, one must use causal filters in the filter bank. In these cases one should remember that the analyzing wavelet and the corresponding filters have identical support.

If one, when using the MF based WT detector, choose an observation window for the reference signal that are to small, the detector performance will decrease. This is especially important when the signal to noise ratio (SNR) is small. When analyzing signals with large SNR, a smaller observation window may be used. The size[34] of the observation window is determined of the correlation between the analyzing wavelet and the reference signal. If the correlation is good, this will result in a smaller window size.

Due to lack of time, no experimental work was done. However, a few examples of applied theory from literature are shown. These few experiments indicate that the pro-

34. The size is both length, which is in the time direction, and width, which is in the scale direction.

posed detector algorithm have good performance with respect to real data. By inspecting some of these data, one can conclude that the SNR is very large. Hopefully the SNR will not be decreased when using FBG strain sensors instead of electrical strain gauges.

During the experiments, the reader probably with suspicion noted that the discrete scaling parameter j not was an integer. In the multiresolution section one require that j should be an integer. As described before, j will only be an integer for certain values for the sampling frequency. If using an approximation of the inner products between the analyzed signal and the scaling function for a chosen integer j, this will cause this error. However, for practical realizations of a system, this should not be of any concern. It is only important if one require proper values on the scaling axis on the transform images.

List of symbols

Symbol	Definition
a	Continuous scaling parameter.
b	Continuous shift (translation) parameter.
ψ	Mother wavelet function.
$\psi_{a,b}$	The wavelet scaled by a and shifted by b, energy is constant.
Ψ	The Fourier transform (FT) of $\psi(t)$, $\Psi(\omega) = \int_{-\infty}^{\infty} \psi(t) e^{-i\omega t} dt$.
Φ	The Fourier transform of $\phi(t)$.
ω	The continuous frequency variable.
i	The imaginary number, $i = \sqrt{-1}$.
*	Denotes complex conjugation.
C_ψ	Redundancy in the continuous transform.
κ_ψ	Inverse redundancy factor in the discrete transform.
$\Re$	All real numbers.
$\mathcal{Z}$	All integers – negative and positive.
$WT(a,b)$	Continuous wavelet transform.
j	Discrete scaling parameter, $a = a_0^{-j}$.
k	Discrete shift (time) parameter, $b = k\, b_0 a_0^{-j}$.
a_0	Scaling grid parameter in DWT.
b_0	Translation grid parameter in DWT.
$DWT(j,k)$	Discrete wavelet transform.

ϕ	Scaling function.
V_j	Subspace spanned by $\phi_{j,k}$.
W_j	Subspace spanned by $\psi_{j,k}$.
$\{\emptyset\}$	The empty space.
L^2	Absolute integrable.
$L^2(\Re)$	Infinite–dimensional Hilbert space ((8)).
$h(n)$	Scaling function coefficients and lowpass FIR filter.
$h_1(n)$	Wavelet function coefficients and highpass FIR filter.
$c_j(k)$	Scaling coefficients.
$d_j(k)$	Wavelet coefficients.
$\delta(t)$	The Dirac delta function.
$\delta(k)$	The Kronecker delta function.
$H(\omega)$	The Discrete–Time Fourier Transform (DTFT) of $h(n)$, $H(\omega) = \frac{1}{N}\sum_{n=0}^{N-1} h(n)e^{-i\omega n}$.
$H_1(\omega)$	The DTFT of $h_1(n)$.
N	The length of the filters.
M	The number of filters in one stage of a decomposition/reconstruction filter bank, i.e. M–band FB.
ρ	Correlation coefficient. Maximum correlation if $\rho = \pm 1$.
λ	The damping coefficient in a transient. Wavelength in Chapter 2.
ξ	Threshold in transient detection.
$\mathcal{O}(n)$	Complexity factor. Typically number of operations or multiplications on a n–length sequence.

References

(1) Rioul O, Vetterli M: *Wavelets and Signal Processing*, IEEE Signal Processing Magazine, Oct. 1991, pp. 14–38.

(2) Burrus C S, Gopinath R A, Guo H: *Introduction to Wavelets and Wavelet Transform*, To be published (summer/fall 1996), Prentice–Hall.

(3) Mallat S G: *A Theory for Multiresolution Signal Decomposition: The Wavelet Representation*, IEEE Transactions on Pattern Analysis and Machine Intelligence, Vol. 11, No. 7, Jul. 1989, pp. 674–693.

(4) Pran K: *Design of Optical Fibre Bragg Gratings*, Diploma thesis, Norwegian Institute of Technology, Jan. 1995.

(5) Graps A: *An Introduction to Wavelets*, IEEE Computational Science and Engineering, Vol. 2, No. 2, summer 1995.

(6) Resnikoff H L: *Wavelets and adaptive signal processing*, Optical Engineering, Vol. 31, No. 6, Jun. 1992, pp. 1229–1234.

(7) Daubechies I: *Where Do Wavelets Come From?–A Personal Point of View*, Proceedings of the IEEE, Vol. 84, No. 4, Apr. 1996, pp. 510–513.

(8) Daubechies I: *Ten Lectures on Wavelets*, SIAM, 1992.

(9) Freeman M O: *Wavelets Signal Representations with Important Advantages*, Optics & Photonics News Aug. 1993, pp. 8–15.

(10) Lee D T L, Yamamoto A: *Wavelets Analysis: Theory and Applications*, Hewlett–Packard Journal, Dec. 1994, pp. 44–54.

(11) Vetterli M, Kovačević J: *Wavelets and Subband Coding*, PTR Prentice–Hall Inc, 1995.

(12) Shensa M J: *The Discrete Wavelet Transform: Wedding the À Trous and Mallat Algorithms*, IEEE Transactions on Signal Processing, Vol. 40, No. 10, Oct. 1992, pp. 2464–2482.

(13) Mallat S G: *Multiresolution approximations and Wavelet othonormal bases of* $L^2(\Re)$, Transactions of The American Mathematical Society, Vol. 315, No. 1, Sep. 1989, pp. 69–87.

(14) Strang G, Nguyen T: *Wavelets and Filter Banks*, Wellesley–Cambridge Press, 1996.

(15) Misiti M, Misiti Y, Oppenheim G, Poggi J–M: *Wavelet Toolbox For Use with MATLAB*, The MathWorks Inc., 1996.

(16) Sweldens W, Piessens R: *Wavelet Sampling Techniques*, Proceedings of the Joint Statistical Meetings, San Fransisco, Aug. 1993.

(17) Walter G G: *A Sampling Theorem for Wavelet Subspaces*, IEEE Transactions on Information Theory, Vol. 38, No. 2, Mar. 1992, pp. 881–884.

(18) Beauchamp K, Yuen C: *Digital Methods for Signal Analysis*, George Allen & Unwin, London, 1979.

(19) Liang J, Parks T W: *A Translation–Invariant Wavelet Representation Algorithm with Applications*, IEEE Transactions on Signal Processing, Vol. 44, No. 2, Feb. 1996, pp. 225–232.

(20) Del Marco S, *Weiss J: M–band wavepacket–based transient signal detector using a translation–invariant wavelet transform*, Optical Engineering, Vol. 33, No. 7, Jul. 1994, pp. 2175–2182.

(21) Vaidyanathan P P: *Multirate systems and filter banks*, PTR Prentice–Hall Inc., 1993.

(22) Frisch M, Messer H: *Detection of a Known Transient Signal of Unknown Scaling and Arrival Time*, IEEE Transactions on Signal Processing, Vol. 42, No. 7, Jul. 1994, pp. 1859–1863.

(23) Frisch M, Messer H: *The Use of the Wavelet Transform in the Detection of an Unknown Transient Signal*, IEEE Transactions on Information Theory, Vol. 38, No. 2, Mar. 1992, pp. 892–897.

(24) Frisch M, Messer H: *Transient Signal Detection Using Prior Information on the Likelihood Ratio Test*, IEEE Transactions on Signal Processing, Vol. 41, No. 6, Jun. 1993, pp. 2177–2192.

(25) Frisch M, Messer H: *Detection of a transient signal of unknown scaling and arrival time using the discrete wavelet transform*, IEEE International Conference on Acoustics, Speech and Signal Processing, Vol. 2, 1991, pp. 1313–1316.

(26) Palmstrøm R E, Wang G: *Detection of Moving Magnetic Dipoles by three–dimensional Metched Filter Techniques*, NDRE report, 1996.

(27) Louisell W: *Radiation and Noise in Quantum Electronics*, McGraw–Hill, 1964.

(28) Messiah A: *Quantum Mechanics, Volume I*, North–Holland Publishing Company, Amsterdam, 1961.

(29) Det Norske Veritas Classification AS: *Advanced FRP Composite Hull Structures: Strain Measurements on Test vessel*, Technical Report, No. 93–0200, Jul. 1993.

(30) Wellstead P E, Zarrop M B: *Self–Tuning Systems: Control and Signal Processing*, John Wiley & Sons, Chichester, 1991.

(31) Proakis J G, Monolakis D G: *Digital signal processing, Principles, Algorithms, and Applications*, 2nd ed., Macmillan, 1992.

(32) Chui C K: *An Introduction to Wavelets, Wavelet Analysis and its Applications Volume 1 & 2*, Academic Press Inc., 1992.

(33) Vetteri M, Herley C: *Wavelets and Filter Banks: Theory and design*, IEEE Transactions on Signal Processing, Vol. 40, No. 9, Sept. 1992, pp. 2207–2234.

(34) Daubechies I: *The Wavelet Transform, Time–Frequency Localization and Signal Analysis*, IEEE Transactions on Information Theory, Vol. 36, No. 5, Sept. 1990, pp. 961–1005.

(35) Weiss L G: *Wavelets and Wideband Correlation Processing*, IEEE Signal Processing Magazine, Jan. 1994, pp. 13–32.

(36) Wickerhauser M V: *Adapted Wavelet Analysis from Theory to Software*, A K Peters, Wellesley, 1994.

(37) Del Marco S, Weiss J, Jagler K B: *Wavepacket–based transient signal detector using a translation–invariant wavelet transform*, Proceedings of SPIE – The International Sociey for Optical Engineering, Vol. 2242, Apr. 1994, pp. 792–802.

(38) Soares C G: *Transient response of ship hulls to wave impact*, International Shipbuilding Progress, Vol. 36, No. 406, Jun. 1989, pp. 137–156.

(39) Aghajan H, Pati Y, Kailath T: *Transient signal detection using high–resolution line detection on wavelet transforms*, Conference Record of the Asilomar Conference on Signals Systems & Computers, Vol. 2, 1994, pp. 1114–1118.

(40) Carter P H: *Unknown transient detection using wavelets*, Proceedings of SPIE – The International Sociey for Optical Engineering, Vol. 2242, Apr. 1994, pp. 803–814.

(41) Leung W–H, Chang F–Y: *Transient analysis via fast wavelet–based convolution*, Proceedings – IEEE International Symposium on Circuits and Systems, Vol. 3, Apr./May 1995, pp. 1884–1887.

(42) Belik O, Price W G: *Comparison of slamming theories in the time simulation of ship responses in irregular waves*, International Shipbuilding Progress, Vol. 29, No. 335, Jul. 1982, pp. 173–186.

(43) Kaiser G: *A Friendly Guide to Wavelets*, Birkhauser, 1994.

(44) Rioul O: *A Discrete–Time Multiresolution Theory*, IEEE Transactions on Signal Processing, Vol. 41, No. 8, Aug. 1993, pp. 2591–2606.

(45) Boashash B, O'Shea P: *Detection and Classification of Underwater Transients by Time–Frequency Analysis*, Journal of Electrical and Electronics Engineering, Australia – IE Australia & IREE Australia, Vol. 9, No. 3, Sep. 1989, pp. 63–74.

(46) Hlawatsch F, Boudreaux–Bartels G F: *Linear and Quadratic Time–Frequency Signal Representations*, IEEE Signal Processing Magazine, Apr. 1992, pp. 21–67.

(47) Matalgah M, Knopp J: *Time–varying spectral analysis of non–stationary signals based on combined wavelet and fourier transforms*, International Journal of Electronics, Vol. 78, No. 3, Mar. 1995, pp. 463–476.

(48) Kirby J T, Chajes M J, Melby J A: *Wavelet Transform Analysis of Several Transient or Nonstationary Phenomena in Engineering Mechanics*, Proceedings of the Ninth Conference on Engineering Mechanics, 1992, pp. 204–207.

(49) Desai M, Shazeer D J: *Acoustic Transient Analysis using Wavelet Decomposition*, IEEE Conference on Neural Networks for Ocean Engineering, Aug. 1991, pp. 29–40.

(50) Petropulu A P: *Detection of Transients using Discrete Wavelet Transform*, Proceedings of IEEE ICASSP, Vol. 2, 1992, pp. 477–480.

(51) Cohen A, Kovačević J: *Wavelets: The Mathematical Background*, Proceedings of the IEEE, Vol. 84, No. 4, Apr. 1996, pp. 514–522.

(52) Dougherty E R: *Probability and Statistics for the Engineering, Computing and Physical Sciences*, Prentice Hall Inc., 1990.

(53) Holschneider M: *Wavelets: An Analysis Tool*, Clarendon Press, Oxford, 1995.

(54) Hartung F: *Image coding and Wavelet theory – Theory and performance evaluation of FIR wavelet coders*, Diploma thesis, Norwegian Institute of Technology, Jul. 1992.

APPENDIX

A OVERVIEW OF AVAILABLE WAVELETS IN MATLAB

The dashed line shows the corresponding scaling function to each wavelet function. For the Morlet wavelet the dashed line indicates the imaginary part of $\psi(t)$, and the continuous line the real part (For the Morlet and Mexican hat wavelet there does not exist any corresponding scaling function, see table 3.1). These figures are generated using the WAVEFUN command in Matlab. This function use the iteration Equation (3.65) with 2^8 iterations. It is possible to construct Daubechies wavelets in Matlab up to $N = 50$. For the biorthogonal wavelets, the decomposition functions is used in the analysis part and the reconstruction functions in the synthesis part.

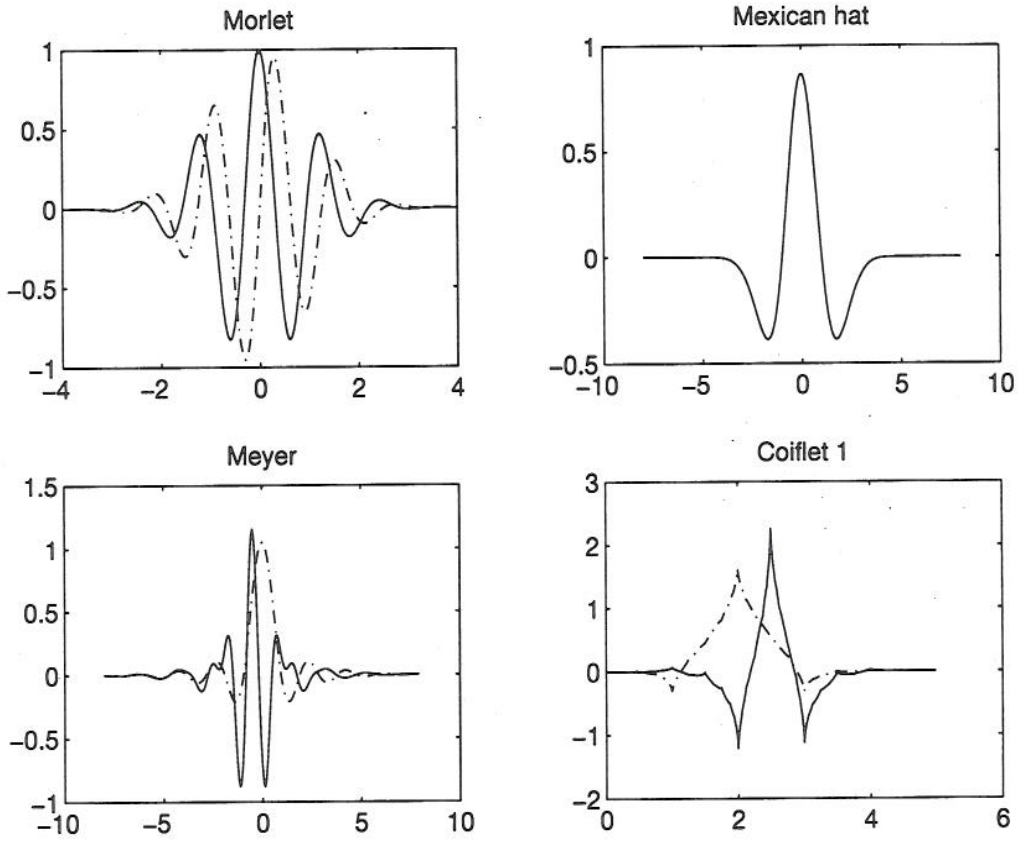

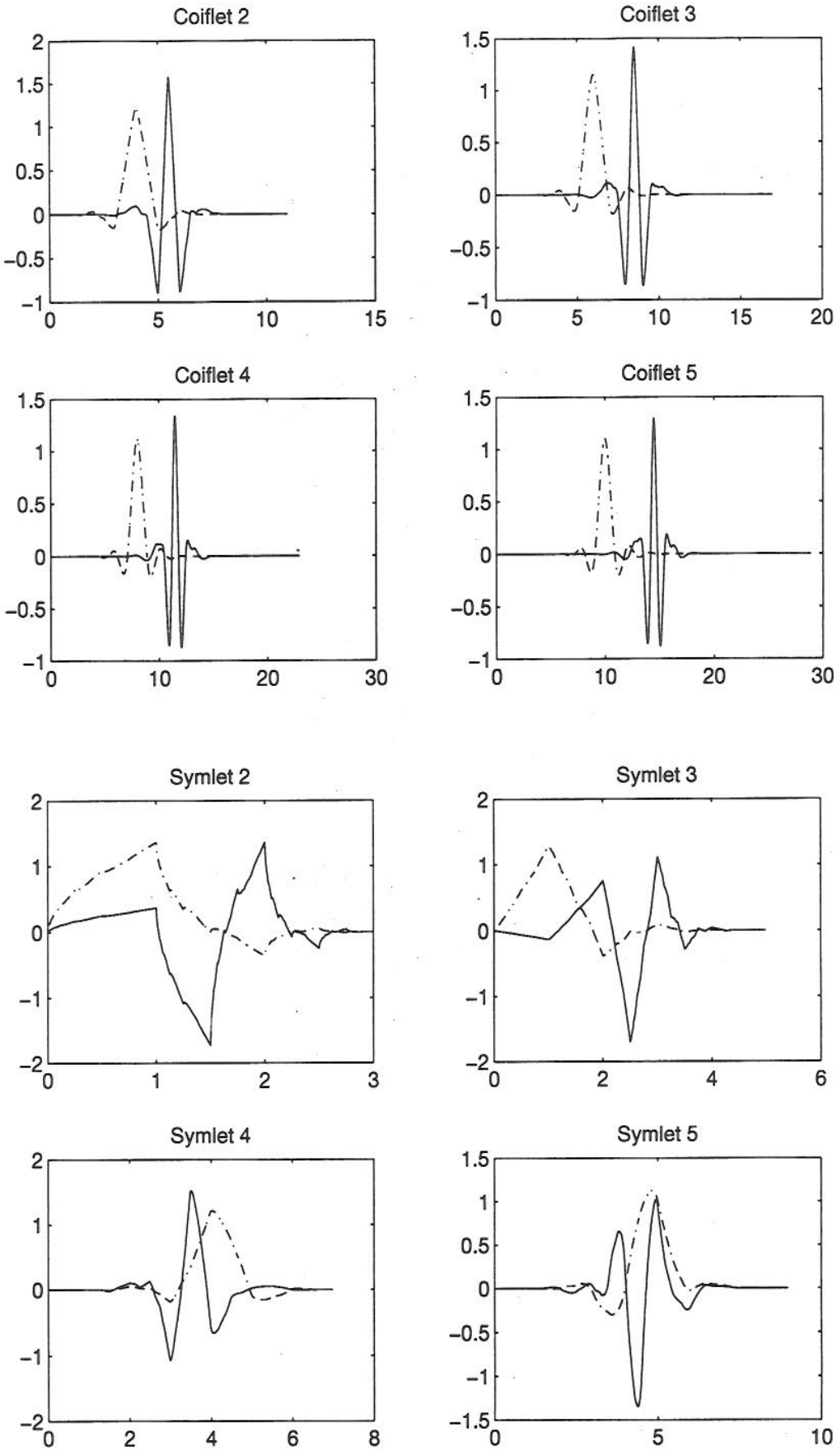
Coiflet 2
Coiflet 3
Coiflet 4
Coiflet 5
Symlet 2
Symlet 3
Symlet 4
Symlet 5

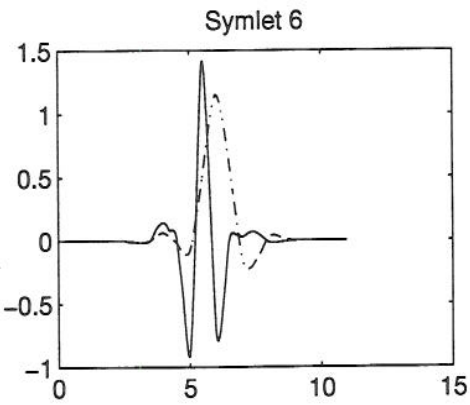
Symlet 6
1.5
1
0.5
0
−0.5
−1
0
5
10
15

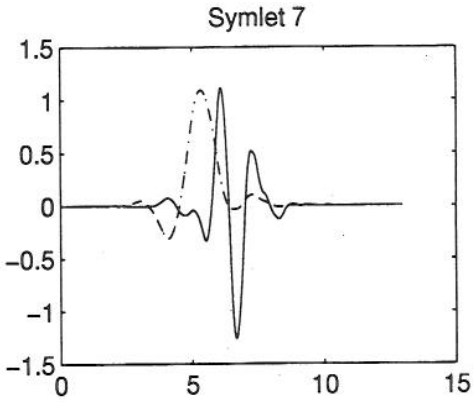
Symlet 7
1.5
1
0.5
0
−0.5
−1
−1.5
0
5
10
15

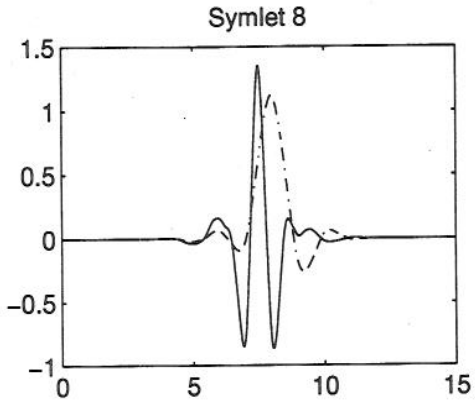
Symlet 8
1.5
1
0.5
0
−0.5
−1
0
5
10
15

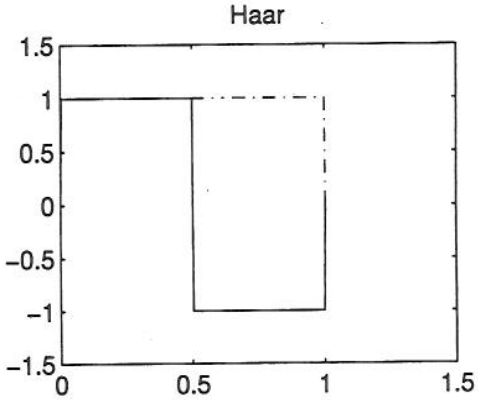
Haar
1.5
1
0.5
0
−0.5
−1
−1.5
0
0.5
1
1.5

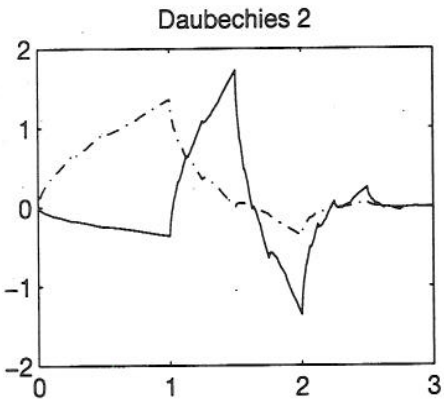
Daubechies 2
2
1
0
−1
−2
0
1
2
3

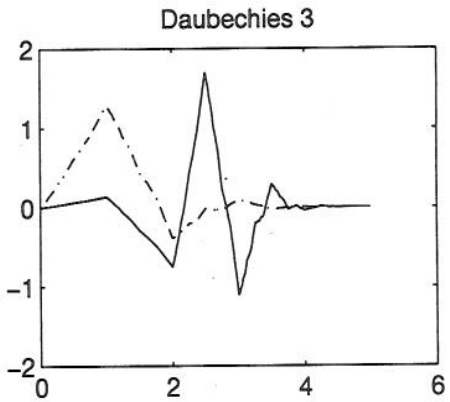
Daubechies 3
2
1
0
−1
−2
0
2
4
6

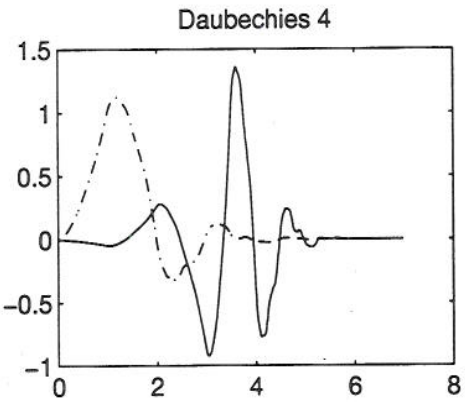
Daubechies 4
1.5
1
0.5
0
−0.5
−1
0
2
4
6
8

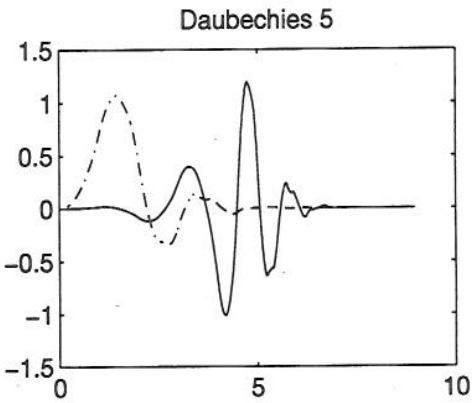
Daubechies 5
1.5
1
0.5
0
−0.5
−1
−1.5
0
5
10

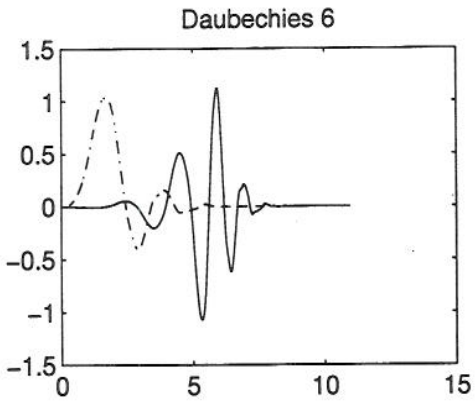
Daubechies 6
1.5
1
0.5
0
−0.5
−1
−1.5
0
5
10
15

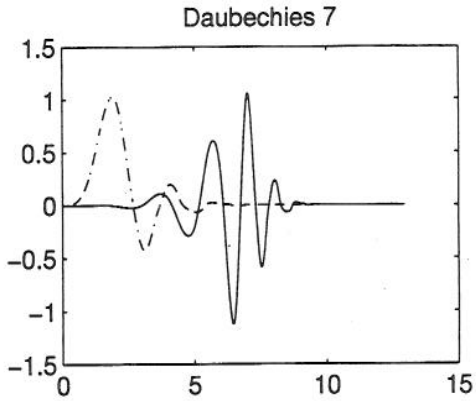
Daubechies 7
1.5
1
0.5
0
−0.5
−1
−1.5
0
5
10
15

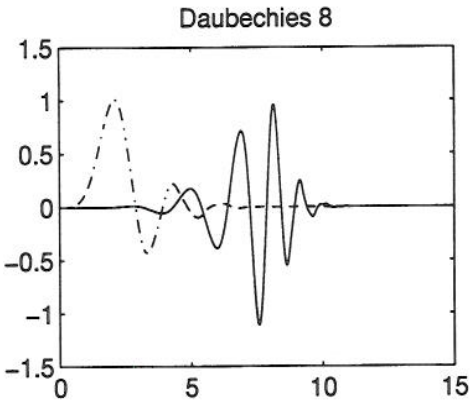
Daubechies 8
1.5
1
0.5
0
−0.5
−1
−1.5
0
5
10
15

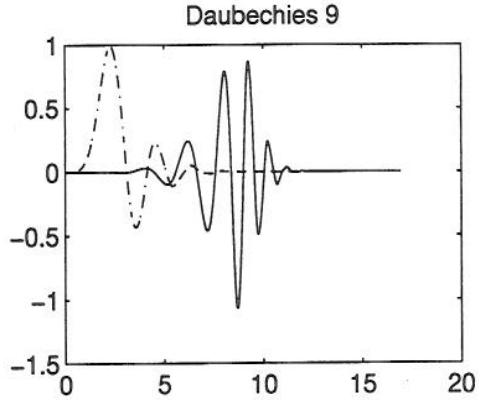
Daubechies 9
1
0.5
0
−0.5
−1
−1.5
0
5
10
15
20

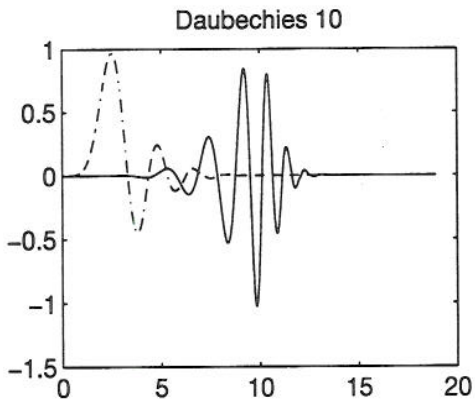
Daubechies 10
1
0.5
0
−0.5
−1
−1.5
0
5
10
15
20

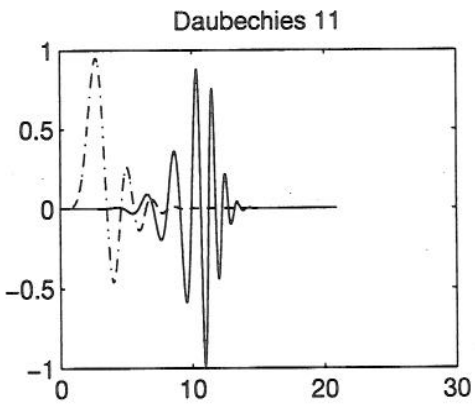
Daubechies 11
1
0.5
0
−0.5
−1
0
10
20
30

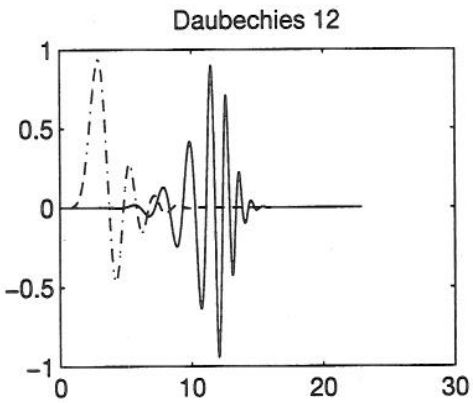
Daubechies 12
1
0.5
0
−0.5
−1
0
10
20
30

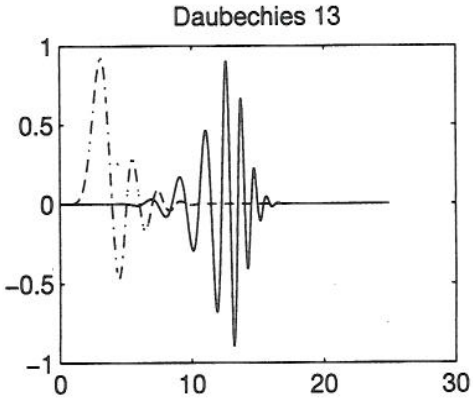
Daubechies 13
1
0.5
0
−0.5
−1
0
10
20
30

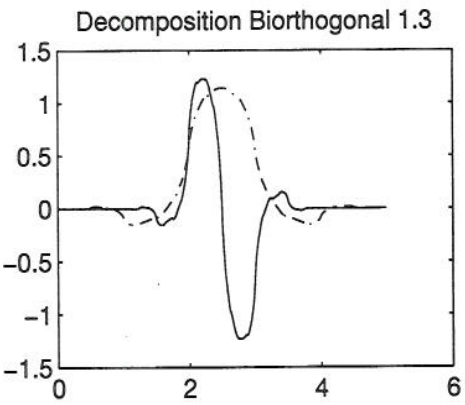
Decomposition Biorthogonal 1.3
1.5
1
0.5
0
−0.5
−1
−1.5
0
2
4
6

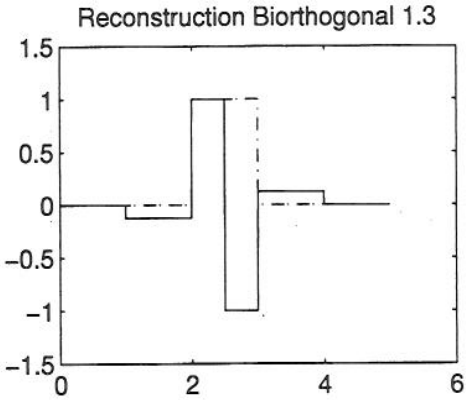
Reconstruction Biorthogonal 1.3
1.5
1
0.5
0
−0.5
−1
−1.5
0
2
4
6

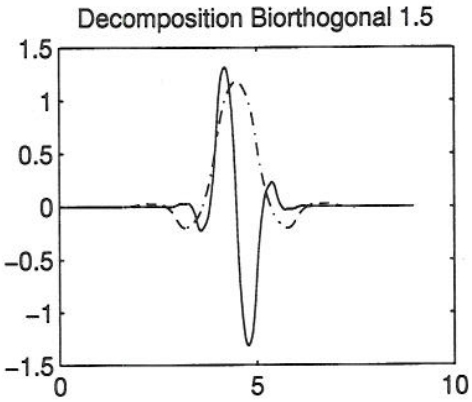
Decomposition Biorthogonal 1.5
1.5
1
0.5
0
−0.5
−1
−1.5
0
5
10

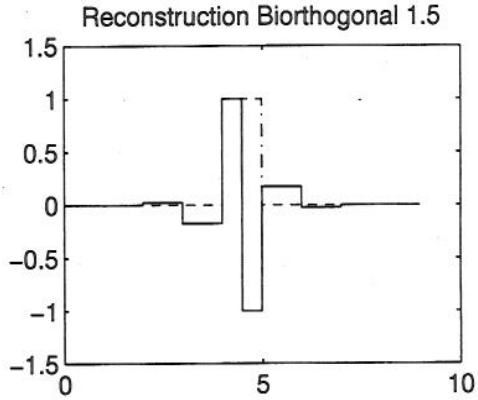
Reconstruction Biorthogonal 1.5
1.5
1
0.5
0
−0.5
−1
−1.5
0
5
10

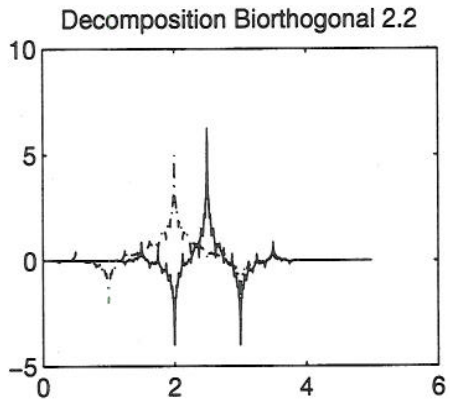
Decomposition Biorthogonal 2.2
10
5
0
−5
0
2
4
6

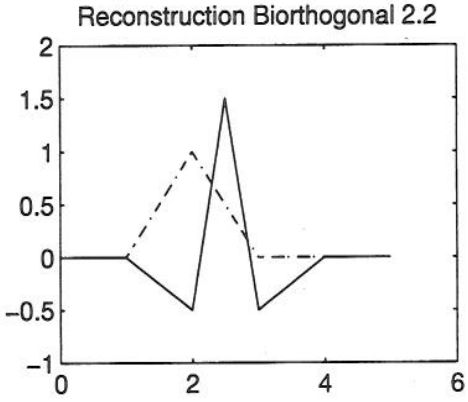
Reconstruction Biorthogonal 2.2
2
1.5
1
0.5
0
−0.5
−1
0
2
4
6

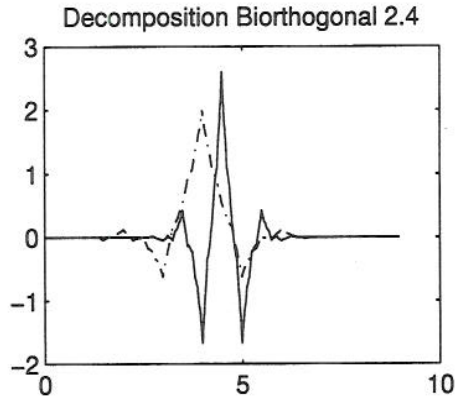
Decomposition Biorthogonal 2.4
3
2
1
0
−1
−2
0
5
10

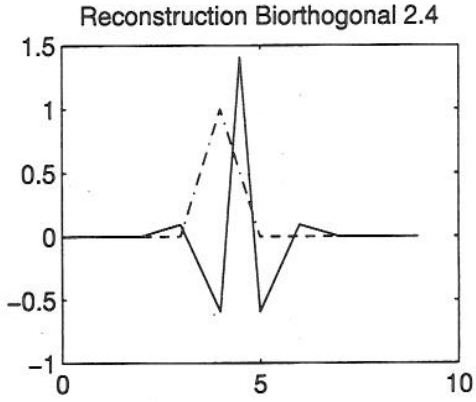
Reconstruction Biorthogonal 2.4
1.5
1
0.5
0
−0.5
−1
0
5
10

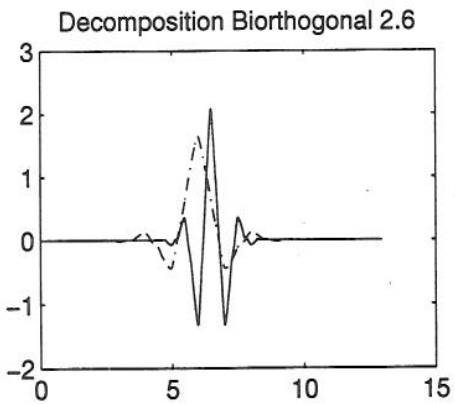
Decomposition Biorthogonal 2.6
3
2
1
0
−1
−2
0
5
10
15

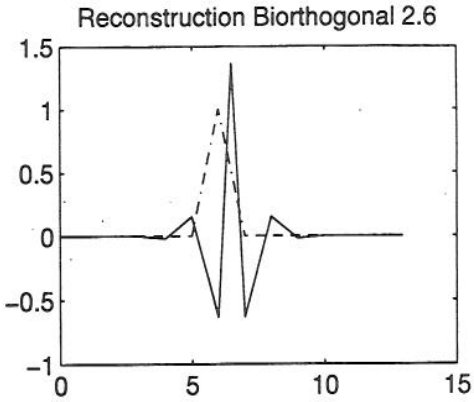
Reconstruction Biorthogonal 2.6
1.5
1
0.5
0
−0.5
−1
0
5
10
15

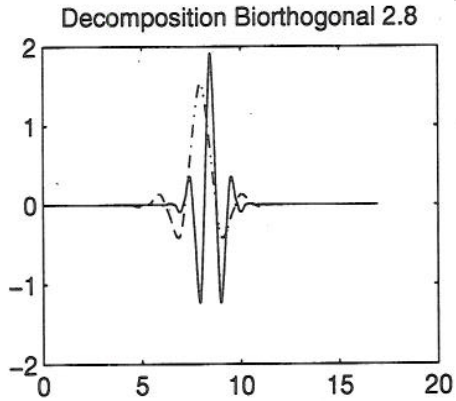
Decomposition Biorthogonal 2.8
2
1
0
−1
−2
0
5
10
15
20

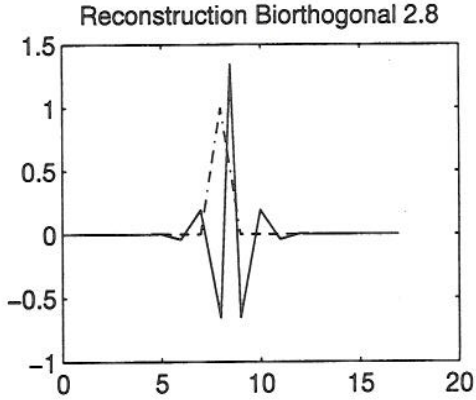
Reconstruction Biorthogonal 2.8
1.5
1
0.5
0
−0.5
−1
0
5
10
15
20

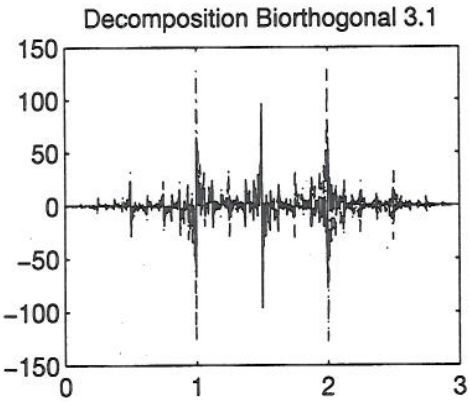
Decomposition Biorthogonal 3.1
150
100
50
0
−50
−100
−150
0
1
2
3

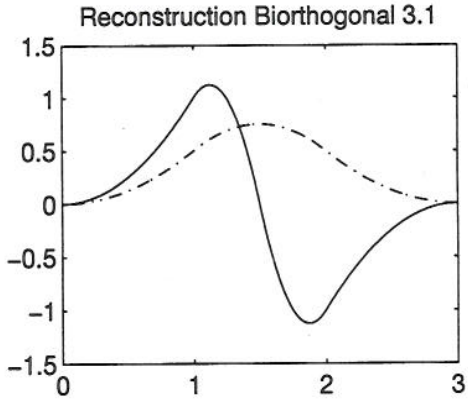
Reconstruction Biorthogonal 3.1
1.5
1
0.5
0
−0.5
−1
−1.5
0
1
2
3

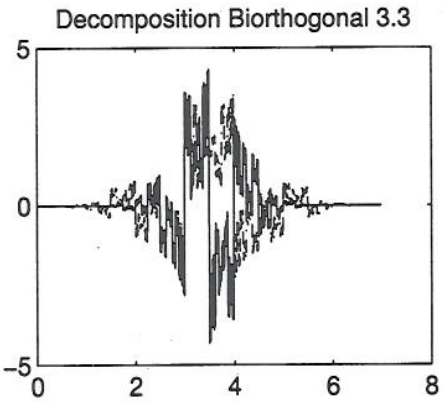
Decomposition Biorthogonal 3.3
5
0
−5
0
2
4
6
8

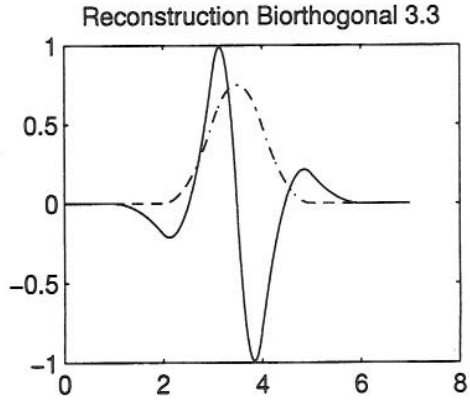
Reconstruction Biorthogonal 3.3
1
0.5
0
−0.5
−1
0
2
4
6
8

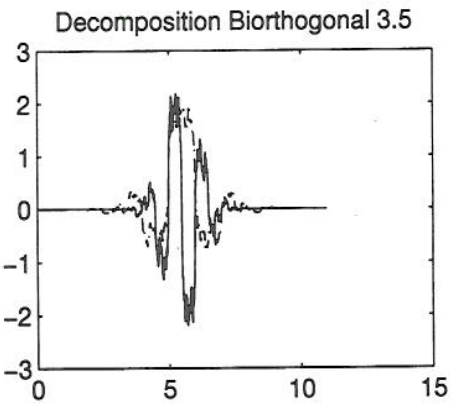
Decomposition Biorthogonal 3.5

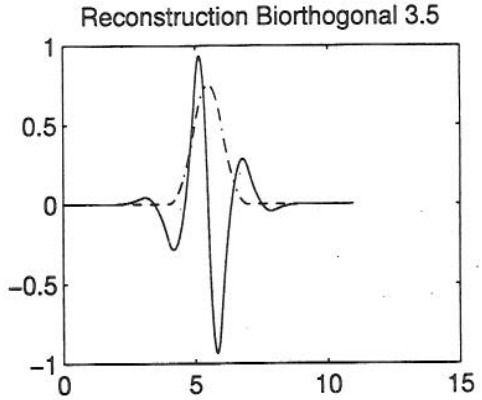
Reconstruction Biorthogonal 3.5

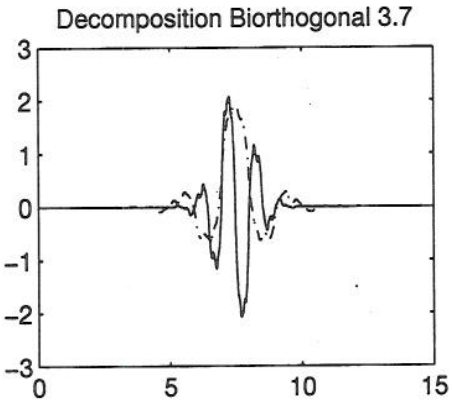
Decomposition Biorthogonal 3.7

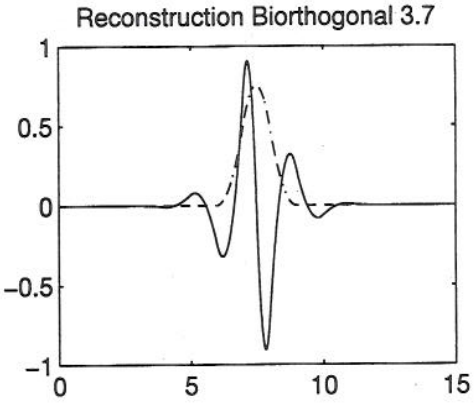
Reconstruction Biorthogonal 3.7

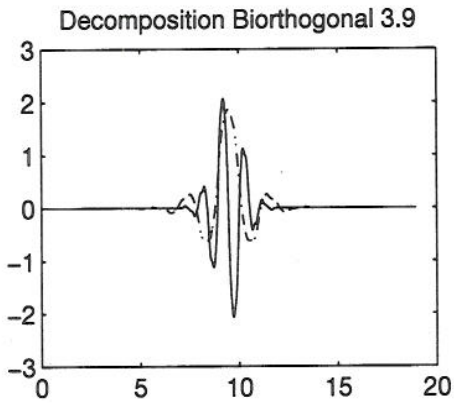
Decomposition Biorthogonal 3.9

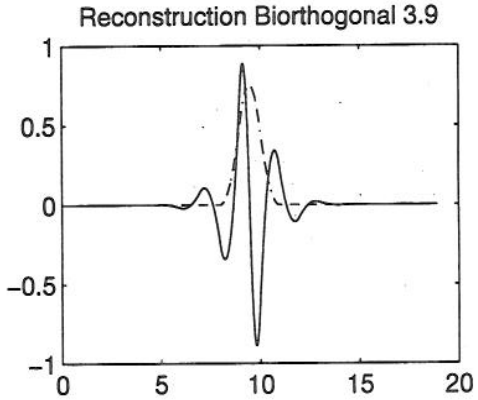
Reconstruction Biorthogonal 3.9

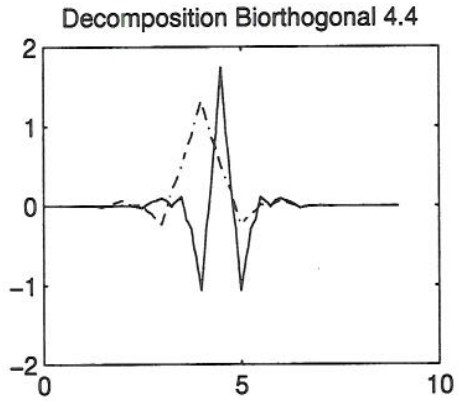
Decomposition Biorthogonal 4.4

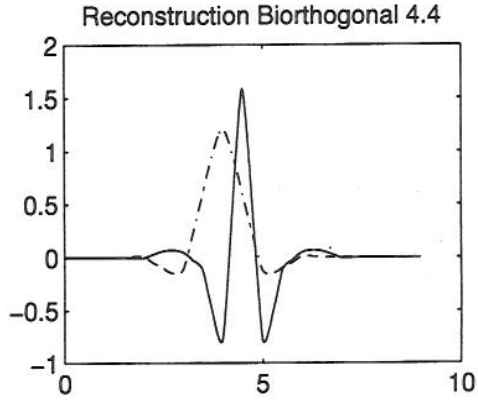
Reconstruction Biorthogonal 4.4

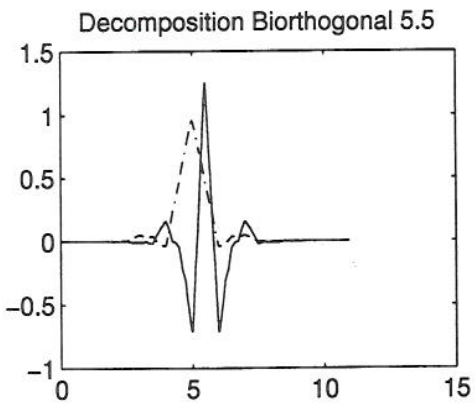
Decomposition Biorthogonal 5.5
1.5
1
0.5
0
−0.5
−1
0
5
10
15

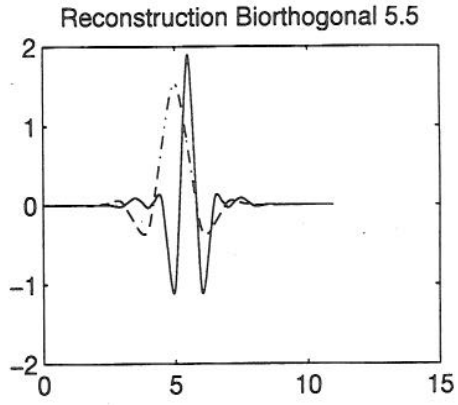
Reconstruction Biorthogonal 5.5
2
1
0
−1
−2
0
5
10
15

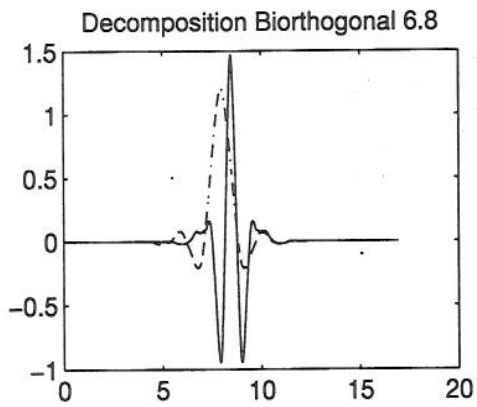
Decomposition Biorthogonal 6.8
1.5
1
0.5
0
−0.5
−1
0
5
10
15
20

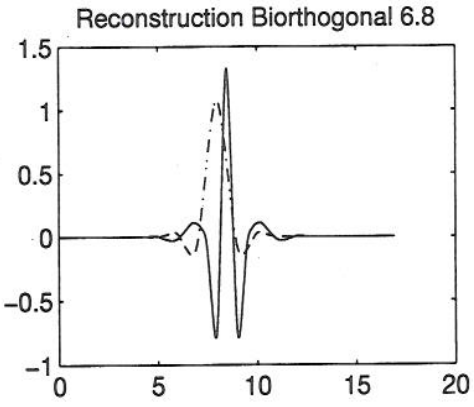
Reconstruction Biorthogonal 6.8
1.5
1
0.5
0
−0.5
−1
0
5
10
15
20

B MATLAB PROGRAMS

In this appenix the most important Matlab procedures/programs that I have used during my work be listed. Each program will have an introduction that in a short way explain what the program does.

`sig_filt.m`: Is used for filtering the analyzed signal. The results of this routine are presented in Section 5.1.2. The GONE variable contain the bands to be ignored during the reconstruction. The number of stages are desided by the largest absolute value in this variable.

```
clear;
Channel = 3;
disp('Loading file ....');
eval(['load cha' num2str(Channel) ';']);
x = eval(['cha' num2str(Channel)]);
x = x(1:2^(floor(log2(length(x)))));
Fs = 6000; % [Hz]
start = 267000;
L = 2^13;
y = x(start:start+L-1);
t = TvsX(x,Fs,start,start+L-1);
wname = 'db2';
GONE = [-14 1 2 3 4]; % Band(s) to be left out
S = max(abs(GONE)); % Number of stages
C = x;

disp('Computing .....');
%%%%%%%%%%%%%%%%%%%%%%%%%%%%%%%%%%%%%%
for s = 1:S,
  [C,D] = dwt(C,wname);
  if member(s,GONE),
    D = zeros(length(D),1);
  end;
  EQ = ['D' int2str(s) ' = D;']; eval(EQ);
  disp(sprintf('D%i ok %i %i',s,length(C),length(D)));
end;
disp('Decomposition ok ');
%%%%%%%%%%%%%%%%%%%%%%%%%%%%%%%%%%%%%%
for s = 1:S,
  EQ = ['D = D' int2str(S-s+1) ';']; eval(EQ);
 % disp(sprintf(' %i %i',length(C),length(D)));
  if length(C) ~= length(D),
    D = [D' 0]';
  end;
  C = idwt(C,D,wname);
  disp(sprintf('D%i ok',S-s+1));
end;
disp('Reconstruction ok ');
%%%%%%%%%%%%%%%%%%%%%%%%%%%%%%%%%%%%%%
```

`TxsX.m`: This function returns a time vector with equal length as the vector x. Fs is the samle rate and start/stop give the boudaries for this time vector.

```
function t = TvsX(x,Fs,start,stop);

tstart = start/Fs;
tstop = stop/Fs;
t = [tstart:1/Fs:tstop];
t = wkeep(t,length(x),'1');
```

`member.m`: Test if a veriable A is a member of a vector B.

```
function T = member(A,B);
% Tests if A is a member of B.
% If so, returning 1, else 0.
% Syntax: answer = member(A,B);

T = 0;
for n = 1:length(B),
  if A == B(n),
    T = 1;
  end;
end;
```

`WTdetector.m`: Is the detector used in Section 5.1.3. Compute first the filters according to second method for TI transform. The Y matrix is the reference representation.

```
clear; clf;
D = 4;
Fs = 6000/D; % [Hz]
J1 = log2(Fs);
wavelet = 'db2';
[H0,H1,RH0,RH1] = wfilters(wavelet);
S = 10; % Number of stages in the FB
j = -[J1-1:-1:J1-1-S+1];

%%% Computing filters in the FB %%%
for s = 1:S,
  EQ = ['FILT' num2str(s) ' = FBfiltNr(' num2str(s)
',2,wavelet);'];
  eval(EQ);
end; disp('Filters ok ...');
%%%%%%%%%%%%%%%%%%%%%%%%%%%%%%%%%%%

%%% Make y %%%
load BA1_4; % Filtered and downsampled signal
y = BA1_4;
for n = 1:D,
  y = dyaddown(y);
end;
ystart = 267000/2^D;
L = 2^(13-D);
y = y(ystart:ystart+L-1)';
```

```
t = TvsX(y,Fs,ystart,ystart+L-1);
%%%%%%%%%%%%%%%

%%% Compute DWT of a known signal y, store it in Y %%%
for s = 1:S,
  EQ = ['Y(' num2str(s) ',:) = filter(FILT' num2str(s) ....
        ',1,y)/(sqrt(2^J1));'];%*2^s);'];
  eval(EQ);
end; disp('Y matrix ok ...');
%%%%%%%%%%%%%%%%%%%%%%%%%%%%%%%%%%%%%%%%%%%%%%%%%%%%%%%%%%%%

%%% Make x %%%
x = BA1_4;
for n = 1:D,
  x = dyaddown(x);
end;
%xstart = 250000/2^D; % hoved eks.
xstart = 660000/2^D;
x = x(xstart:xstart+50000/2^D)';
%%%%%%%%%%%%%%%

%%% Compute DWT of the unknown signal x, store it in X %%%
for s = 1:S,
  EQ = ['X(' num2str(s) ',:) = filter(FILT' num2str(s) ....
        ',1,x)/(sqrt(2^J1)*2^s);'];
  eval(EQ);
end; disp('X matrix ok ...');
%%%%%%%%%%%%%%%%%%%%%%%%%%%%%%%%%%%%%%%%%%%%%%%%%%%%%%%%%%%%
disp('DWT matrices ok ...');

ly = length(y);
lx = length(x);
MF = wkeep2(X,ly,'l');
for n = 1: lx,
  if ly+n > lx,
    new = zeros(S,1);
  else,
    new = X(:,ly+n);
  end;
  %MF = [new wkeep2(MF,ly-1,'l')];
  MF = [wkeep2(MF,ly-1,'r') new];
  matching(n) = sum(sum(Y.*MF));
end; disp('Detection done!');

MAX = maxindex(matching,'abs');
Tmax = MAX/Fs;
g = matching;
hold off; plot(g); grid on;
etmp = axis; axis([1 length(g) etmp(3) etmp(4)]);
xlabel('Time step (k)'); ylabel('Detector output');
title('Detection using WT based MF technique');
```

```
[phi,psi,xval] = wavefun(wavelet);
DWTplot(Y,y,[1:1:ly],j,psi)
DWTplot(X,x,[1:1:lx],j,psi)
colormap(hot);
```

`FBfiltNr.m`: Construct the filters used in the filter bank without downsamplers.

```
function H = FBfiltNr(S,D,wavelet);
%Use the 1st Noble identity to compute the impulse response
%to the FIR filter at a specific stage. All the downsamplers
%is moved to the right, which means that a signal is filtred
%before dovnsampling.
%
% Syntax: hs = FBfiltNr(s,D,'wname');
%
%s is the stage number at which the filter hs is located.
%D is the downsample factor in each stage BEFORE moving the
%downsamplers to the right.

% Made by Roger Eriksen 17/6-96. Ver.2

[H0,H1,RH0,RH1] = wfilters(wavelet);
if S == 1,
  H = H1;
elseif S == 2,
  H = conv(H0,nobelid1(H1,D));
else,
  tmp = H0;
  for s = 1:S-2,
    tmp = conv(tmp,nobelid1(H0,D*2^(s-1)));
  end;
H = conv(nobelid1(H1,D*2^s),tmp);
end;
```

`nobleid1.m`: Realization of the first Noble identity.

```
function F = nobelid1(H,D);
% Computes the Noble identity from left to right
% according to the figure in [9], page 100.

% Made by Roger Eriksen, Spring 96. Ver.2

tmp = H(2:length(H));
F = zeros(1,(length(H)-1)*D+1);
F(1) = H(1);
for n = 1:length(H)-1,
  F(n*D+1) = H(n+1);
end;
```

`wkeep2.m`: Extracts a part of a matrix.

```
function y = wkeep2(x,arg2,arg3);

[r,c] = size(x);
if arg3 == 'l',
  y = x(:,1:arg2);
elseif arg3 == 'r',
  y = x(:,c-arg2+1:c);
else,
  y = wkeep(x,arg2);
end;
```

`maxindex.m`: Finds the indexes for the maximum, minimum or absolute maximum in a vector or a matrix.

```
function M = maxindex(X,type);
%Finds the index in the vector or matrix X
%that corresponds to a maximum ('max'),
%minimum ('min') or absolute maximum ('abs')
%value.

% Made by Roger Eriksen 27/6-96. Ver.4.

if type == 'abs',
  m = max(max(abs(X)));
elseif type == 'min',
  m = min(min(X));
elseif type == 'max',
  m = max(max(X));
else,
  error('Wrong arguments, read help!');
end;

s = size(X);
[A B] = find(X == m);
if A == 1, % X is a vector
  M = max(M);
else,
  M = [A B];
end;
```

`DWTplot.m`: Plot the dircrete wavelet representation of a analyzed signal. Used for the DWT plots in Section 5.1.3.

```
function DWTplot(c,f,time,scales,psi);
%
%imageplot of the DWT(a,b), with the analyzing
%wavelet in the rigth corner. The analyzed signal
%is plotted over the DWT plot.
%
%  syntax: DWTplot(c,f,time,scale,psi)
%
```

```
% c     - the wavelet representation matrix
% f     - the analyzed signal
% time  - time vector
% scale - scaling vector
% psi   - the analyzing wavelet
%
%If the analyzing wavelet is complex, both the
%real and the imaginary part is shown. The
%imaginary part is plotted as a dashed line.
%When the DWT is complex the absolute valve is
%plotted.

% Made by Roger Eriksen 16/6-96. Ver. 2. Based on CWTplot

clf;
NBC = 64;
caxis([1 NBC]);
axis off;

% Plot of analyzed signal
WINDOW1 = [0.075 0.8 0.85 0.15];
axes('position',WINDOW1);
plot(time,f,'g-');
axis([min(time) max(time) 1.5*min(f) 1.5*max(f)]);
title('Analyzed signal');

% Plot of DWT
WINDOW2 = [0.075 0.14 0.85 0.55];
axes('position',WINDOW2);
if ~(imag(c) == 0),
  c = abs(c);
end;
C = wcodemat(c,NBC,'mat',0);
image(time,fliplr(scales),NBC-abs(C));
xlabel('Time step (k)');
ylabel('Scale (j)');
title('DWT(j,k)');
grid off;

% Plot of the analyzing wavelet
WINDOW3 = [0.77 0.55 0.13 0.11];
axes('position',WINDOW3);
if ~(imag(psi) == 0),
  plot(imag(psi),'r-.');
end;
hold on;
plot(real(psi),'b-');
axis([1 length(psi) min(real(psi)) max(real(psi))]);
hold off;
axis off;
grid off;

% Plot of colorbar
CBAR = [0.3 0.05 0.4 0.0125];
```

```
axes('position',CBAR);
for n = 1:NBC,
  bar(1,n) = NBC-n+1;
  bar(2,n) = NBC-n+1;
end;
image(bar);
axis off;
axes('position',[0 0 1 0.00001]);
axis off;
title('Colorscale from MIN to MAX');
```

CWTplot.m: Used to produce the plots in Section 3.1.

```
function CWTplot(c,f,time,scales,psi);
%
%imageplot of the CWT(a,b), with the analyzing
%wavelet in the rigth corner. The analyzed signal
%is plotted over the CWT plot.
%
%  syntax: CWTplot(c,f,time,scale,psi)
%
% c     - the wavelet representation matrix
% f     - the analyzed signal
% time  - time vector
% scale - scaling vector
% psi   - the analyzing wavelet
%
%If the analyzing wavelet is complex, both the
%real and the imaginary part is shown. The
%imaginary part is plotted as a dashed line.
%When the CWT is complex the absolute valve is
%plotted.

% Made by Roger Eriksen 14/5-96. Ver. 2.

clf;
NBC = 64;
caxis([1 NBC]);
axis off;

% Plot of analyzed signal
WINDOW1 = [0.075 0.8 0.85 0.15];
axes('position',WINDOW1);
plot(time,f,'g-');
axis([min(time) max(time) 1.5*min(f) 1.5*max(f)]);
title('Analyzed signal');

% Plot of CWT
WINDOW2 = [0.075 0.14 0.85 0.55];
axes('position',WINDOW2);
if ~(imag(c) == 0),
  c = abs(c);
end;
C = wcodemat(c,NBC,'mat',0);
```

```
image(time,fliplr(scales),NBC-abs(C));
xlabel('Time (b)');
ylabel('Scale (a)');
title('CWT(a,b)');
grid off;

% Plot of the analyzing wavelet
WINDOW3 = [0.77 0.55 0.13 0.11];
axes('position',WINDOW3);
if ~(imag(psi) == 0),
  plot(imag(psi),'r-.');
end;
hold on;
plot(real(psi),'b-');
axis([1 length(psi) min(real(psi)) max(real(psi))]);
hold off;
axis off;
grid off;

% Plot of colorbar
CBAR = [0.3 0.05 0.4 0.0125];
axes('position',CBAR);
for n = 1:NBC,
  bar(1,n) = NBC-n+1;
  bar(2,n) = NBC-n+1;
end;
image(bar);
axis off;
axes('position',[0 0 1 0.00001]);
axis off;
title('Colorscale from MIN to MAX');
```